2017

Advanced materials for stable Li-S and Li-organic batteries

Yuede Pan
University of Wollongong

UNIVERSITY OF WOLLONGONG

Institute for Superconducting & Electronic Materials

Advanced materials for stable Li-S and Li-organic batteries

Yuede Pan

This thesis is presented as part of the requirements for the

Award of the Degree of Doctor of Philosophy

University of Wollongong

February 2017

CERTIFICATION

I, Yuede Pan, declare that this thesis, submitted in partial fulphilment of the requirements for the award of Doctor of Philosophy, in the Institute for Superconducting & Electronic Materials (ISEM), Faculty of Engineering, University of Wollongong, NSW, Australia, is wholly my own work unless otherwise referenced or acknowledged. This thesis has not been submitted for qualifications at any other academic institutions.

Yuede Pan

February 2017

DEDICATION

To my family and friends, who stand by me all the time.

ACKNOWLEDGEMENTS

I would like to deliver my utmost gratitude to my supervisors, Prof. Shixue Dou, and Dr. Shulei Chou, for their invaluable supervision, suggestions, encouragement and understanding during my PhD study at University of Wollongong (UOW). Thank Prof. Huakun Liu and Prof. Jiazhao Wang for their supervision and guidance. I also would like to thank Dr. Tania Silver for her critical reading of my manuscripts.

During my PhD study, I have stayed for some time in China on cooperation projects. I would like to thank Prof Jiang Lei from Chinese Academy of Sciences (CAS) and Beihang University (Beijing) for his supervision. His wisdom, leadership, passion for the career of science and his philosophy of how to understand and how to do research will be helpful to me during my research career. I also would like to thank Prof Chen Jun from Nankai University (Tianjin). His vision, diligence and devotion to the research career has always inspired me. I also would like to thank Prof. Cheng Fangyi, A/Prof. Zhanliang Tao and A/Prof Jing Liang for their help during my stay in Prof Chen Jun's laboratory. The supervisors are always excellent examples for me to follow.

I would like to thank UOW for my international postgraduate tuition award (IPTA) and University postgraduate award (UPA) for supporting my PhD study.

I am grateful to my collaborators, Yuhai Dou (UOW), Dr Yahong Zhou (Technical institute of physics and chemistry, TIPC, CAS), Qing Zhao (Nankai University), Junran Hao (Beihang University) and Xuanbo zhu (Jilin University) for their joint contribution to the works during my PhD study.

Technical assistance and instruction from the staff at UOW, particularly those at Institute for Superconducting and Electronic Materials (ISEM), such as Dr. Germanas

Peleckis (XRD), Dr. Dongqi Shi (XPS), Dr. Tony Romeo (FESEM), Dr. Darren Attard (FESEM), Dr. Kosta Konstantinov (TGA, BET) and Dr. Gilberto Casillas-Garcia (TEM) are greatly appreciated. Other staff, like Ms. Joanne George (Laboratory and Safety Operations Officer), Ms. Crystal Mahfouz (Administrative Assistant), Ms. Narelle Badger (Administrative Assistant) are highly appreciated for their administrative and safety education assistance.

I would like to thank staff in Prof Jiang Lei's group (some of them have stayed at UOW as visiting scholars), such as Prof. Shutao Wang, Prof. Liping Wen, A/Prof. Dongliang Tian, Prof. Kesong Liu, Dr. Tianye, Prof. Prof. Jingxia Wang, Dr. Yahong Zhou, Dr, Lingjuan Zhang, Dr. Yan Liu, Dr. Xiqi Zhang, Dr. Hongliang Liu, Dr. Mingxuan Kuang, Dr. Kan Li, Dr. Zhichao Dong, Dr. Yuchen Wu, Dr. Xiangyu Jiang,

I also would like to thank my colleagues and friends in CAS and Beihang, like Dr. Yanan Jiang, Dr. Kang Sun, Dr. Siheng Li, Dr. Huacheng Zhang, Dr. Jue Hou, Dr. Jingwen Liao, Dr. Huijie Wang, Dr. Weiwei Xiong, Dr, Hainan Gao, Dr. Moyuan Cao, Dr. Chunming Yu, Dr. Xiangyu Kong, Dr. Bing Bao, Dr. Jian Wagn, Dr. Li Wang, Dr. Junbing Fan, Dr. Li He, Dr. Zhen Gu, Mr. Chuangqi Zhao, Mr. Kang Ruan, Mr. Zhandong Gu, Mr. Feilong Zhang, Mr. Yongyang Song, Ms. Junran Hao, Mr. Xuanbo Zhu, Mr. Yi Ding, Mr. Lie chen, Mr. Xiaoxun Li, Mr. Bing Dai, Mr. Yuefeng Wang, Mr. Zhe Xu, Ms. Yanxia Chen, Ms. Lili Wang, Ms. Qian Kang, Mr. Yang Wang, Mr. Yun Peng, Mr. Yi Zhou, etc.

I would like to thank those staff, colleagues and friends in UOW, such as, Prof. Xiaoling Wang, Dr. Dr Lin Lu, Dr. Yi Shi, Dr. Jiantie Xu, Dr. Yunxiao, Dr. Zhijia Zhang, Dr. Yuhai Dou, Dr. Xuanwen Gao, Dr. Mohammad Ihsn, Dr. Qi Li, Dr. Jun

Wang, Dr. Xin Liang, Dr. Weijie Li, Dr Wenbin Luo and Dr. Lanling Zhao, for their valuable suggestions and help.

Finally, I would like to thank my parents and my brother for their love and support. I would like to thank my girlfriend Rong Zhang, whether she will be my wife or not I cannot 100% ascertain, but thank her for dragging me out of my psychological marsh and giving me confidence facing to my or our future. Ms Zhang plays a critical role in this stage of my life and will influence my whole life, of which I am 100% sure.

ABSTRACT

Lithium ion batteries (LIBs) are playing an increasingly important role in our everyday life. LIBs are powering consumer electronics (e.g., cameras, smartphones, laptops), electric vehicles and large-scale industrial facilities. Also, LIBs are important energy storage systems for renewable energies like solar and wind. With respect to conventional LIBs, typically, the cathode material is $LiCoO_2$ and the anode material is graphite. However, the upper limit of the conventional LIBs cannot meet the long-term needs of the rapidly developing society, for instance, extended-range of electric vehicles. In this regard, next-generation battery types are highly needed to build up a more sustainable society.

Li-S batteries, with high theoretical capacity of 1675 mA h g^{-1} and high theoretical energy density of 2600 W h kg^{-1}, is a promising candidate for next-generation high-energy batteries. Also, the low cost and abundance of sulphur is an attracting advantage for Li-S batteries. In order to achieve the high capacity and high energy density of Li-S batteries, two severe problems should be overcome, that is, the poor electrical conductivity, as well as the dissolution and shuttling of the intermediate products of lithium polysulphides.

In addition to Li-S batteries, another lithium-based battery type, Li-organic batteries, are also attracting great interest. Organic molecules as cathode materials for lithium batteries show great promise for their sustainability and structure tunability. However, similar to Li-S batteries, the dissolution problem of the electroactive organic species leads to severe self-discharge and quick capacity decay.

Considering the similar problems between Li-S and Li-organic batteries, i.e., the dissolution and shuttling of the electroactive species (polysulphides anions or organic molecules/anions), strategies based varied membrane materials have been applied in order to achieve stable Li-S and Li-organic batteries. Several works based on this similar concept have been carried out and the main points are stated as below.

An integrated sulphur cathode with ion-transport regulating polymer membrane wrapping the sulphur/mesoporous carbon (CMK-3) composite is reported. Sulphonated poly (ether ether ketone), an ion-containing polymer, possesses excellent film-forming ability. The polymer film contains both hydrophobic domain of polymer backbone and hydrophilic domain of sulphonate groups. The ion interactions of negative sulphonate groups form negatively charged nanochannels. Thus, the novel cathode with asymmetric nanochannels system composed of the nanoporous membrane and the carbon nanochannels regulates the ion transport by facilitating lithium ions and rejecting polysulphides; meanwhile, the electron conductivity is ensured. Our novel design of the integrated cathode renders faster lithium-ion transport, which significantly reduces the resistance. Besides, the polysulphide rejection alleviates the active material loss. Therefore, these merits together enable superior high-rate long-cycle Li-S batteries. For instance, at an ultrahigh rate of 18 C, a high specific capacity of 612 mA h g^{-1} is retained over 250 cycles, with excellent capacity retention of 91%.

A new lithium-sulphur battery with a hydrothermally treated graphite film sandwiched between the separator and the sulphur cathode shows increased capacity, enhanced cycling stability and improved Coulombic efficiency. After 50 cycles, a high capacity of 631 mA h g^{-1} is maintained, compared to 203 mA h g^{-1} for the Li-S battery with conventional configuration. Moreover, the Coulombic efficiency is increased to near

100% from around 94%. This improved electrochemical performance could be attributed to the new cell configuration, for the graphite film greatly retains the active material by alleviating the polysulphide shuttling problem and providing extra reaction sites for sulphur species.

A thin bicomponent laminate composed of graphene oxide (GO) and nanoscale conductive carbon coated on the microporous polymer substrate as a new configured separator for stable lithium-organic batteries is presented. The sub-laminate with reconstructed GO sheets forms numerous negatively charged nanochannels, which permselectively allow the transport of lithium ions and reject the electroactive organic anions; meanwhile, the other sub-laminate with the nanoscale conductive carbon functions as the upper current collector for reactivating the electroactive organic species. In this work, two typical carbonyl electrode materials with respectively two (anthraquinone, AQ) and four (perylene-3,4,9,10-tetracarboxylic dianhydride, PTCDA) carbonyl groups are applied as examples. Compared to the pristine polymer separator, the coating of the bicomponent laminate enables significantly alleviated self-discharge, improved Coulombic efficiency and enhanced cycling stability.

TABLE OF CONTENTS

LIST OF FIGURES

LIST OF TABLES

LIST OF ABBREVIATIONS

Abbreviation	Full name
AQ	anthraquinone
a.u.	Arbitrary unit
BET	Brunauer Emmett Teller
cm	Centimeter
CNT	Carbon nanotubes
CPE	Constant phase element
CV	Cyclic voltammetry
DOL	1,3-dioxolane
DME	1,2-dimethoxyethane
EDS	Energy dispersive X-ray spectroscopy
EIS	Electrochemical impedance spectroscopy
EV	Electric vehicle
FTIR	Fourier transform infrared spectroscopy
G	graphene
GO	Graphene oxide
GO/SP-P	GO/SP coated separator
GO/G-P	GO/G coated separator
GPC	Gel Permeation Chromatography
HRTEM	High-resolution transmission electron microscopy
LIBs	Lithium-ion batteries
LiTFSI	lithium bis (trifluoromethanesulphonyl) imide
LLS	laser light scattering (LLS) spectrometer

M	Metal element
mm	Millimeter
nm	Nanometer
NMR	Nuclear magnetic resonance
NMP	N-methyl-2-pyrrolidone
OCV	open-circuit voltages
P	Pristine separator
PE	polyethylene
PEEK	poly (ether ether ketone)
PP	polypropylene
PTCDA	perylene-3,4,9,10-tetracarboxylic dianhydride
PTFE	Poly(tetrafluoroethylene)
PVDF	Polyvinylidene fluoride
SAXS	1D small-angle X-ray scattering
SEI	Solid electrolyte interphase
SEM	Scanning electron microscopy
SHE	Standard hydrogen electrode
SP	Super P
SPEEK	sulphonated poly (ether ether ketone)
TEM	Transmission electron microscopy
TGA	Thermogravimetric analysis
XPS	X-ray photoelectron spectroscopy
XRD	X-ray diffraction

LIST OF SYMBOLS

Symbol	Name	Unit
2θ	Detection angle in XRD	Degree
C-rate	Charge or discharge rate	mA g^{-1}
I	Current	A
V	Voltage	V
^{o}C	Degrees Celsius	-
R_{ct}	Charge transfer resistance	Ω
R_{e}	Electrolyte resistance	Ω
R_{sei}	Solid-electrolyte interface resistance	Ω
T	Temperature	K or °C
t	Time	h or s
W	Warburg impedance	Ω
wt.%	Weight percent	-
Z_{re}	Real part of the impedance	Ω
Z_{w}	Warburg impedance	Ω
η_{e}	Coulombic efficiency	%
β	Coherence factor	-
λ	Wavelength	nm
σ	Ionic conductivity	S cm^{-1}

LIST OF ORGANIZATIONS

Abbreviation	Full name
ISEM	Institute for Superconducting and Electronic Materials
UOW	University of Wollongong
CAS	Chinese academy of sciences
TIPC	Technical institute of physics and chemistry

CHAPTER 1 INTRODUCTION

Energy is one of the key factors that drives the world forward to supply a better life for every human being. Since the industrial revolution in the 18th century, the world has been transformed at a much faster speed than before, owing to many key inventions, many of which are related to energy. The exploitation of fossil fuels such as coal and petroleum in the last two centuries has brought a better life and brighter future for our generations living in the 21st century. The consumption of fossil fuels has helped to build up the modern world, but constant energy crises have inspired the exploration of renewable forms of energy.

Renewable forms of energy such as wind and solar power have a formidable common problem, that is, they are affected by the natural environment and are hard to control and manage. Therefore, energy storage systems have become very important for better exploitation of renewable energy. Rechargeable lithium ion batteries (LIBs), due to their high capacity, high energy density and reliability, have become an important option among the many electrochemical energy storage systems like redox flow cells and Na-S batteries, etc. LIBs have so far been the most favorable and widely-used battery type, as compared with nickel metal hydride (Ni-MH) batteries, lead-acid batteries, etc. Their attractive characteristics, as well as their high safety and low cost, has caused LIBs to be widely used in consumer electronics (e.g., cameras, cellular phones, laptop computers), electric vehicles, and large-scale industrial facilities.

With the research and development during the last two decades, LIBs have almost reached the theoretical limit of capacity and energy density, which, however, need further improvement to meet the ever-growing demand for high energy density and requirements such as light weight, small size, low cost, and environmental compatibility.

In this context, next-generation batteries are gaining increasingly greater attention. In this thesis, two lithium-based battery types, that is, Li-S and Li-organic batteries, are investigated. In the case of Li-S batteries, sulphur has a high theoretical specific capacity (1675 mA h g-1) and energy density (2600 kW h kg-1) approximately 10 and 5 times those of the conventional intercalation cathode, respectively. The low cost and the abundance of the sulphur are also great advantages. With respect to the organic molecules as cathode materials, they have merits including cost-effectiveness, sustainability, chemical tunability and environmental-friendliness, etc., and hence are attracting world-wide attention for application in rechargeable lithium batteries.

Both the sulphur cathode and the organic cathode have a similar common problem, that is, both the intermediate products of lithium polysulphide in Li-S batteries and the organic molecules/anions in Li-organic batteries are soluble the aprotic electrolytes and result in shuttling problems. The active material loss causes rapid capacity decay and poor Coulombic efficiency.

To overcome these formidable drawbacks, approaches related to the main components (the electrodes, the electrolyte and the separator) and the cell configuration (insertion of interlayers) have been reported. A wide range of carbon materials have been utilized to form composites with sulphur or organic molecules. Other applied materials include conductive polymers, metal oxides, etc. With respect to the electrolytes, for examples, varied additives are used in order to mitigate the polysulphide shuttling problem in Li-S batteries. Ion selective materials used for independent or dependent separators in Li-S or Li-organic batteries achieve highly stable batteries and improve the Coulombic efficiencies. In this thesis, through membrane design, the utilization of the active material is greatly improved, the capacity and cycling stability are significantly enhanced.

The structure of this thesis is presented as follows.

Chapter 1 introduces the general background, major problems, the approaches that have been applied in addressing these problems in Li-S and Li-organic batteries, and the general strategies utilized in this thesis.

Chapter 2 presents a literature review on Li-S and Li-organic batteries, including the history of batteries, general principles, working mechanisms, basic concepts, and recent advances in these areas.

Chapter 3 includes the list of materials used in this thesis, as well as the experimental procedures, synthesis approaches, electrode preparation, cell assembly, and physical and electrochemical characterization methods.

Chapter 4 studies the synthesis of a new polymer material, sulphonated poly(ether ether ketone), and its application as the binder material for the sufur cathode in Li-S batteries. The ion-regulation property of this polymer material was researched from both theoretical and experimental aspects. By demonstration with Li-S batteries, the cycling stability and the rate capability have been greatly improved.

Chapters 5 investigate a simple strategy by inserting a piece of graphite paper between the separator and the sulphur cathode to modify the cell configuration of the Li-S battery. The sandwiched graphite film greatly improves the active material utilization and enhances the cycling stability, as well as the Coulombic efficiency.

Chapters 6 presents the investigation of Li-organic batteries with the molecules of AQ and PTCDA, respectively, as the cathode active material and modified separators coated with GO/G and GO/SP, respectively, as the separator. With the ion-selectivity of GO and the reactivating ability of the conductive carbon, the stability of the Li-organic

batteries has been greatly improved. Further, the open circuit voltages have been significantly stabilized and the Coulombic efficiencies have been impressively ameliorated.

Chapter 7 is the general conclusions of this thesis and recommendations for further research based on them, followed by the lists of references and publications during the PhD study.

CHAPTER 2 LITERATURE REVIEW

2.1 Lithium-ion batteries

2.1.1 General Background

Lithium ion batteries (LIBs) are playing an important role in our everyday lives.[1-16] Commercial cell phones and laptop computers rely on LIBs for supplying their electrical power. The rapid development of transportation electrification depends on the high energy density and the relatively acceptable price of LIBs. To build a more sustainable society, renewable sources of energy such as solar and wind power need

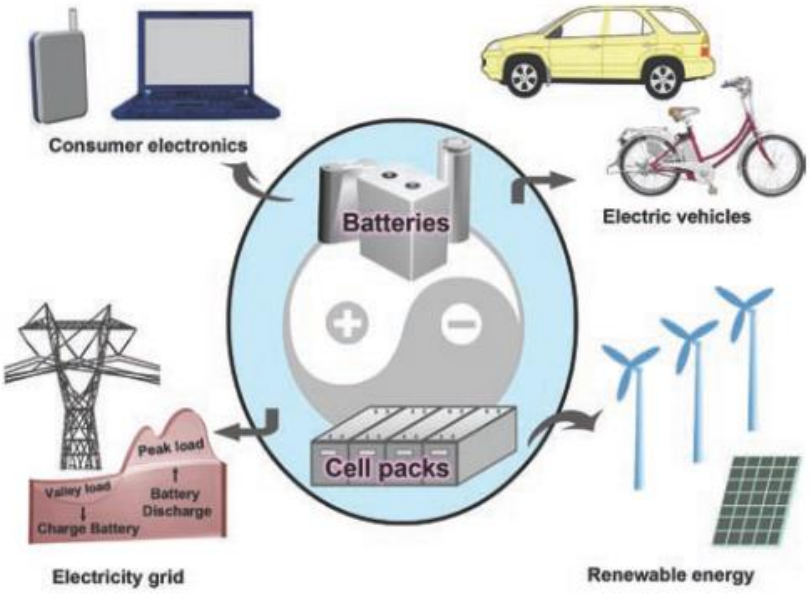

Figure 2.1 The wide-ranging applications of rechargeable batteries.[4]

energy storage systems for better exploitation and utilization of such intermittent energy systems, and for this purpose, LIBs have been an important candidate. LIBs can also be

used as energy storage and conversion devices for large-scale industrial facilities. Typical applications of LIBs, as well as some high-energy rechargeable batteries, are shown in Figure 2.1.

2.1.2 Brief History

LIBs can be considered the most favorable battery system in the market, but the evolution of batteries has required more than two centuries. The history of battery development has witnessed the control and use of electricity and electrical energy, and the design of new power sources with increasingly improved energy storage capabilities, lower cost, evolved electrochemical systems, and dependence on advanced materials sciences and technologies.[17] Compared to other commercialized battery systems, LIBs exhibit appealing advantages in terms of energy and power densities, and they dominate a large proportion of market for application in portable electronics and electrified transportation.[3]

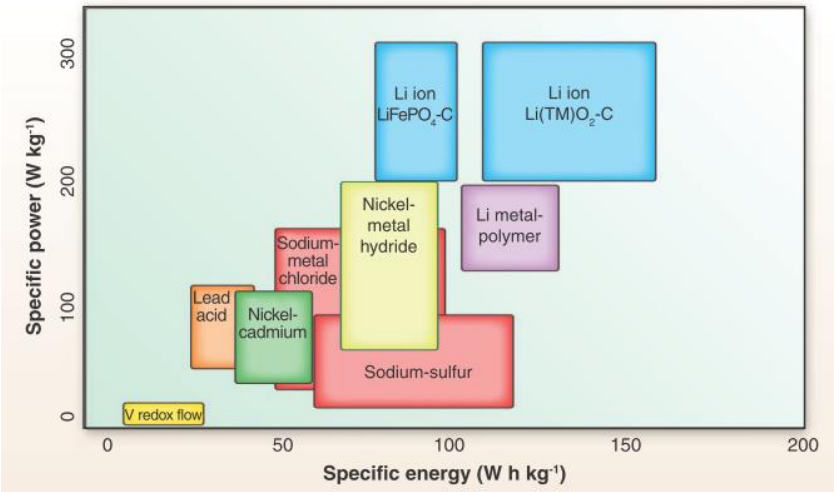

Figure 2.2 Comparison of energy and power densities of LIBs with some other types of batteries.[3]

The invention of batteries can be dated back to more than two centuries ago. In 1800, Alessandro Volta invented the first power source in human history, for which achievement, his name was chosen to name the unit of potential. Then, the lead-acid battery, one of the most important rechargeable power sources, was commercialized in 1882. Even nowadays, lead-acid batteries are still being widely used due to their low price, although their capacity and energy density are relatively low. The reversible electrochemical reactions in the lead-acid battery are presented in Equation (2.1).

$$PbO_2 + 2H_2SO_4 + Pb \;\Leftrightarrow\; 2PbSO_4 + 2H_2O \qquad (2.1)$$

Later, at the beginning of the 20th century, nickel-cadmium batteries were commercialized and greatly developed in the 1980s. Their reversible reaction is shown in the equation below.

$$Cd + 2NiOOH + 4H_2O \;\Leftrightarrow Cd\;(OH)_2 + 2Ni\;(OH)_2 \cdot H_2O, \qquad E_0 = 1.30\ V \quad (2.2)$$

where E_0 is the standard electrode potential.

Nevertheless, because of the toxicity of cadmium and their troublesome memory effect, nickel-cadmium batteries were partly replaced by nickel-metal (M) hydride batteries. The charge/discharge reaction is as follows.

$$M + xNi(OH)_2 \;\Leftrightarrow MH_x + xNiOOH, \qquad E_0 = 1.30\ V \qquad (2.3)$$

The aforementioned battery systems use poisonous heavy metals such as lead or cadmium, which causes serious environmental problems. In addition, their low discharge voltages, low capacities and low energy densities have been unable to satisfy the ever-growing demands due to rapid technological development, particularly on consumer electronics, electric vehicles, and new energy sources such as solar and wind. Therefore, high-performance rechargeable batteries with high energy density and low price are highly desirable. To define a high-performance battery, there are 16 important

parameters to meet: (1) a high and stable discharge voltage plateau; (2) high energy density relative to the weight (W h/kg) or the volume (W h/L); (3) low internal resistance; (4) high power density (W/kg or W/L); (5) a wide range of working temperature; (6) long shelf life; (7) long cycle life; (8) low price; (9) high safety, high reliability, and high stability; (10) good sealing, without electrolyte leakage; (11) feasible and environmental friendly electrode materials; (12) recyclability of the utilized materials; (13) high charge/discharge efficiency; (14) high-rate property; (15) durable under over-charge and over-discharge; and (16) easily maintained. Although the specific requirements are different for varied types of batteries, some of them are common, for instance, high energy density, high output power density, long cycle life, stable discharge voltage plateau, and high-rate charge and discharge.

Owing to the properties of lithium, with the lightest weight among all the metals, the lowest oxidation/reduction potential, and the highest energy density (W h/kg), rechargeable lithium batteries have been a promising alternative new energy source. Li is the most electronegative metal, with electrochemical potential of -3.04 V (vs. standard hydrogen potential, SHE) and molecular weight of 6.94 g mol^{-1} (specific gravity ρ = 0.53 g cm^{-3}), respectively. LIBs possess energy density approximately 3 times higher and power density 6 times higher than those of nickel metal hydride (Ni-MH), Ni-Cd, and lead acid batteries, respectively.

Before the 1980s, the research on the rechargeable LIBs was focused on those with anodes composed of lithium metal and lithium alloys. In the charge process, however, the rough surface of the lithium metal causes uneven surface potential and uneven lithium deposition. During the deposition of the lithium metal, in some specific areas, lithium is deposited much more rapidly and produces lithium dendrites. The lithium dendrites grow as the battery is cycled. On the one hand, some of the dendrites break

and form “dead lithium”, which is unrecyclable; on the other hand, more seriously, the lithium dendrites penetrate through the separator, electrically connect the cathode and the anode, cause an internal short circuit, produce much heat, and make the battery catch fire or even explode.

In the 1970s, the Exxon Company invented a Li//TiS_2 battery system, with the charge/discharge process shown below:

$$x\mathrm{Li} + \mathrm{TiS_2} \Leftrightarrow \mathrm{Li}_x\mathrm{TiS_2} \quad (2.4)$$

Although the effort of commercializing this product failed, this invention was a landmark attempt in the decades’ long effort to finding the proper material and structure for a commercial rechargeable LIB. Researchers concluded that the cycle life of the Li//TiS_2 battery system could not be further prolonged for practical application owing to the following two important reasons. First, the utilization of lithium metal as the anode causes a serious safety issue due to the formation of lithium dendrite. Second, the lithium metal might react with the electrolyte and result in unstable operation.

The first breakthrough came when John B. Goodenough proposed $LiCoO_2$ as the cathode material for rechargeable LIBs in 1980. Lithium ions could be intercalated into or deintercalated out of the layered structure of $LiCoO_2$ during charge/discharge.

$$\mathrm{LiCoO_2} \Leftrightarrow \mathrm{Li}_{1-x}\mathrm{CoO_2} + x\mathrm{Li}^+ + xe^- \quad (2.5)$$

After a decade’s effort, researchers found that graphite performed very well as the anode material. In charge, lithium ions intercalate between the graphene layers and form the intercalation compound LiC_6. In discharge, the lithium ions deintercalate out of the layered structure of graphite. By coupling the $LiCoO_2$ cathode and the graphite anode, the new structure for the lithium ion battery greatly decreased the safety hazard caused by the usage of lithium metal as the anode and was successfully commercialized in

1991 by the SONY Company. The working mechanism of the graphite//$LiCoO_2$ cell is shown in Figure 2.2.

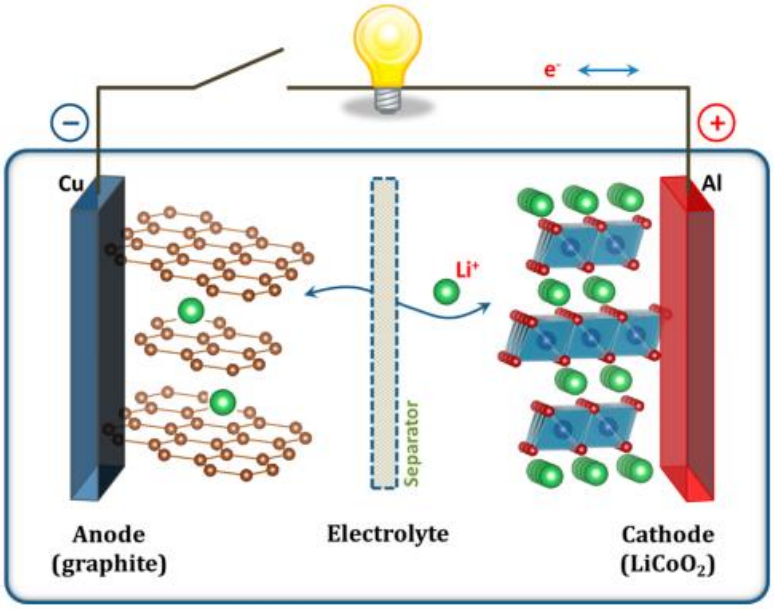

Figure 2.3 Working mechanism of a "rocking-chair" lithium ion battery with graphite as the anode, organic liquid electrolyte, and $LiCoO_2$ cathode.[8]

Since the successful commercialization of the LIBs, the research on power sources has opened up a new chapter, considering the evident merits of the LIBs compared to the aforementioned power supply systems, due to advantages including (1) high output voltage (3.6 V), triple those for Ni-Cd and Ni-MH batteries; (2) high energy density, (3) high power density; (4) low self-discharge, significantly outperforming Ni-Cd and Ni-MH batteries; (5) no memory effect, unlike Ni-Cd and Ni-MH batteries, and excellent cycling stability; (6) high-rate performance; (7) high charge/discharge efficiency; (8) wide range of working temperature; and (9) long cycle life, generally above 1000 cycles, with $LiFePO_4$ cells achieving more than 3000 cycles. As can be seen from Figure 2.3, both the energy and power densities of LIBs are significantly higher than for other types of commercial batteries.[3]

2.1.3 Basic concepts

Batteries are an important type of electrochemical energy storage system. Each cell of a battery has several important components: the cathode, the anode, the porous separator, and the liquid electrolyte. The battery converts chemical energy to electrical energy. Chemical reactions take place on the cathode (reduction half-reaction) and the anode (oxidation half-reaction) and drive the ionic component to migrate inside the cell. Meanwhile, to keep the charge equilibrium, electrons are forced to pass along the external electric circuit between the cathode and the anode. Hence, an external electronic current I at a voltage V for a time period Δt is produced. In relation to LIBs, some important concepts are listed as below.

1. Primary battery: a battery that can only be discharged once, as it is unable to be recharged and reused.

2. Rechargeable/secondary battery: a battery that can be charged/discharged repeatedly.

3. Cathode: the oxidant electrode, where electrochemical reduction occurs in discharge. In the charge process, the oxidation reaction takes place.

4. Anode: the reductant electrode, where electrochemical oxidation occurs in discharge. During the charge process, the reduction reaction takes place.

5. Intercalation: the process by which lithium ions migrate into the layered structure of a cathode material.

6. Deintercalation: the process by which lithium ions are removed from the layered structure of a cathode material.

7. Open-circuit voltage (OCV): the voltage between the cathode and the anode when there is no current flow along the external electric circuit.

8. Discharge: the process in which chemical energy is turned into electric energy, during which, electric current flows along the external electric circuit.

9. Charge: the process in which electrical energy is turned into chemical energy, for which a power source is used to restore the voltage and capacity of the cell.

10. Discharge/charge curve: the voltage-time curve in discharge/charge.

11. Discharge/charge capacity: the quantity of electric charge released in discharge/charge, with units of A h, or mA h.

12. Depth of discharge (DOD): the percentage of the released capacity with respect to the whole discharge capacity.

13. Discharge/charge rate: A measure of how fast the discharge takes place and how long it takes for the whole discharge/charge process. For example, if the whole discharge/charge process is completed in 1 h, the discharge rate is 1 C; if it takes 5 h, then the discharge/charge rate is 0.2 C.

14. Coulombic efficiency: Under certain charge/discharge conditions, the ratio between the discharged quantity of electric charge and the charged quantity of electric charge.

15. Self-discharge: The capacity loss when the battery is stored but has no electrical connection with other devices.

16. Internal resistance: the overall resistance between the cathode and the anode, including the resistances assigned to the current collectors, the electrode laminates, the separator, and the electrolyte.

17. Internal shortage: the state in which the cathode and the anode are electrically connected inside the cell, normally because of damage to the separator, lithium dendrites, impurities, etc.

18. Shelf/storage life: The period of time during which the electrochemical performance of a battery degrades to a specific extent (normally defined artificially).

19. Cycle life: Under certain conditions, the cycle number at which the capacity or other electrochemical properties can no longer be retained above a certain level after repeated charge and discharge.

20. Capacity density: the quantity of electric charge released by one unit (weight or volume) of electrode material, with units of mA h/L or mA h/kg.

21. Energy density: the energy released by one unit (weight or volume) of electrode material, with units of W h/L or W h/kg.

22. Power density: the power released by one unit (weight or volume) of electrode material, with units of W/L or W/kg.

23. Lithium-sulphur battery: a type of lithium battery with sulphur as the cathode material and lithium metal as the anode.

24. Lithium-organic battery: a type of lithium battery with an electroactive organic molecule or polymer as the cathode material and lithium metal as the anode.

2.1.4 Cathode materials

The development of suitable cathode and anode materials has been the key obstacle for low-cost high-performance LIBs (Figure 2.4). Materials scientists and engineers have endeavored to advance the material chemistry and physics of LIBs.

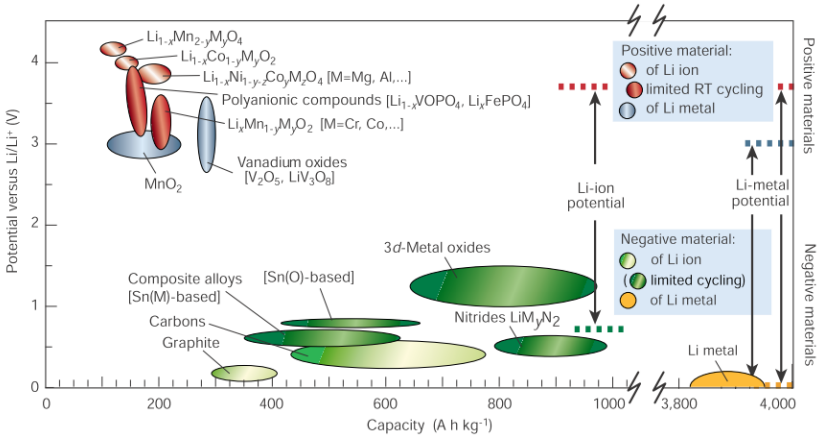

Figure 2.4 Cathode and anode materials for LIBs, and their capacities and potentials.[5]

The cathode materials can be broadly divided into three important categories according to their crystalline structures. They are the α-NaFeO2, spinel, and olivine structures. $LiCoO_2$, which is the most important representative of the α-$NaFeO_2$ structured cathode materials, is the most widely applied and the first cathode material to be successfully commercialized (Figure 2.5).[18, 19] α-$NaFeO_2$ has a distorted rock-salt structure, in which the cations are ordered in alternating planes (Figure 2.5). This type of material can also be called a layered structure material. Because the first-generation LIBs are assembled with $LiCoO_2$ cathodes and graphite anodes, both of which are layered structure materials, LIBs are also called "rocking-chair" batteries.

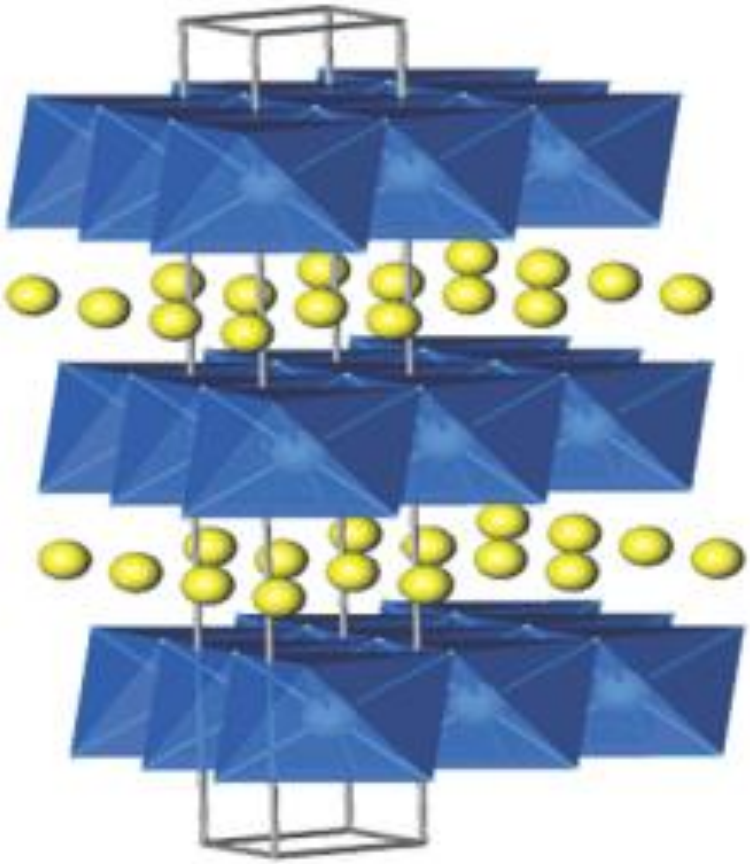

Figure 2.5 Layered α-$NaFeO_2$ structure with lithium ions between the transition metal planes.[20]

Although $LiCoO_2$ has had both historical and practical importance during the last two decades, great efforts have been put into developing alternative cathode materials to lower the cost, improve the environmental friendliness, and enhance the stability. The transition metal in the $LiCoO_2$ is more expensive, less abundant, and more unfriendly to the environment compared to other transition metals such as Fe, Ni, and Mn. Also, the stability of $LiCoO_2$ needs further improvement, because it can degrade when overcharged, causing performance decay or failure.[21, 22] The capacity can be improved by increasing the charging voltage, but the cycling stability is greatly harmed at the same time.[23] The reasons for the cycling degradation are stated as follows: First, the Co can be dissolved in the electrolyte during the processes of lithium intercalation and

deintercalation.[24] Second, the CoO_2 layer is stripped from the electrode surface after full delithiation.[25] Third, the lattice parameters undergo significant change during the lithiation and delithiation, leading to stresses and cracking of the $LiCoO_2$ particles.[26]

Another α-$NaFeO_2$ structured cathode material is $LiNiO_2$, which has a lower cost and has higher energy density, but it is less ordered and more unstable compared with $LiCoO_2$. The lower degree of order impedes the lithium intercalation and deintercalation. A solution to this problem involves doping with Co in order to maintain the performance while taking advantage of the low cost and high energy density of Ni. $LiMnO_2$ has a monoclinic structure, which is transformed to a layered hexagonal structure during cycling. The addition of Ni, or both Ni and Co, results in the formation of the α-$NaFeO_2$ structure. This ternary cathode material, i.e., $LiNi_{1/3}Mn_{1/3}Co_{1/3}O_2$, exhibits a high operating voltage, and improved capacity and rate performance.[27]

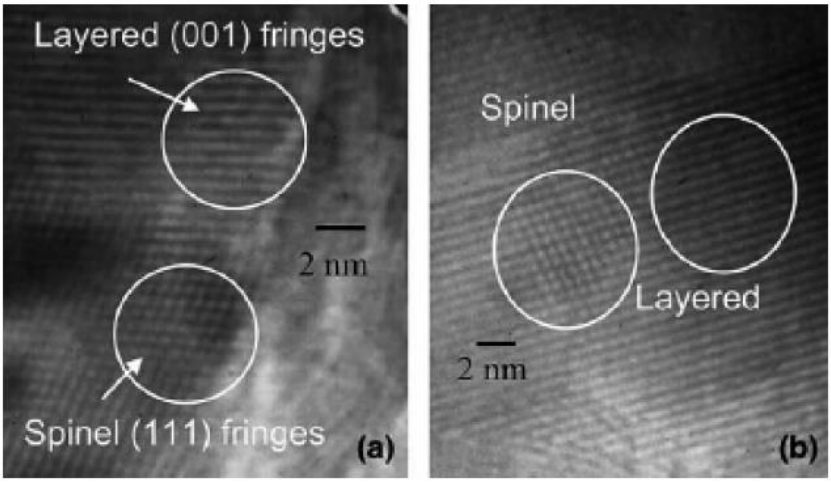

Figure 2.6 (a ,b) High-resolution TEM images of $0.7Li_2MnO_3 \cdot 0.3Li_4Mn_5O_{12}$ showing the co-existence of layered (Li_2MnO_3) and spinel ($Li_4Mn_5O_{12}$) domains.[28]

The spinel structure, as represented by $LiMn_2O_4$, is another important structure for commercialized LIB cathode materials.[20, 29-33] In the spinel structure, Mn occupies the octahedral sites and lithium occupies the tetrahedral sites. The difference between the

layered and the spinel structure can be clearly seen in Figure 2.6. The nanoparticle in the transmission electron microscope (TEM) images of $0.7Li_2MnO_3 \cdot 0.3Li_4Mn_5O_{12}$ is composed of layered Li_2MnO_3 and spinel $Li_4Mn_5O_{12}$ structures.[28] In the spinel structure, the lithiation and delithiation paths are through a three-dimensional network rather than planes as in the α-$NaFeO_2$ structure. $LiMn_2O_4$ features lower cost and higher safety than $LiCoO_2$, but it has lower capacity. A major challenge for $LiMn_2O_4$ as LIB cathode material is the phase change during cycling. Another problem is the capacity loss due to Mn dissolution in the electrolyte or changes in the particle crystallinity. In order to further improve the electrochemical performance, the crystalline structure of $LiMn_2O_4$ can be doped with various transition metal elements.[34-37] The addition of Co improves the cycling stability by stabilizing the spinel crystal structure, and Fe leads to an additional discharge plateau at high voltages. More commonly, Ni is added to decrease the lattice parameter and improve the electrical conductivity of $LiMn_2O_4$.

Another successful cathode material, $LiFePO_4$, has the olivine structure. In this crystalline structure, P occupies tetrahedral sites, Fe or other transition metals occupies octahedral sites, and Li is located in one-dimensional chains along the [010] direction. During the charge process, i.e. the delithiation process, the Fe^{2+} in the $FePO_4$ is oxidized to Fe^{3+}. In the change from $LiFePO_4$ to $FePO_4$, some Fe ions occupy lithium sites to maintain charge neutrality in the crystal structure. $LiFePO_4$ has a flat discharge profile, which is favorable for practical application. Nevertheless, the electronic conductivity is relatively low (10^{-9} S cm^{-1}) for pure $LiFePO_4$. Typically, additives are added to increase the conductivity. Fe_2P is a typical additive, although the amount should be carefully controlled, because larger amounts might block the lithium ion pathways in $LiFePO_4$.

Two other phosphate candidates are $LiCoPO_4$ and $LiMnPO_4$, both of which have higher open circuit voltages but lower capacities.

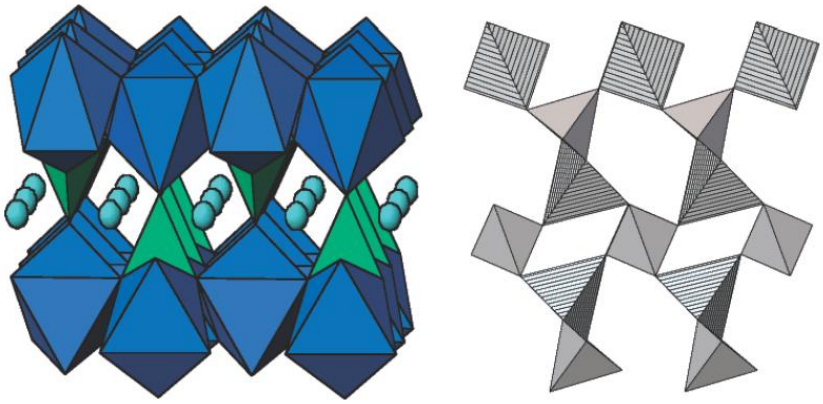

Figure 2.7 Structures of orthorhombic $LiFePO_4$ and trigonal $FePO_4$.[20]

2.1.5 Anode materials

The most successful anode material for LIBs is graphite, which enabled the commercialization of LIBs by the SONY Company in 1991. Lithium metal is the most promising anode material due to its high capacity, but the safety problem is still unresolved. Here, several typical anode materials are presented as examples.

The first type of anode material is graphite, which was coupled with $LiCoO_2$ in the first successful commercialized LIB by the SONY Company in 1991. The theoretical specific capacity is 372 mA h g^{-1}, with LiC_6 as the final lithiation product. Typical voltage profiles of the graphite anode and the lithiation/delithiation mechanism can be seen in Figure 2.8. It should be noted that a stable solid-electrolyte interphase (SEI) is critical for the stable operation of the graphite anode.[38-40]The electrolyte[41], the binder[42, 43], or the electrode additive can be all tuned to encourage the deposition of a stable SEI.

In addition, artificial SEI layers have been reported for long-cycling graphite anodes.[44, 45]

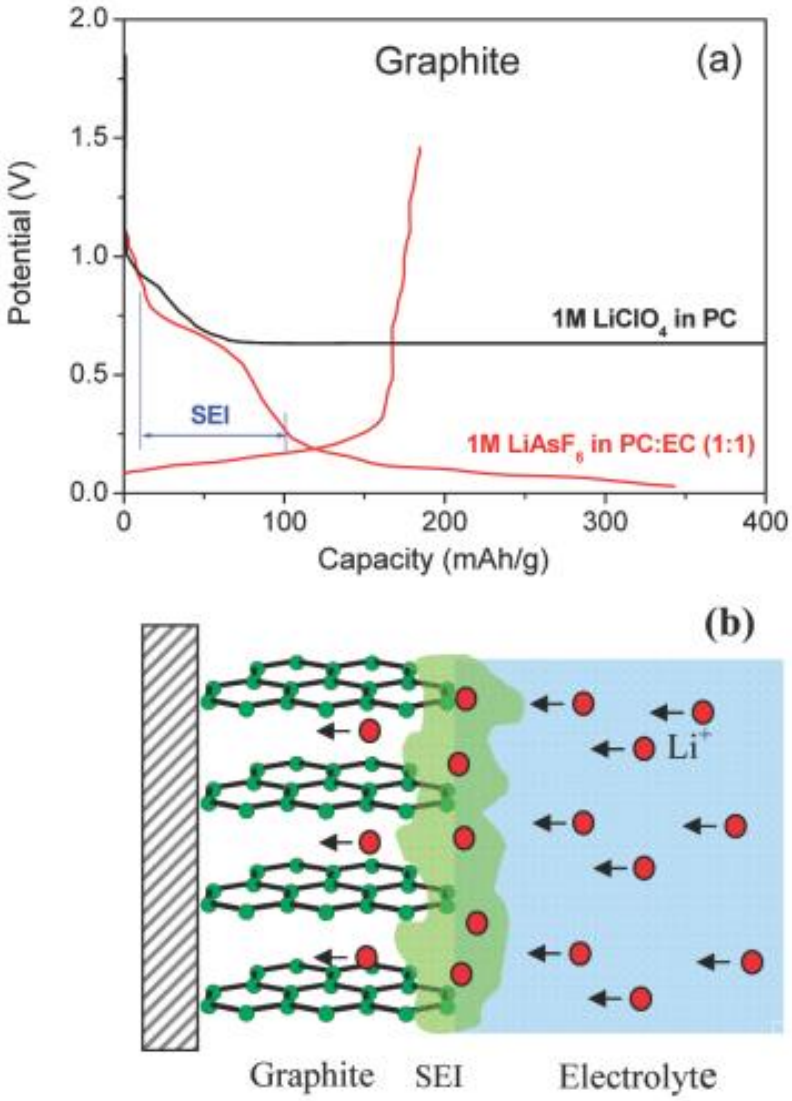

Figure 2.8 Voltage curves of graphite tested in 1 M $LiClO_4$ in propylene carbonate (PC) and 1 M $LiAsF_6$ in PC: ethylene carbonate (EC) (1:1, v/v) electrolytes. (b) Schematic illustration of the formation of the SEI layer by decomposition of EC-based electrolyte.[7]

Another kind of anode materials is composed of the Group IV elements that form lithium alloys, including Si, Ge, Sn, and Pb (Figure 2.9). These four elements all have higher capacities than graphite. In particular, the capacity of Si, 4200 mA h g^{-1}, is the highest among all these elements (Figure 2.10). For this reason, Si has received the most

attention, although Si is also severely plagued by the problems of unstable SEI films and the large volume expansion (300%). Prof. Cui Yi's group has conducted a series of excellent works on this interesting material by exploiting nanotechnology.[46-48]

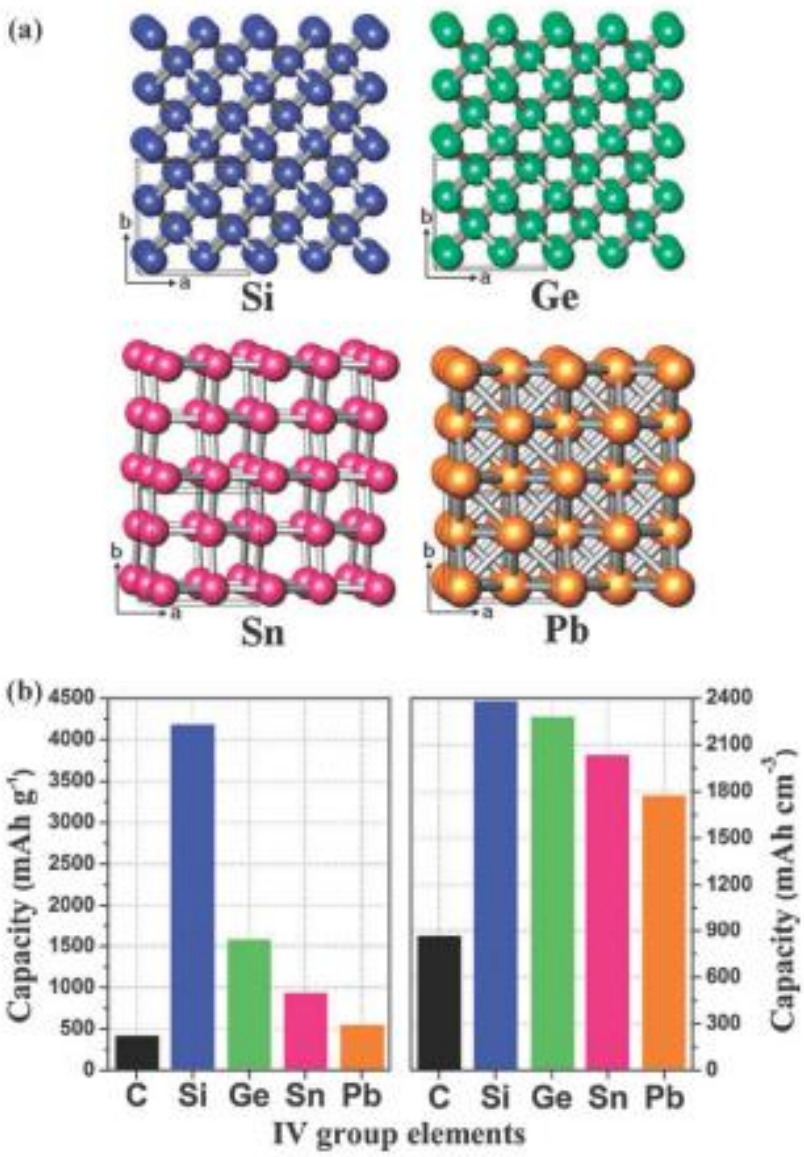

Figure 2.9 Crystal structures and capacities of Group IV elements. (a) Crystal structures of cubic Si (blue), cubic Ge (green), tetragonal Sn (red), and cubic Pb (orange). (b) Gravimetric (left) and volumetric (right) capacities of graphite (LiC_6), Si ($Li_{4.4}Si$), Ge ($Li_{4.25}Ge$), Sn ($Li_{4.25}Sn$), and Pb ($Li_{4.25}Pb$).[49]

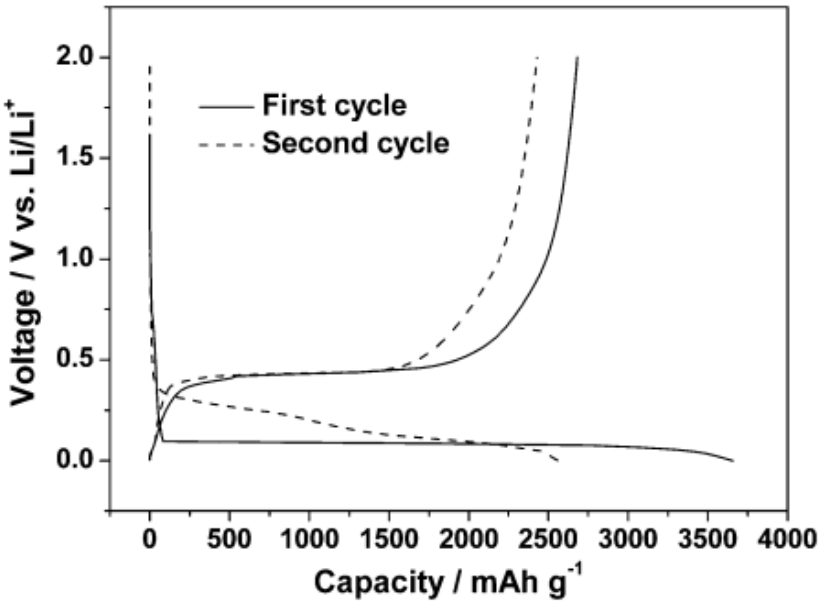

Figure 2.10 Typical charge/discharge voltage profiles of Si anode for the first and second cycles.[49]

The third important type of anode material consists of metal oxides, which have already been very well reviewed.[50] Roughly, the metal oxide anodes can be categorized into the following several groups: Li intercalation-deintercalation anodes, Li alloying-dealloying anodes, conversion-reaction anodes, and those based on both alloying and conversion reactions (Figure 2.11).

Lithium metal, which has proved dangerous for usage as the anode, is now regaining interest. On the one hand, the high capacity and energy density of the lithium metal makes it very attractive for building high-energy battery systems. On the other hand, with the quick development of nanotechnology and characterization techniques such as in-situ TEM, researchers have gradually been equipped with the necessary methods and tools for the study of the lithium metal anode. The main approach to improving the safety and cycling stability of lithium metal anode is to construct stable SEI films and suppress the lithium dendrites.[51-54] For instance, Zheng et al. applied a thin-film coating

consisting of interconnected carbon spheres on lithium metal anode to suppress the lithium dendrite growth and improve the cycling stability.[51]

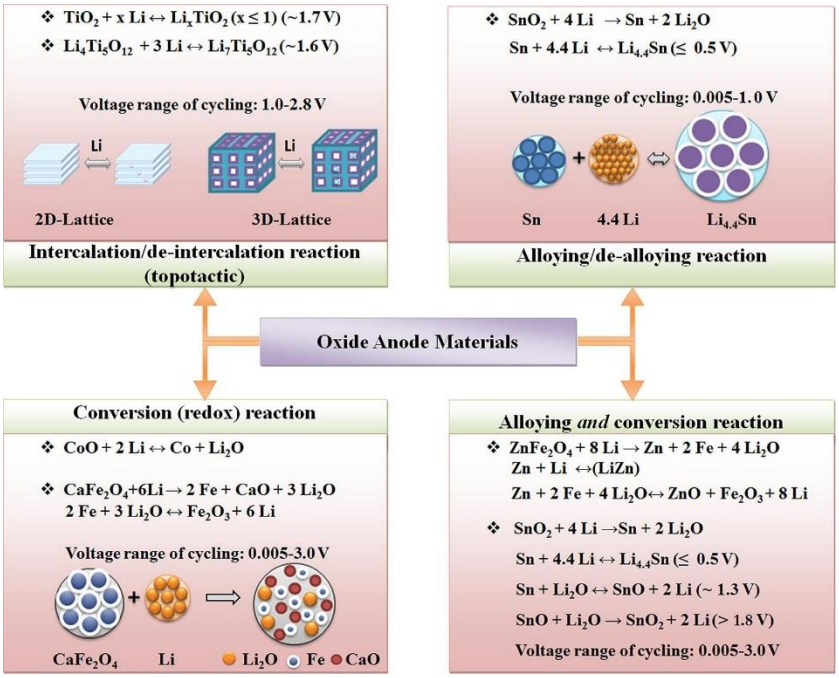

Figure 2.11 Metal oxide materials as anode in LIBs.[50]

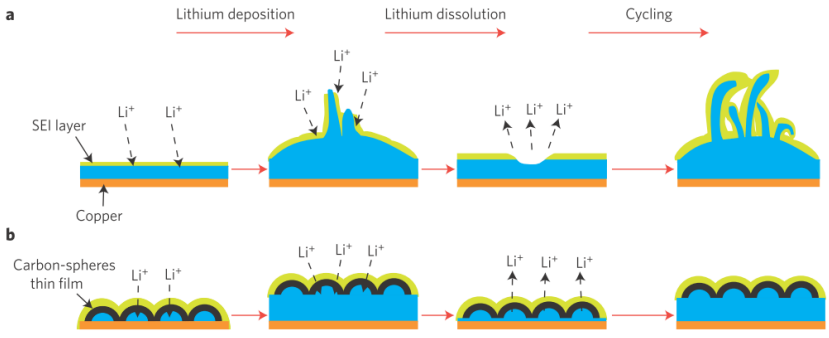

Figure 2.12 (a, b) Schematic diagram of lithium dendrite suppression by coating a thin film composed of carbon spheres on the surface of the lithium metal.[51]

2.1.6 Separators

The separator is an important component in the LIB, which is located between the cathode and the anode. The separator protects the cathode and the anode from direct electrical contact, while it also functions as the reservoir for the electrolyte and allows the transport of lithium ions. A detailed description of the development of separators can be seen in several important review papers on LIB separators.[55, 56]

Typically, there are three types of separators, including microporous polymer membranes, non-woven fabric mats, and inorganic composite separators. Some basic requirements on LIB separators relate to chemical stability, thickness, porosity, pore size, permeability, mechanical strength, wettability, dimensional stability, thermal shrinkage, thermal shutdown, and cost. In order to improve some key properties of separators, several approaches can be applied, including surface modification and polymer or ceramic coating of the separator surface.

In this thesis, the most widely used type of separator, i.e. the microporous polymer separator, is introduced. Some important companies that produce this kind of separator include Celgard, Degussa, Exxon, and Entek. The main separator polymer materials are polyethylene and polypropylene, and the production processes can be divided into two categories (Figure 2.13). One is the dry process, which consists of heating, extruding, annealing, and stretching steps. That is, the polymer is heated to its melting point and then extruded to form a nonporous polymer film, which is annealed and then stretched to form the final product. The other one is the wet process, which employs the solvent extraction, including four steps. The first step is mixing and heating the polymer, hydrocarbon liquid, and additives to form the polymer solution. Then, the polymer

solution is extruded into a nonporous polymer film. The third step is solvent extraction to produce a microporous polymer film, which is then stretched into a microporous polymer membrane as the final product. The difference in morphology between the dry-process and wet-process separators is revealed in Figure 2.14.

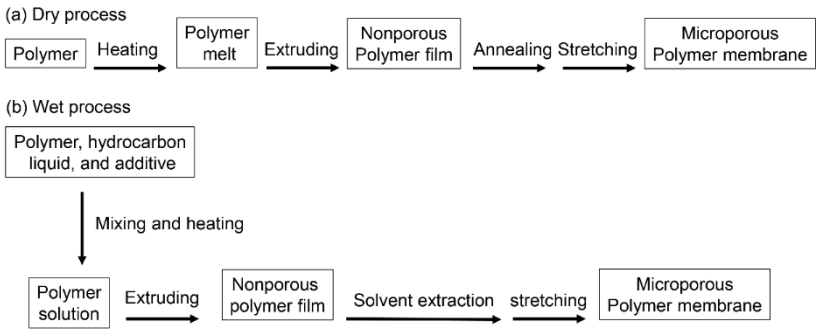

Figure 2.13 Fabrication processes for microporous polymer membrane separators: (a) dry and (b) wet processes.[56]

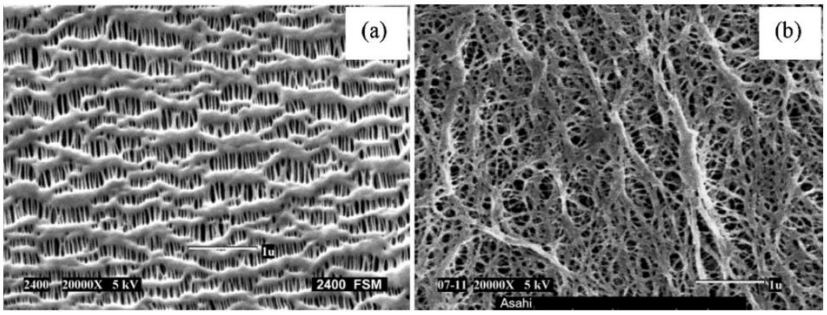

Figure 2.14 SEM images of separators fabricated by the (a) dry and (b) wet processes.[57]

2.1.7 Electrolytes

Nonaqueous liquid electrolytes are solutions composed of carbonate based solvents and Li salts. The typical carbonate solvents are propylene carbonate (PC), ethylene carbonate (EC), and linear dialkyl carbonates, such as dimethyl carbonate (DMC), diethyl carbonate (DEC), ethylmethyl carbonate (EMC), and propylmethyl carbonate

(PMC). The Li salts are lithium perchlorate ($LiClO_4$), lithium hexafluoroarsenate ($LiAsF_6$), lithium tetrafluoroborate ($LiBF_4$), lithium trifluoromethanesulphonate (LiTf), lithium bis(trifluoromethanesulphonyl)imide (LiIm), and lithium hexafluorophosphate ($LiPF_6$). Other systems of electrolytes include ionic liquids, polymers, inorganic ceramics, etc. Some typical electrolytes are listed in Table 2.1.

Table 2-1 Nonaqueous electrolytes for LIBs.[7]

Electrolytes	Example of classical electrolytes	Ionic conductivity ($\times 10^{-3}$ s/cm) at room temp	Electrochemical window (V) vs Li^+/Li^0		Remark
			Reduction	Oxidation	
Liquid organic	1M $LiPF_6$ in EC:DEC (1:1) 1M $LiPF_6$ in EC:DMC (1:1)	7[3] 10[3]	1.3[7] 1.3[7]	4.5[6] >5.0[3]	Flammable
Ionic liquids	1M LiTFSI in EMI-TFSI 1M $LiBF_4$ in EMI-BF_4	2.0[15] 8.0[15]	1.0[15] 0.9[16]	5.3[15] 5.3[16]	Non-flammable
Polymer	LiTFSI-P(EO/MEEGE) $LiClO_4$−PEO_8 + 10 wt % TiO_2	0.1[24] 0.02[26]	<0.0[24] <0.0[26]	4.7[24] 5.0[26]	Flammable
Inorganic solid	$Li_{4-x}Ge_{1-x}P_xS_4$ (x = 0.75) $0.05Li_4SiO_4 + 0.57Li_2S + 0.38SiS_2$	2.2[28] 1.0[30]	<0.0[28] <0.0[30]	>5.0[28] >8.0[30]	Non-flammable
Inorganic liquid	$LiAlCl_4 + SO_2$	70[20]	-	4.4[20]	Non-flammable
Liquid organic + Polymer	$0.04LiPF_6$ + 0.2EC + 0.62DMC + 0.14PAN $LiClO_4$ + EC + PC + PVdF	4.2[38] 3.0[39]	- -	4.4[38] 5.0[39]	Flammable
Ionic liquid + Polymer	1M LiTFSI + P_{13}TFSI + PVdF-HFP	0.18[43]	<0.0[43]	5.8[43]	Less flammable
Ionic liquid + Polymer + Liquid organic	56 wt % LiTFSI−Py_{24}TFSI + 30 wt % PVdF-HFP + 14 wt % EC/PC	0.81[44]	1.5[44]	4.2 [44]	Less flammable
Polymer + Inorganic solid	2 vol % $LiClO_4$-TEC-19 + 98 vol% 95 ($0.6Li_2S + 0.4Li_2S$) + $5Li_4SiO_4$	0.03[46]	<0.0[46]	>4.5[46]	Non-flammable
Ionic liquid + Liquid organic[19]		-	-	-	Non-flammable

2.2 Li-S batteries

2.2.1 Background and principles of Li-S batteries

The state-of-the-art LIBs have almost completely dominated the battery market for applications in portable electronics and electric vehicles, although the theoretical capacity and energy density of the LIBs have limited the further improvement of this

battery technology. In order to construct a more sustainable and cost-effective energy storage system, battery types with higher specific capacity and energy density are desired.

Li-S batteries, with compelling high specific capacity of 1675 mA h g^{-1} and high energy density of 2600 W h kg^{-1}, have been a promising candidate for next-generation high-energy lithium batteries.[58-73] With a long history dating back to the 1960s, Li-S batteries have recently been back in vogue owing to the ever-growing demand for batteries with high energy density for application in transportation and stationary energy storage. It can be expected that packed Li-S batteries are able to extend the range of electric vehicles to the standard of 500 km per charge. In addition, the abundance, low cost, and non-toxicity of elemental S endow Li-S batteries with important characteristics such as economic sustainability and environmental friendliness.

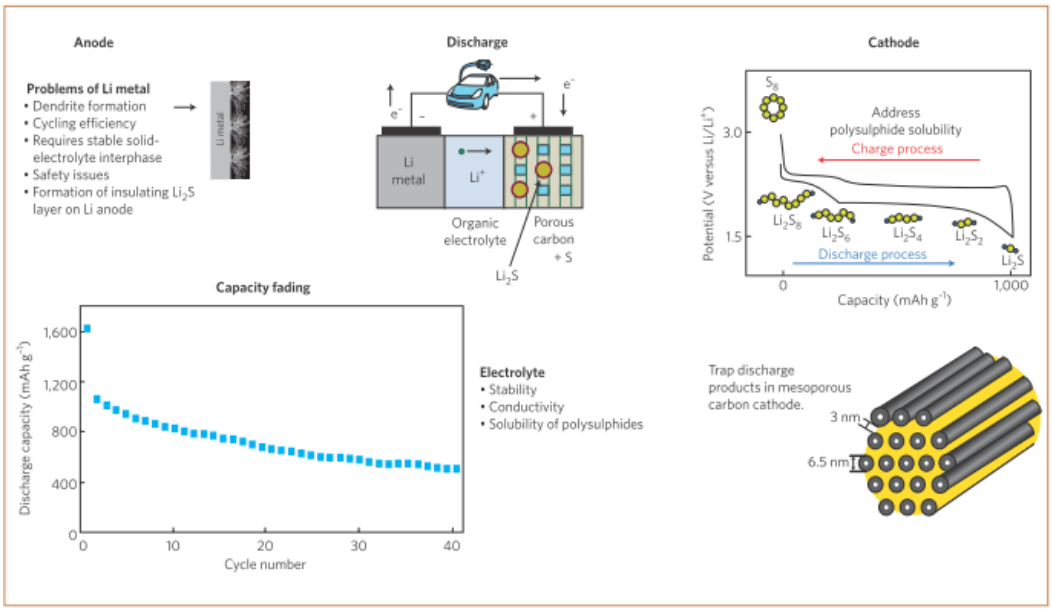

Figure 2.15 The challenges of Li-S batteries.[60]

Elemental sulphur is reduced to soluble lithium polysulphides and then solid Li_2S/Li_2S_2 in discharge, and vice versa in charge. The Li-S batteries face several critical challenges

(Figure 2.15).[60] First, both the S and the Li_2S/Li_2S_2 are insulating solids, and hence are plagued by sluggish electrochemical kinetics. Second, the i lithium polysulphide intermediate products can dissolve in the electrolyte and shuttle between the cathode and the anode, causing quick capacity decay and poor Coulombic efficiency. To overcome these issues, varied strategies have been applied. The most important work that marked the revival of Li-S batteries was reported in 2009 by Prof. Nazar's group.[74] They described a significantly improved Li-S cell with high practical capacity and stable cycling. Since then, the Li-S battery has gained ever-growing attention and undergone rapid development. All the main components of the Li-S battery have been investigated based upon varied principles and strategies. In this thesis, recent developments on the cathode material, the polymer binder, the cell configuration, the separator, and the electrolyte will be briefly reviewed.

2.2.2 Advanced sulphur composite cathodes

Sulphur as the electroactive material is plagued by two critical problems, i.e., its poor electrical conductivity, and the dissolution and shuttling of the intermediate products of polysulphide anions. To address these two key challenges, the development of novel sulphur composite cathode materials has received the most attention. Nano-confining sulphur inside a carbon framework can both increase the conductivity and alleviate the dissolution of the polysulphides. In this section, the three most important sulphur composites: sulphur-carbon[75-82], sulphur-conductive polymer[83, 84], and sulphur-metal oxide[85, 86], are presented.

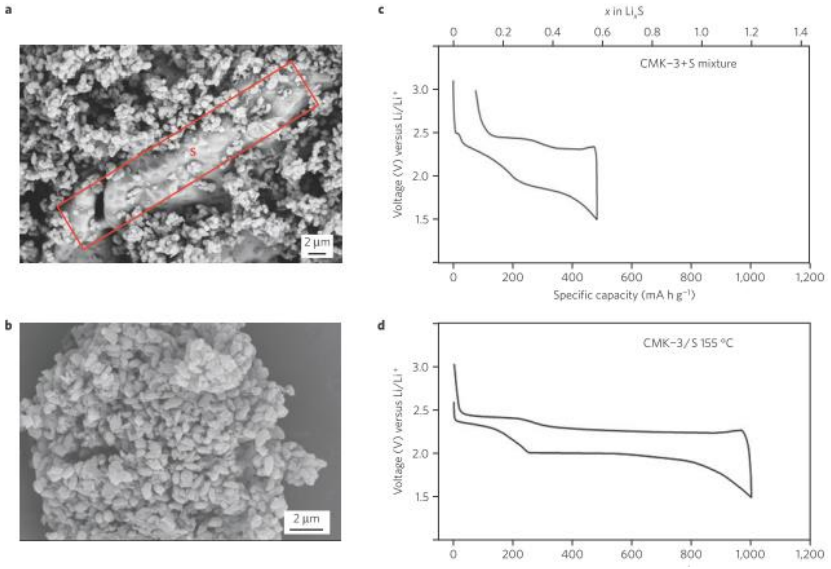

Figure 2.16 Scanning electron microscope (SEM) images of the S/CMK-3 composite (a) before and (b) after heating and (c, d) the corresponding charge/discharge voltage profiles, respectively.[74]

The most typical sulphur/carbon composite used in Li-S batteries was reported by Prof. Nazar's group (Figure 2.16).[74] Sulphur was mixed with a type of mesoporous carbon, CMK-3, and heated at 155ºC. At this temperature, the sulphur has already been melted, and the viscosity reaches its lowest value. Under capillary forces, the sulphur flows into the pores of CMK-3. Hence, the sulphur is confined in the mesopores of CMK-3 and has intimate contact with the carbon nanofibers, which significantly facilitates the electron transfer. In addition, this highly ordered structure of CMK-3 allows quick lithium-ion ingress/egress for reaction with sulphur. The confinement of sulphur in the nanopores inhibits the diffusion of the intermediate polysulphide products and decreases the dissolution of the polysulphides, thereby retaining the sulphur species inside the electrode for electrochemical reactions. Moreover, a chemical gradient was formed on the carbon surface to further retard the sulphur species. In result, a high capacity of 1320 mA h g^{-1} was obtained, compared to the typical 300−500 mA h g^{-1} using other

approaches, as previously reported by other groups. This novel "melt-diffusion" strategy has since been broadly applied for preparing a wide range of sulphur/carbon composites.[76, 77, 87-89] A new chapter has been opened in the development of advanced sulphur composite cathodes.

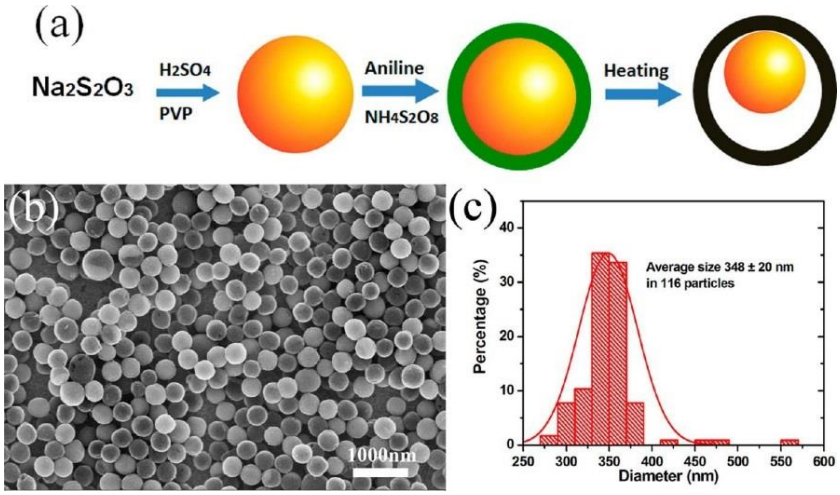

Figure 2.17 (a) Preparation of a core-shell sulphur-polyaniline composite, with the yellow balls representing sulphur, the dark green shell representing polyaniline, and the black shell representing vulcanized polyaniline. (b) SEM image of the core-shell S-polyaniline composite, and (c) the corresponding particle size distribution.[90]

Sulphur/conductive polymer composites have also been reported to be capable of stabilizing electrochemical charge/discharge cycling. Zhou et al. prepared a S-polyaniline yolk-shell composite for advanced sulphur composite cathodes (Figure 2.17).[90] The rapid capacity decay of a typical Li-S battery is due to the poor conductivity of sulphur, the polysulphide dissolution, and the volume expansion. In this yolk-shell design, the conductivity of polyaniline and the internal void space inside the polyaniline shell can alleviate all three problems. The authors compared the performances of the core-shell and yolk-shell designs and found that the latter one presents improved cycling, because the internal void space inside the polyaniline shell

accommodates the volume expansion during the sulphur lithiation process. The yolk-shell structure exhibits stable cycling over 200 cycles and a high capacity of 765 mA h g^{-1} at 0.2 C. In the case of sulphur/conductive polymer composites, a series of sulphur/polyacrylonitrile[91-95] or sulphur/polyacrylonitrile/carbon[84, 96-98] composites have been prepared by Wang et al. for advance sulphur composite cathodes. This sulphur/conductive polymer composite strategy was reviewed in 2011 by Yang et al.[99]

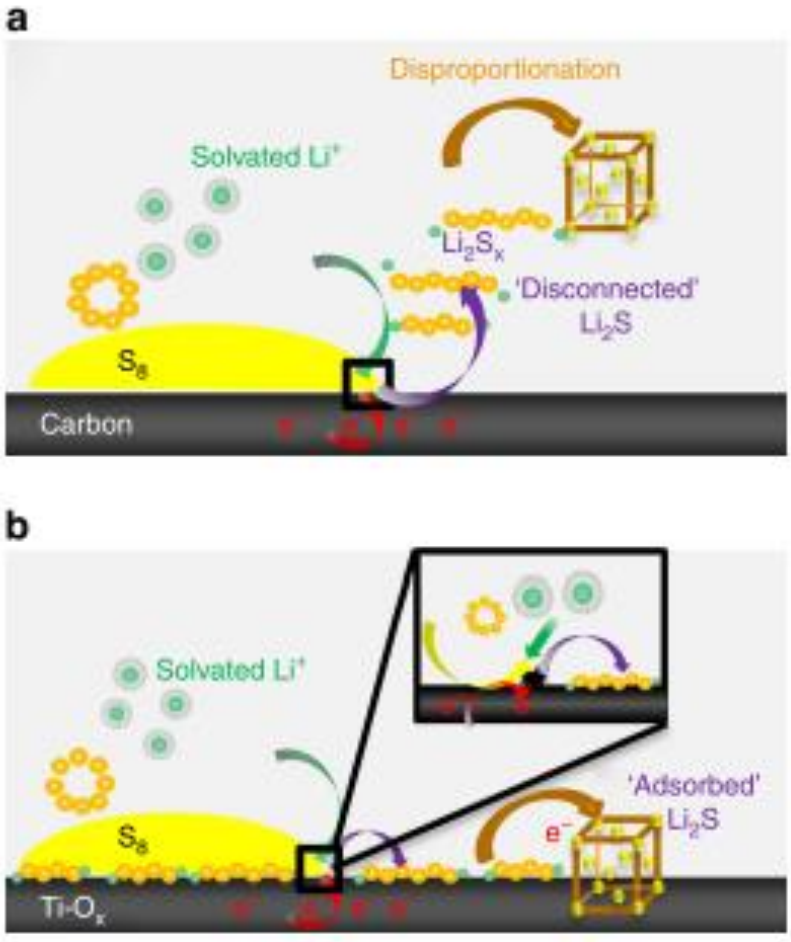

Figure 2.18 Diagram illustrating the chemical/physical processes in the reduction of sulphur on a solid surface. (a) On reduction of S_8, the polysulphides on the carbon surface are directly dissolved in the electrolyte for further electrochemical reduction. (b) On reduction of S_8, the polysulphides on the Ti_4O_7 surface are adsorbed for further reduction to the final solid product Li_2S.[85]

Recently, metal oxides have been found to be a useful type of material for forming composites with sulphur for high-performance sulphur cathodes. Compared to carbon hosts, which cannot adsorb the polysulphide intermediates or adhere to the solid Li_2S/Li_2S_2 products, metal oxides normally can form a favorable interface with Li_2S. The inherently polar metal oxides provide strong binding points for both polysulphides and Li_2S, leading to improved retention of the sulphur species for more stable cycling. Pang et al. prepared Ti_4O_7/S cathodes, which exhibited high capacity of 1070 mA h g^{-1} at intermediate rates and a long life of 500 cycles at high rates (Figure 2.18).[85] This sulphur/metal oxide composite approach has been widely applied by various research groups and proved successful for retaining the sulphur species in the electrode and achieving stable cycling.[86, 100, 101]

2.2.3 Polymer binders for sulphur cathodes

Lithium-sulphur (Li-S) batteries utilize sulphur as the cathode and lithium metal foil as the anode. Although the main attention has been given to the cathode, there are some interesting research papers on the binder. The choice of binder materials for Li-S batteries has been dominated by two kinds of polymers: polyethylene oxide (PEO) and poly(vinylidene difluoride) (PVDF). In the earlier stage of research on Li-S batteries, PEO was widely used as the binder. Cheon et al.[102] compared sulphur cathodes with different amounts (8%, 13% and 18%) of PEO as the binder and found that, with the binder taking up a larger weight percentage in the cathode, the cycling performance improved correspondingly. Researchers have made efforts to find a better binder than PEO, and two successful alternatives were gelatin[103-105] and

poly(acrylamide-co-diallyldimethylammonium chloride) (AMAC)[106]. Regarding the composite binders carboxymethyl cellulose (CMC) and styrene butadiene rubber (SBR), there have been two papers reporting opposite results, with Rao et al.[107] claiming that CMC + SBR is better than PEO, while Lacey et al.[108] reported that PEO is better than CMC + SBR. Concerning these two opposite results, the factors that contribute might be the differences in various aspects: the sulphur materials (carbon nanofiber (CNF)-S composite vs. pure sulphur), the current collectors (carbon-coated Al foil vs. uncoated Al foil), the electrolytes (1 M kg^{-1} lithium bis(trifluoromethylsulphonyl)imide (LiTFSI) in N-methyl-N-butylpyrrolidinium bis(trifluoromethaneulphonyl)imide / poly(ethylene glycol) dimthyl ether vs. 1 M LiTFSI and 0.25 M $LiNO_3$ in 1, 2-dimethoxyethane/1,3-dioxolane), and the electrode preparation methods (unknown vs. ball milling for 2 h).

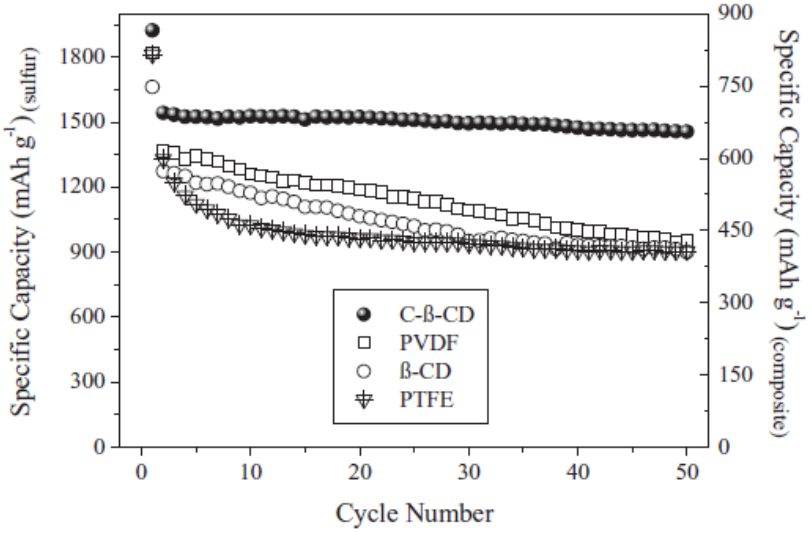

Figure 2.19 Cycling performance of polyacrylonitrile (PAN)-S composite cathode with PTFE, β-CD, PVDF and C-β-CD (carbonyl β-CD prepared through treatment of β-CD with H_2O_2) at 0.2 C.[109]

Later, PVDF became the mainstream binder for Li-S batteries. Nevertheless, when PVDF is applied as the binder, the toxic dispersant N-methyl-2-pyrrolidone (NMP) and the longer heating time that are needed for the electrodes are two major disadvantages. Therefore, researchers have been searching for environmentally friendly water soluble binders which can contribute to better cell performance. Various materials have been proved to be better choices than PVDF, and they are CMC + SBR[110], polyacrylic acid (PAA)[111], Na-alginate[112] and poly(vinylpyrrolidone) (PVP)[113]. A recent work[114] also demonstrated the excellent performance of Li-S batteries with PAA as the binder. Through ball milling with polydopamine (PD), sulphur, and carboxylic-acid-functionalized multiwall carbon nanotube (MWCNT-COOH), covalent bonds that were formed through crosslinking between PD/PAA and PD/MWCNT-COOH demonstrated a strong binding effect with sulphur, and good cycling performance in the Li-S batteries was achieved.

Schneider et al[115] applied three kinds of water soluble binders (i.e. Nafion®, Teflon®, and polyacrylonitrile-CMC) in Li-S batteries and demonstrated them to be promising environmentally friendly binders. Carbonyl β-cyclodextrin (C-β-CD)[109], which was prepared through treatment of β-cyclodextrin (β-CD) with H_2O_2, can be a better binder in Li-S batteries compared with PVDF, polytetrafluroethylene (PTFE), and β-CD.

2.2.4 Functional separators for Li-S batteries

Sulphur has been considered a promising candidate as a next-generation cathode material due to its high capacity (1675 mA h g^{-1}), abundance, and low cost. Typically, the sulphur cathode is a composite between sulphur and a conductive material such as

carbon, a conductive polymer, or a metal oxide.[116] The sulphur cathode can be coupled with lithium metal or sodium metal anodes to construct Li-S or Na-S batteries.

The elemental sulphur in the sulphur cathode of an Li-S battery is reduced to solid Li_2S/Li_2S_2 via intermediate polysulphide products of Li_2S_x ($4 \leq x \leq 8$). The lithium polysulphide is soluble in the electrolyte, resulting in not only the loss of active material from the cathode, but also diffusion of the species to the lithium metal anode to form an unstable solid electrolyte interphase on the lithium surface. An unwanted shuttling problem is also produced, i.e., the dissolved sulphur species with higher oxidation state migrate to the anode for reduction in the charge stage and then return back to the cathode for re-oxidation, and so on.

The separator, which is located between the electrodes and provides channels for the ion transport, can be expected to play a critical role in blocking the polysulphide anions from diffusing to the anode side. Therefore, an ion-selective membrane allowing the transport of lithium ions and rejecting the polysulphide anions is very much needed for a stable Li-S or room-temperature Na-S battery.

One important ion-selective polymer material is Nafion, a commercial product developed and produced by the DuPont Company. Nafion is synthesized by copolymerization of tetrafluoroethylene (TFE) and a perfluorinated vinyl ether comonomer. In 2012, Li-Nafion film was first reported as a functional separator for Li-S cells (Figure 2.20).[117] The Nafion-212 film was purchased from the Dupont Company and ion exchanged with lithium ions in a LiOH solution (solvent: H_2O/ethanol) at 80°C; the residual salt was then flushed away using boiling deionized water. The successful preparation of Li-Nafion was characterized by Fourier transform infrared spectroscopy (FTIR), which showed the disappearance of the peak at 924 cm^{-1}

for S-OH stretching and the appearance of a peak at 1630 cm^{-1} related to the lithium ions. By applying the steady-state current method, the transference number of Li^+ was measured to be 0.986, indicating high permeability for Li^+ and low permeability against anions. Combined with a commercial Sulphur cathode and ether-based electrolyte, both the cycling stability and the Coulombic efficiency were significantly improved (Figure 2.20). The enhanced cycling performance resulted from the polysulphide-blocking property of the Li-Nafion film, as proved by the smooth surface of the lithium anode after 50 cycles, while the battery with the conventional separator showed much more corrosion and cracks.

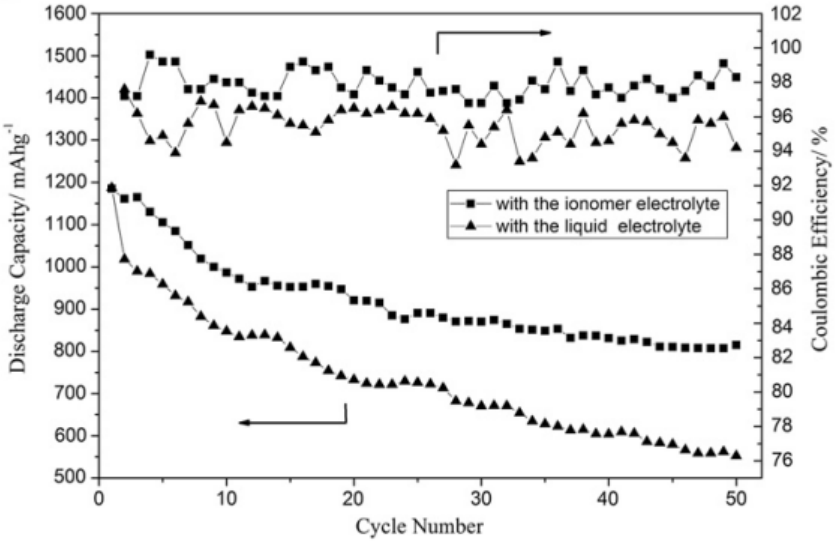

Figure 2.20 Improved cycling stability and Coulombic efficiency of the Li-S battery with the Nafion separator.

In 2014, Bauer et al. reported a Li-Nafion coating on polyethylene separator for application in Li-S batteries. Nafion was first drop coated on a polyolefin substrate and then transformed to Li-Nafion by ion exchange in LiOH solution. The authors investigated the influence of the coating density and found that 0.25 mg cm^{-2} of Li-Nafion coating resulted in significantly improved rate performance and charge

efficiency compared to the pristine polyolefin separator. Free-standing Li-Nafion membrane was also studied as a control separator, which was found to cause a voltage drop of approximately 0.2 V, in agreement with the results of a former similar work[118]. That is, a thin layer of Li-Nafion coated on the polyolefin separator can enhance the discharge voltage, compared to a lithiated thick commercial Nafion membrane. To demonstrate the polysulphide-blocking behavior of the Nafion-coated separator, a diffusion experiment was carried out (Figure 2.21). It can be clearly seen that the pristine polyolefin separator allows the transport of the polysulphide anions, while the Li-Nafion coated separator successfully suppresses the polysulphide diffusion.

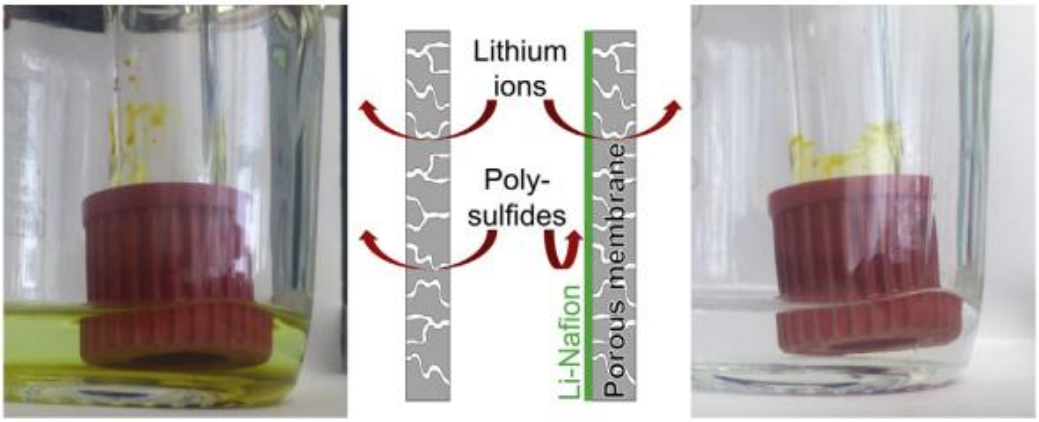

Figure 2.21 The Nafion coating on a porous membrane blocks the polysulphide anions and allows the transport of lithium ions, as shown by the visual experiment.[117]

In 2014, more research on Nafion-coated porous polyolefin substrate as the separator for Li-S batteries was reported by Huang et al.[119] Unlike the former works on applying the lithiated form of the Nafion membrane, here, the protonated Nafion was directly utilized, and no further ion exchange with lithium salts was conducted. A coating of 0.7 mg cm^{-2} was found to be the optimal choice among three different amounts (0.7, 0.15 and 3.5 mg cm^{-2}), and the battery with this separator exhibited a long life of 500 cycles and greatly improved Coulombic efficiency. With the lower loading of 0.15 mg cm^{-2},

however, it was impossible to form a complete compact film on the porous substrate, and there was almost no effect on the electrochemical performance, while the higher loading of 3.5 mg cm^{-2} resulted in severe polarization and degraded cell performance. In terms of the underlying mechanism, the authors propose that the sulphonate groups form channels with dimensions of several nanometers. Owing to the Coulombic interactions, the channels allow the transport of cations (e.g., Li^+) by ion hopping and reject the anions (e.g., polysulphide anions). This cation selectivity of the Nafion-coated separator greatly retards the diffusion of the polysulphides, which is demonstrated by a visual experiment, and hence, leads to significantly improved cycling stability (Figure 2.22).

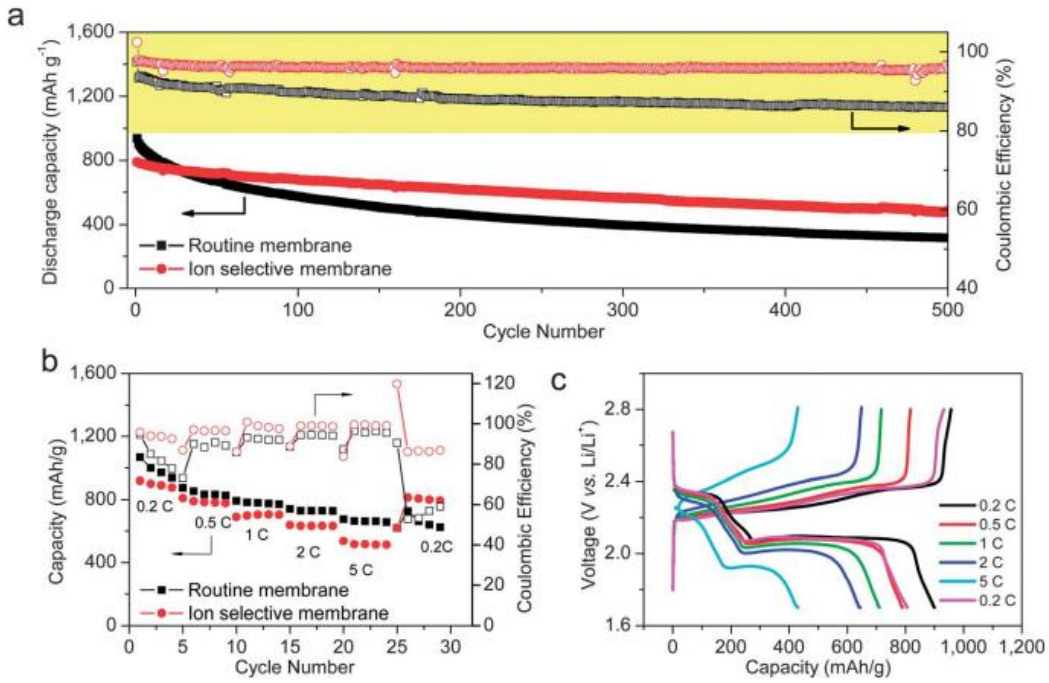

Figure 2.22 (a) Improved cycling stability and (b, c) rate capability of the separator coated with Nafion.[119]

The polysulphide-blocking property of the Nafion-based separator was also proved in an in-operando imaging experiment in Li-S cells.[120] Based on the characteristic color of

the intermediate products of polysulphides in the charge/discharge process in Li-S batteries, an in-operando imaging setup was applied to directly visualize the temporal and spatial distribution of polysulphides, in order to obtain detailed evidence of the electrochemical reactions in Li-S cells. Compared with the pristine polyolefin separator, the Nafion coated polyolefin separator shows a significant blocking effect on the polysulphides, which can be easily understood from the change in the grey level of the electrolyte in different degrees of charge/discharge using the in-operando Li-S cell design.

Nafion, whether in its protonated or lithiated form, is selectively permeable for cations and against anions, owing to the Coulombic interaction with the inherent negative charge borne by the sulphonate groups along the perfluorinated ionomer backbone. The successful application of the Nafion-based separator in Li-S batteries can be ascribed to its rejection property against the soluble polysulphide anions, which are the intermediate products of the sulphur cathode during charge and discharge. In the following part, a range of other functional separators with selective permeability are presented for application in Li-S batteries.

Following their own research on Li-Nafion[118], Jin et al. developed another perfluorinated ionomer polymer, lithium perfluorinated sulphonyl dicyanomethide (Li-PFSD), as a functional separator for application in Li-S batteries (Figure 2.23). [121] The Li-PFSD was prepared by adding the perfluorinated sulphonyl fluoride (PFSF) precursor into a mixed solution of lithium hydride (LiH) and malononitrile ($CH_2(CN)_2$).[122] The Li-PFSD membrane was prepared by the solution-casting method. The as-prepared Li-PFSD membrane possesses high ionic conductivity (0.00012 S cm^{-1}) and has an excellent transference number (0.958), both of which are evidently improved

compared to those parameters for the conventional polyolefin or poly(vinylidenefluoride-hexafluoropropylene) (P(VDF-HFP)) membrane. Although the three separators show similar initial capacities, the cell with Li-PFSD retains the highest capacity (830 mA h g^{-1}) after 100 cycles, and the cells with polyolefin and the P(VDF-HFP) separators exhibited much lower capacities of 543 and 509 mA h g^{-1}, respectively. Moreover, the Li-PFSD separator possesses much higher Coulombic efficiency than the control separators. In a similar way to their former work, scanning electron microscope (SEM) images of the lithium metal anodes after cycling were obtained to explain the polysulphide-retarding behavior of the Li-PFSD membrane and the significantly enhanced Li-S battery performance.

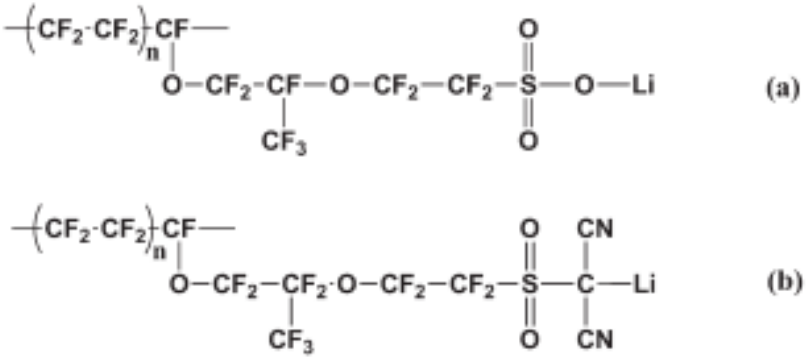

Figure 2.23 Molecular structures of (a) Li-Nafion and (b) Li-PFSD.[121]

In 2015, Li et al. described a polymer with intrinsic microporosity (PIM) as a functional membrane separator for Li-S batteries.[123] The PIM is a non-networked ladder polymer that is mechanically and thermally robust. It was solution-casted into a flexible free-standing membrane (thickness: 10 μm) for utilization as separator. The specific area of the polymer was around 800 m^2 g^{-1} with a nominal pore size of 0.77 nm, which was ideal for selectively blocking polysulphide anions in the ether solvent of diglyme, triglyme, or tetraglyme. The reason is that the molecular dynamics (MD) simulations of

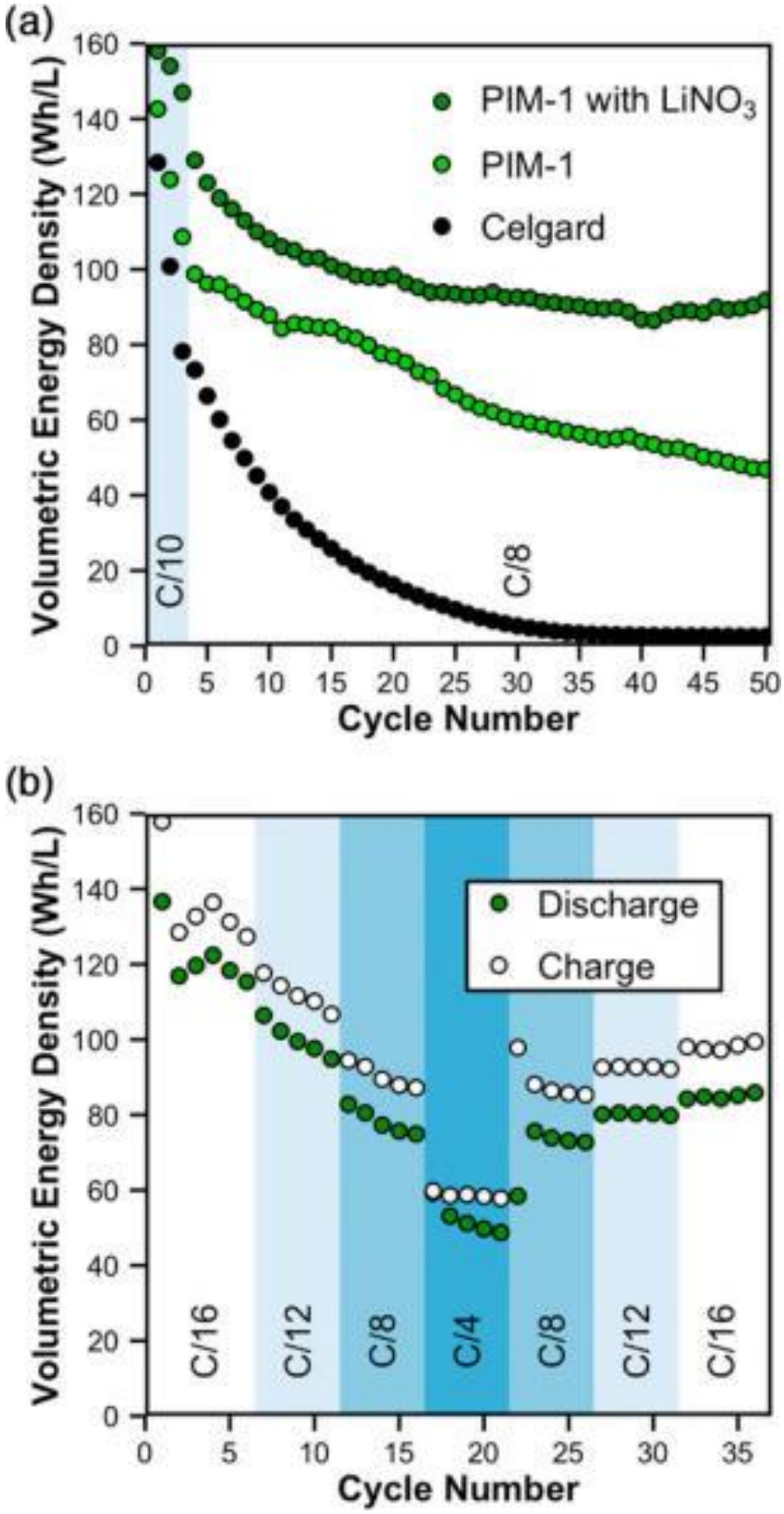

Figure 2.24 Significantly improved cycling stability (a) and very good rate performance (b) of the Li-S battery with the PIM separator.[123]

the radii of gyration of the solvated polysulphide anions resulted in values between 1.2 and 1.7 nm, which is larger than the pore size of the PIM. The nominal pore size (17 nm) of the polyolefin membrane is far too large, however, for preventing the migration of polysulphide anions through the separator. This remarkable difference was investigated by a membrane crossover experiment, which showed a 500 times improved polysulphide blocking ability of the PIM membrane compared to the polyolefin membrane. Given the impressive polysulphide blocking behavior, the PIM membrane was employed as the separator in a Li-S flow battery, which showed very significantly higher cycling stability than the one with the mesoporous polyolefin separator (Figure 2.24).

Ma et al. prepared a cation selective membrane separator based on a cross-linked poly (ethylene glycol) (PEG) network for application in Li-S batteries (Figure 2.25).[124] To enable the function of ion selectivity, sulphonate groups were grafted onto the PEG network by copolymerizing poly (ethylene glycol) dimethacrylate (PEGDMA) and vinylsulphonic acid salt (VS) under ultraviolet radiation. The as-synthesized membrane facilitates electrolyte wetting and lithium ion transport, but it prevents the migration of polysulphide anions due to both the small tortuous pores between the PEG molecules and the electrostatic repulsion of the polysulphide anions by the pendant negatively charged sulphonate groups. The transference number for lithium ions is approximately 0.99, and the blocking effect for polysulphides was visually observed, demonstrating the impressive ion selective transport behavior of the new membrane material. Without the need for $LiNO_3$ additive in the electrolyte that is normally used for protecting the lithium anode, the Li-S battery employing this novel membrane demonstrated highly stable cycling.

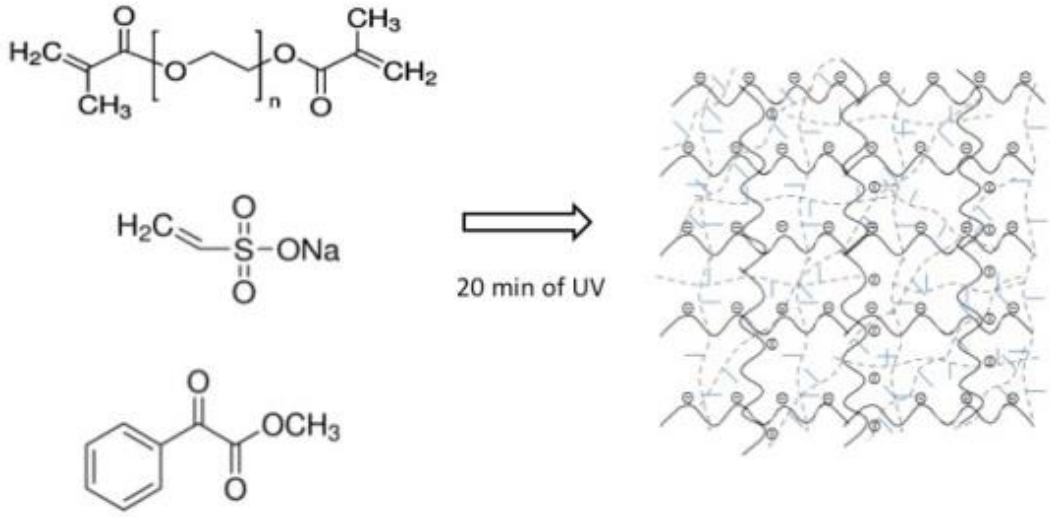

Figure 2.25 Preparation process for cross-linked PEG membranes with sulphonate groups.[124]

Polymer materials, including Nafion-based, Li-PFSD, PIM, and PEG-based, have been demonstrated as functional separators for Li-S batteries. Other materials that have been used as the coating layer or as independent membranes for the Li-S battery separator to effectively retard the crossover of the soluble polysulphides will be presented, including V_2O_5, graphene oxide (GO), metal organic framework (MOF), and lithium superionic conductor (LISICON).

In 2014, Li et al. employed a V_2O_5-based separator for Li-S batteries, exploiting V_2O_5 as solid-state lithium-ion conductor and polysulphide anion barrier.[125] In order to supply sufficient lithium ion transport through the separator, a thin V_2O_5 layer (1 μm thick) was coated on a polyolefin separator substrate, because the lithium-ion diffusion coefficient of V_2O_5 is inferior to that of the liquid electrolyte (~3×10^{-12} vs. 4×10^{-9} cm^2 s^{-1}). Moreover, to achieve a well-adhered crack-free V_2O_5 coating to strongly prevent the crossover of polysulphide anions, a V_2O_5 sol-gel was coated on the polyolefin separator with a surfactant coating. The authors investigated a series of experimental conditions

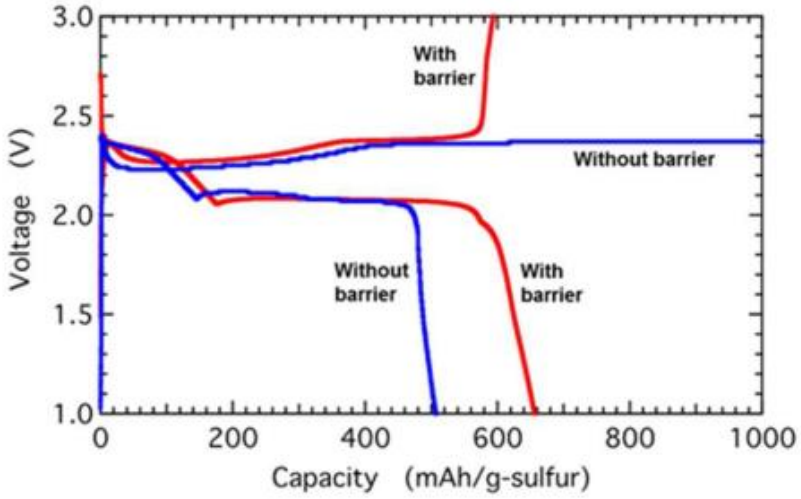

Figure 2.26 Charge/discharge profiles of the Li-S cells with and without the V_2O_5 barrier, indicating that the one without the V_2O_5 barrier cannot be charged to 3 V while the one with the barrier can.[125]

and successfully obtained a complete, dense, nonporous, and pinhole free coating layer. The V_2O_5-coated separator was demonstrated with a S/C composite cathode in a pouch cell. The coated separator exhibited significantly enhanced charge/discharge properties (Figure 2.26). Under low rate, a capacity of ~800 mA h g^{-1} was attained, almost without capacity fade compared to the initial cycle, over 300 cycles over around 1 year.

In 2016, Bai et al. prepared a MOF/graphene oxide (GO) composite membrane separator for Li-S batteries.[126] An in-situ approach was applied for the synthesis of the MOF material, identified as HKUST-1, in the process of vacuum-filtration of the MOF/GO membrane. The MOF/GO composite possesses a microporous nature with pore size of 0.9 nm, significantly smaller than the diameters of lithium polysulphides. In this regard, the MOF/GO separator can effectively suppress the migration of polysulphides to the anode side, while it does not affect the lithium ion transfer. The suppression of polysulphides was visually verified by a permeation experiment. In terms of the battery performance, a long life of 1500 cycles was achieved,

demonstrating the excellent polysulphide-suppression capability of this functional separator (Figure 2.27).

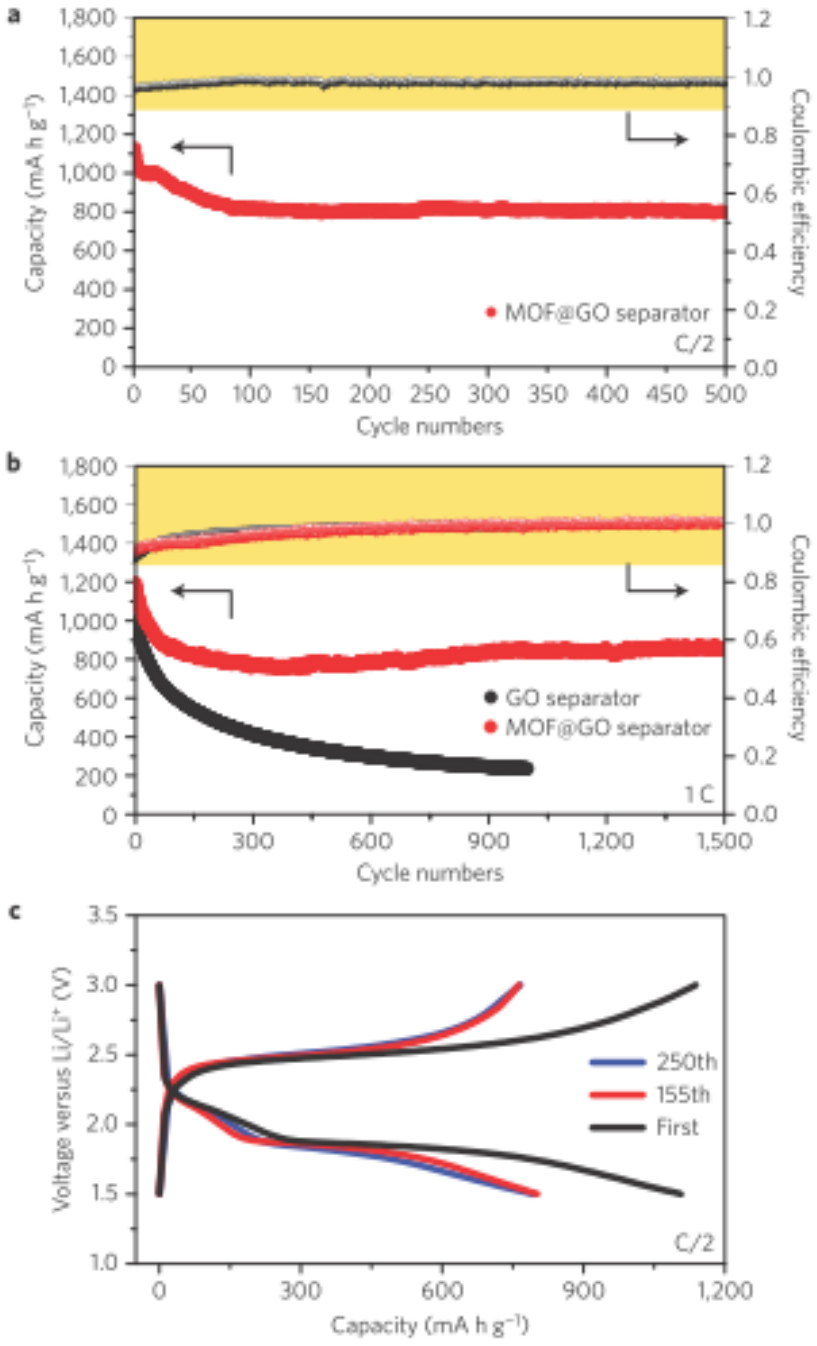

Figure 2.27 (a, b, c) Electrochemical performance of the Li-S battery with a MOF@GO separator.[126]

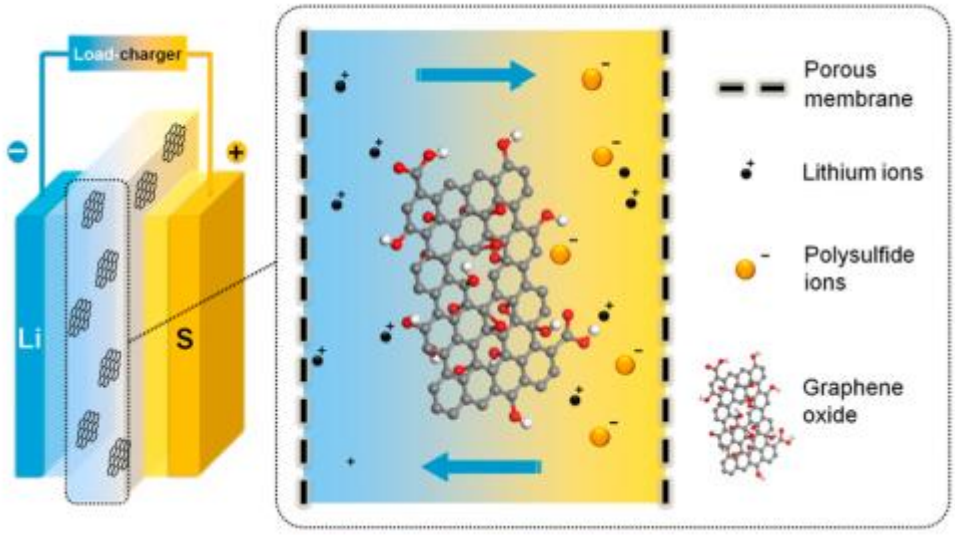

Figure 2.28 Schematic illustration of GO membrane as the separator in Li-S batteries.[127]

Reconstructed GO membranes prepared by some specific methods such as vacuum filtration possess numerous nanochannels between the GO sheets, which bear negative charge originating from functional groups such as carboxylic acid and phenolic hydroxyl.[128, 129] The typical dimension of the nanochannels (1 nm) is comparable to the Debye length, facilitating the transport of cations and blocking the migration of anions. A permselective GO membrane was employed by Huang et al. for application as a thin coating layer on a porous polyolefin separator to improve the cycling stability and inhibit the self-discharge of Li-S batteries (Figure 2.28).[127] Compared to the pristine separator, the GO membrane improved the Coulombic efficiency from 67 – 75% to 95 – 98% at 0.1 C, reduced the capacity decay rate from 0.49 to 0.23% per cycle, and enhanced the stability of the open circuit voltage from 5 h to 30 h. Following their work on the GO separator, Zhuang et al. carried out a proof-of-concept experiment by coating a GO/Nafion composite layer on a porous polyethylene (PP) substrate as the separator for Li-S batteries.[130] The ultrathin GO layer blocks the macropores of the PP substrate and functions as both a physical and an electrostatic barrier against polysulphide

shuttling. The dense layer of Nafion on top, together with the GO layer, retards the polysulphide migration through the separator, endowing the Li-S battery with high Coulombic efficiency and excellent cycling stability.

Lithium superionic conductors (LISICONs), although typically used as the electrolyte separator for solid-state lithium-ion batteries, can also be applied in liquid-electrolyte Li-S batteries as the separator due to their pronounced lithium-ion conductivity and polysulphide-blocking ability. To utilize LISICON as the separator in a liquid-electrolyte Li-S battery, however, the applied cell configuration can no longer be the coin cell but needs a special design. The cell is composed of two glass cylinders with the LISICON membrane inserted between them. A solution or suspension of sulphur species (S, Li_2S, or lithium polysulphide) is injected into the cathodic compartment and an organic electrolyte into the anodic part. The lithium anode is fixed at the bottom of the anodic cylinder. Up to the present, researchers normally have employed a commercial LISICON film of $Li_{1+x+y}Al_xTi_{2-x}Si_yP_{3-y}O_{12}$ (LATP). Although the thick and fragile LATP might have impaired the battery performance to some extent, the works applying LATP separator and the new cell configuration have opened a new avenue for the development of high-energy Li-S batteries. Further advances in this Li-S battery technology require exploration of LISICON films with higher ionic conductivity, thinner thickness, improved flexibility, and more robustness. To illustrate this new Li-S battery technology enabled by LATP film as the separator, two examples are presented in the following paragraphs.

Li et al. described an aqueous Li-S battery with an aqueous solution of Li_2S_4 as the catholyte, lithium metal as the anode, and LATP as the separator (Figure 2.29).[131] The lithium ion conductive LATP separator suppresses the polysulphide shuttling, which is

a critical feature for the cycling stability. The cell configuration is (–) Cu mesh / Li metal / organic electrolyte // LATP membrane // aqueous Li_2S_4 alkalic catholyte l CoS/brass mesh (+). The aqueous Li_2S_4 catholyte can achieve a high concentration (maximum of ~2.3 M), and it therefore enables a fast Li_2S_4/Li_2S redox reaction compared to solid electrolytes and has a high specific energy density of ~654 W h kg^{-1}. Furthermore, solid sulphur was dissolved in the aqueous Li_2S_4 solution as the catholyte, increasing the reversible capacity from 1030 to 1202 mA h g^{-1}.

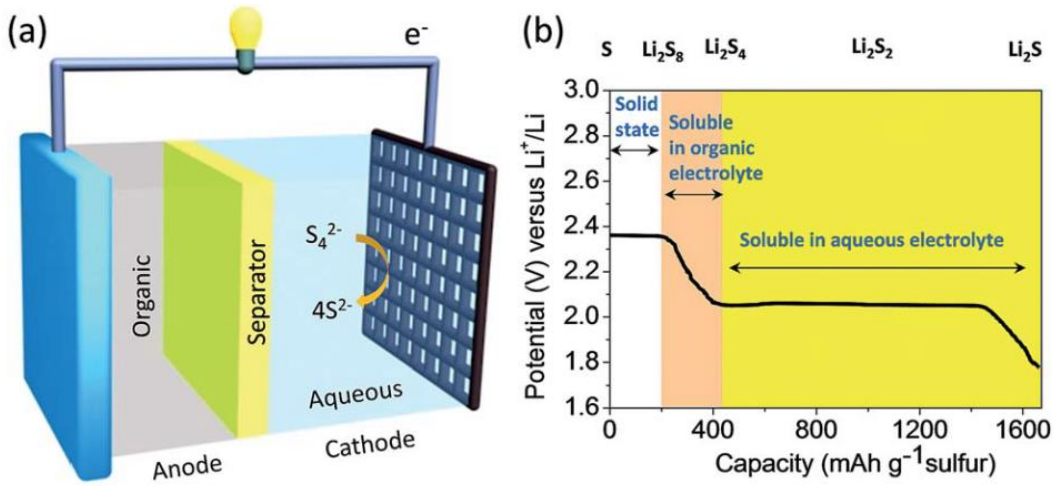

Figure 2.29 (a) Schematic illustration of an aqueous cathode with short-chain polysulphides for Li-S batteries. (b) Typical discharge voltage profile of a conventional Li-S battery showing a two-step reaction producing long-chain polysulphides that are soluble in organic electrolyte and short-chain polysulphides that are soluble in aqueous electrolyte.[131]

Wang et al. prepared a Li_2S suspension in 1 M $LiClO_4$/tetrahydrofuran (THF) as the catholyte for the Li-S battery with a LATP separator (Figure 2.30).[132, 133] The cell configuration is (–) Cu foil / Li metal / carbonate-based organic electrolyte // LATP membrane // Li_2S / $LiClO_4$/THF catholyte / Super P carbon / Ti foil (+). Because the fully lithiated Li_2S was applied as the cathode material, the lithium metal anode could be replaced by various lithium-free anode materials; two examples, aluminum and

graphite, were given in this work. This flexibility in choosing the electrolyte and the anode material paves the way for developing the lithium-ion sulphur battery into a practical energy storage technology.

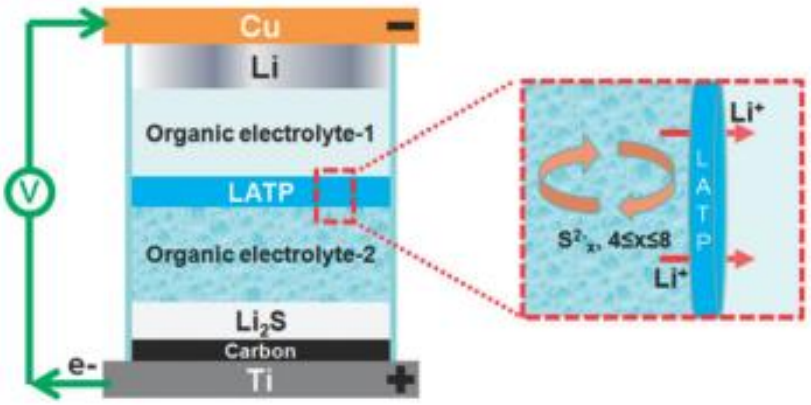

Figure 2.30 Cell configuration of the Li-S battery based on a LATP separator, dissolved Li_2S cathode and dual-phase electrolyte.[132]

2.2.5 New Li-S cell configuration with an interlayer

The most serious problem in Li-S batteries is the polysulphide shuttling problem, which causes low utilization of the active material and quick capacity decay. Manthiram's group invented a novel approach by inserting a microporous carbon layer between the sulphur cathode and the separator (Figure. 2.31).[134] The insertion of the carbon interlayer significantly decreases the charge transfer resistance and plays the role of an upper current collector for improving the utilization of the active material. His group later utilized the same strategy by using a multiwall carbon nanotube (MWCNT) interlayer[135] and a treated commercial Toray carbon interlayer[136], both of which resulted in pronounced high cycling stability and lower charge transfer resistance.

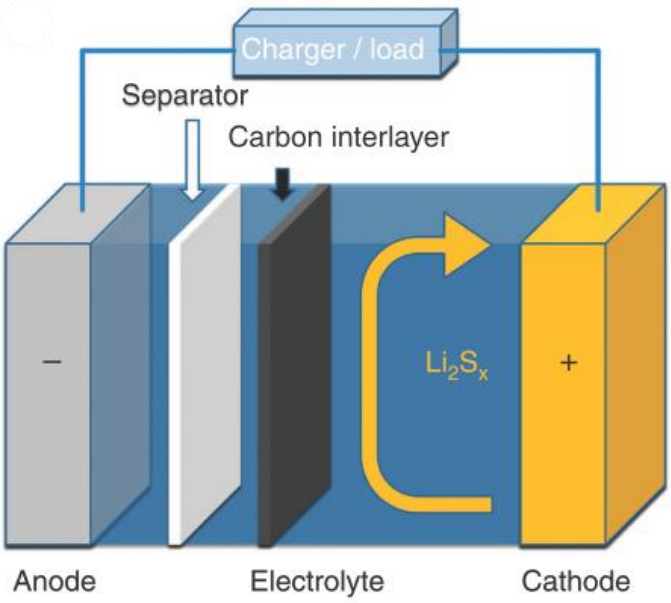

Figure 2.31 A new Li-S cell configuration with a microporous carbon interlayer inserted between the cathode and the separator.[134]

In 2015, Yu et al. reported a CNF interlayer for the Li-S battery, as well as a free-standing Li-Nafion membrane as the separator and lithium polysulphide catholyte (Figure 2.32).[137] This work combines the strategies of using a functional separator and using an interlayer. The lithium polysulphide catholyte was prepared by adding a certain amount of lithium polysulphide, which was synthesized by the reaction between Li_2S and S, into a blank ether-based electrolyte to obtain a catholyte with the desired concentration of sulphur. The catholyte was then infused into carbon nanofiber (CNF) paper to form a cell configuration of Li//Li-Nafion//CNF/activated carbon-lithium polysulphide. In addition, compared to the lithiation process for the protonated Nafion membrane in aqueous solution at 80°C, in this work, the Nafion membrane was immersed in a common liquid electrolyte for Li-S batteries for 7 days at room temperature to allow the ion exchange to take place and for some of the liquid electrolyte to be absorbed. This as-obtained Li-Nafion membrane was directly utilized

in the cell and greatly improved cycling stability was attained, compared to the cell with the porous polyolefin separator.

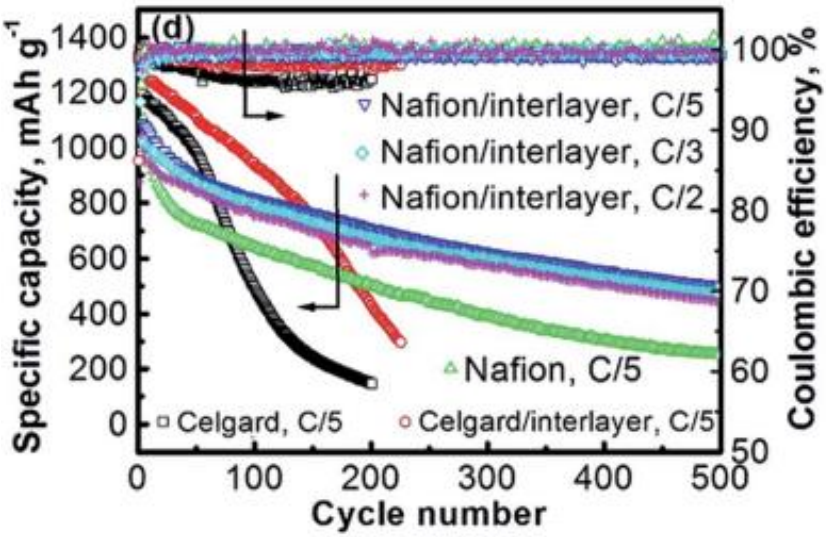

Figure 2.32 Cycling stability of Li-S batteries with Nafion separator and carbon nanotube (CNT) interlayer.[137]

2.2.6 Electrolytes for Li-S batteries

The electrolytes applied in Li-S batteries are normally different from those in LIBs.[63, 64, 138-141] In LIBs, the typical electrolyte is prepared by dissolving a lithium salt, $LiPF_6$ or $LiClO_4$, in carbonate-based mixed solvents. In contrast, the most commonly used lithium salt in Li-S batteries is LiTFSI and the solvent is a mixture of 1,3-dioxolane (*DOL*) and dimethoxyethane (*DME*), both of which are ethers. The reason for choosing ether-based electrolytes rather than carbonate-based electrolytes is that the carbonates can react with the dissolved polysulphides, which causes quick consumption of the active material and short cycle life. When the sulphur is confined in nanopores smaller than 0.5 nm, however, the soluble long-chain polysulphides will not form, and in this

case, the carbonate-based electrolytes can be used and normally will result in better electrochemical performance.[142-144] Some typical Li salts and solvents are listed in Figures 2.33 and 2.34, respectively.

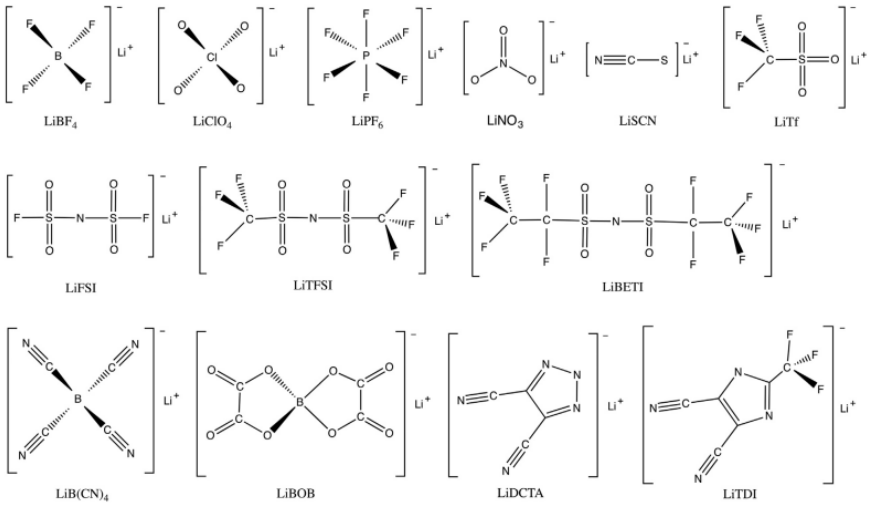

Figure 2.33 Lithium salts applied in Li-S battery electrolytes.[64]

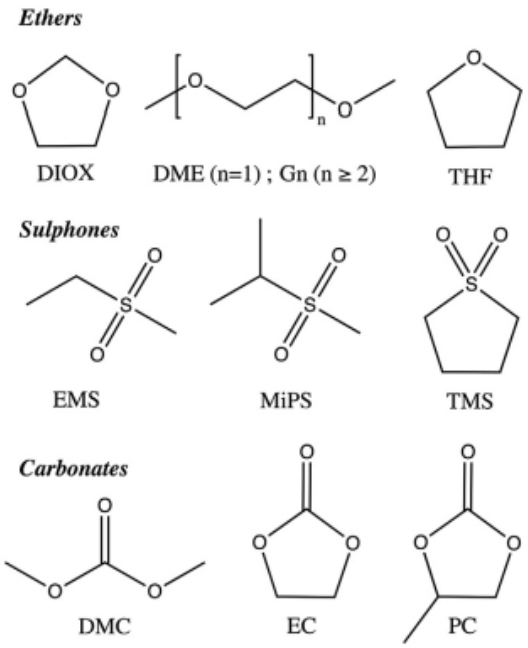

Figure 2.34 Organic solvents for use in Li-S battery electrolytes.[64]

2.3 Lithium-organic batteries

2.3.1 General background and brief history

Electroactive organic molecules as cathode materials have regained researchers' interest in recent years, after being overwhelmed by $LiCoO_2$ and similar intercalation cathode materials for decades.[14, 16, 28, 145-149] Li-organic batteries, like Li-S and Li-O_2 batteries, are not a new concept but have a long history dating back to 1969, almost half a century ago. With the intensive research and development that has been conducted both in the academy and in industry, the insertion cathode materials have gradually met their intrinsic limits in terms of capacity and energy density. In addition, the pressure on the environment and resources has become increasingly larger due to the great demand for the metal oxide ores. Therefore, greater attention has been paid to next-generation cathode materials with high energy density and a low ecological footprint. Organic molecules, owing to merits such as cost-effectiveness, sustainability, chemical tenability, and environmental friendliness,[150-153] have been considered as a promising alternative to the intercalation cathode materials (Figure 2.35).

In particular, electroactive organic molecules originating from biomass could open up a new chapter for the next-generation lithium-based batteries (Figure 2.36). Organic molecules have been widely applied in the semiconducting field, in transistors, solar cells, and light-emitting diodes. The development of Li-organic batteries could be a historic chance for the penetration of organic molecules into the energy storage industry. Despite all their significant advantages in terms of low ecological footprint and environmental friendliness, it should be noted that the organic molecules could be

limited by their noticeable solubility in electrolytes, low specific gravity, and thermal stability.

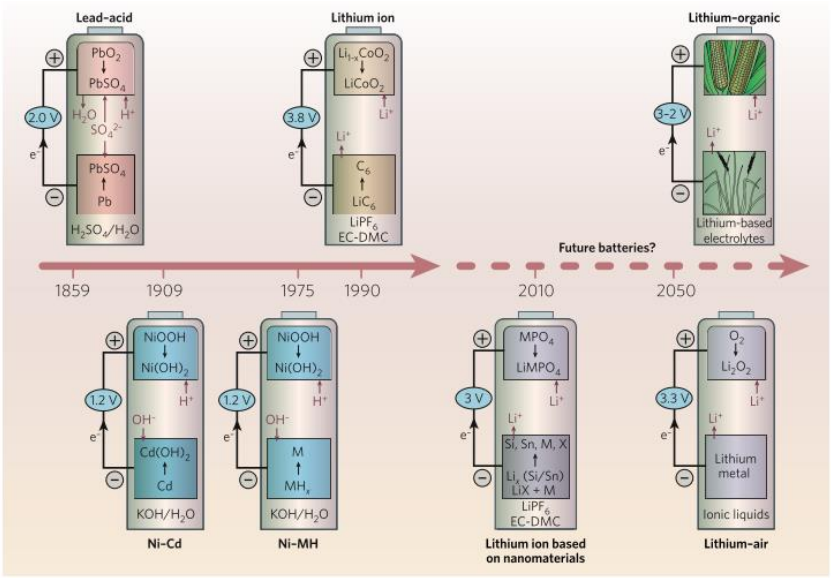

Figure 2.35 Battery chemistry from lead-acid batteries to LIBs and then next-generation batteries such as lithium-organic batteries.[16]

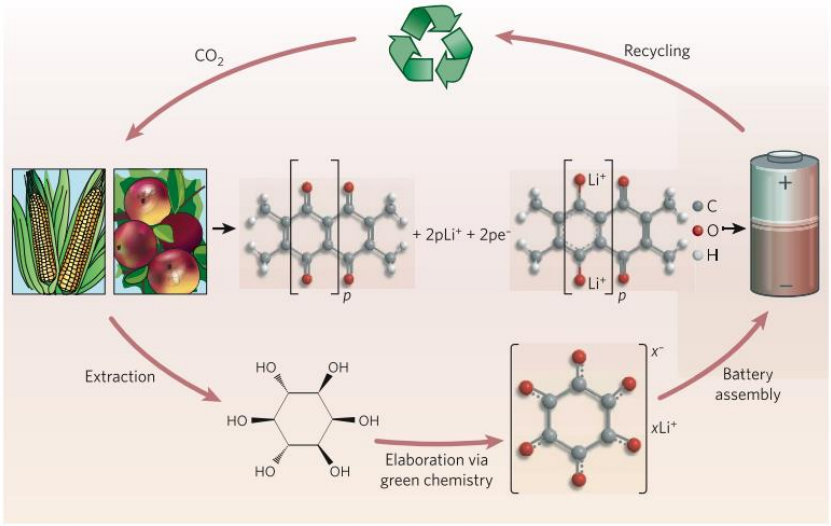

Figure 2.36 The circulation of electroactive organic molecules from biomass to application in batteries.[16]

2.3.2 Basic principles and concepts

The basic requirement for an electrode material is that it can undergo reversible redox reactions. For inorganic electrode materials, the valence of the transition metal normally changes during charge/discharge processes. With respect to the organic molecules, the charge state of the electroactive organic groups or moieties changes in the lithiation/delithiation processes.[145]

According to the different redox reaction mechanisms, the electroactive organic molecules can be divided into three categories (Figure 2.37).[154] Those transforming between neutral and anion states can be classified as *n*-type and those between neutral and positive states as *p*-type. The other type consists of the bipolar organics, for which the neutral state can be either oxidized to the positive state or the negative state. The anions can be ClO_4^-, PF_6^-, BF_4^-, or $TFSI^-$ in nonaqueous electrolytes or Cl^- and NO_3^- in aqueous electrolytes.

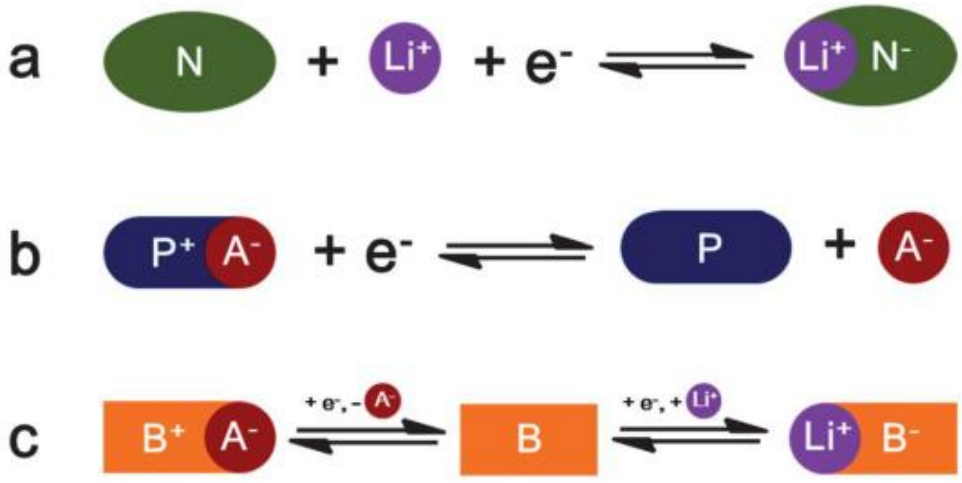

Figure 2.37 Redox chemistries of three types of electroactive organics: (a) *n*-type; (b) *p*-type and (c) bipolar. A^- denotes an anion in the electrolyte.[154]

In the Li-organic battery, the cathode material is an electroactive organic molecule, and the anode material is lithium metal. In this regard, the electroactive organic molecules should have redox voltage belonging to the cathode area, at least > 2V vs. Li^+/Li. One typical type of organic cathode consists of molecules with carbonyl groups. As can be seen below, the redox reactions of two typical carbonyls, anthraquinone (AQ) and perylenetetracarboxylic dianhydride (PTCDA) undergo two steps. The reason is that there are two carbonyl groups being reduced in the lithiation process with an intermediate state with one carbonyl group reduced.

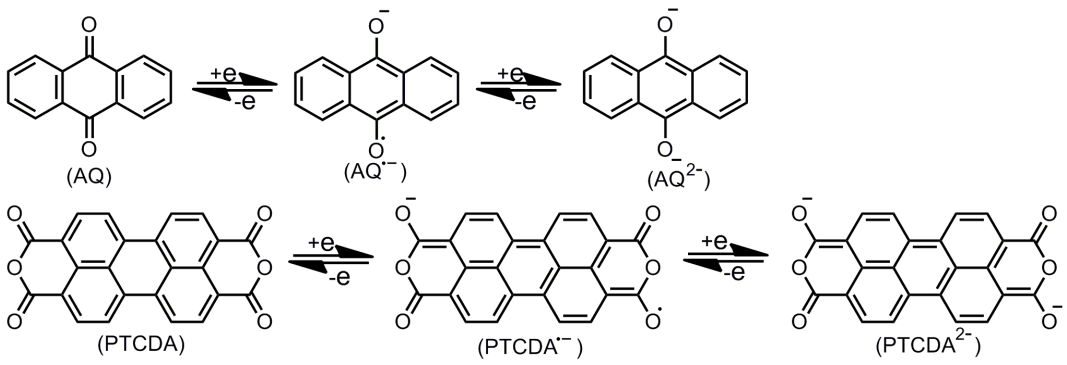

Figure 2.38 Reversible electrochemical reaction of two typical carbonyl organic molecules, AQ and PTCDA.

2.3.3 Organic cathodes

In the Li-organic batteries, most of the focus has been on the development of new organic species. A wide range of organic molecules or polymers have been applied as the electrode materials in Li-organic batteries, including organosulphur compounds, organic free radical compounds, organic carbonyl compounds, conducting polymers, non-conjugated redox polymers, and layered organic compounds.[151, 152, 155-160]

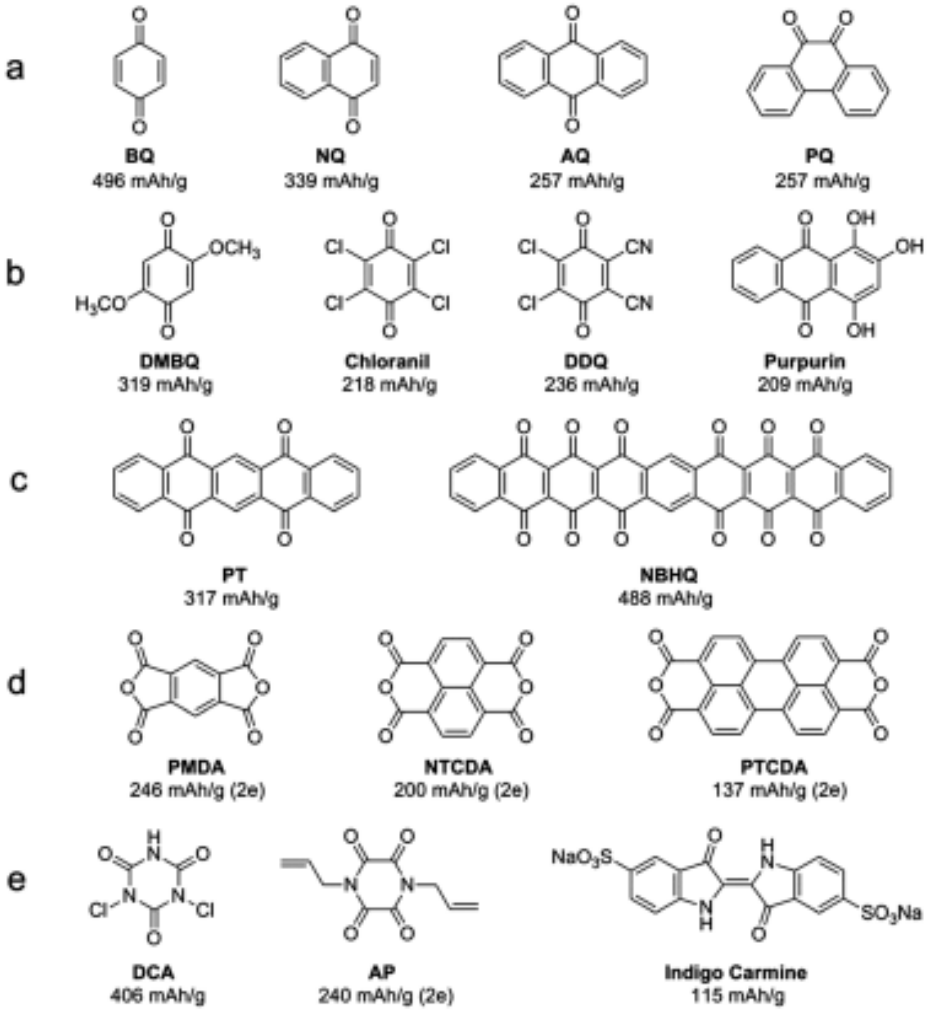

Figure 2.39 Typical small organic molecules with carbonyl groups and their theoretical capacities: (a) quinones: BQ (benzoquinone), NQ (naphthoquinone), AQ (anthraquinone), PQ (phenanthraquinone). (b) Quinone derivatives: DMBQ (2,5-dimethoxy-1,4-benzoquinone), Chloranil (2,3,5,6-tetrachloro-1,4-benzoquinone), DDQ (2,3-dichloro-5,6-dicyano-1,4-benzoquinone), purpurin (1,2,4-trihydroxyanthraquinone). (c) Multi-carbonyl quinones: PT (5,7,12,14-pentacenetetrone), NBHQ (nonylbenzohexaquinone). (d) Dianhydrides: PMDA (pyromellitic anhydride), NTCDA (1,4,5,8-naphthalenetetracarboxylic dianhydride, PTCDA (3,4,9,10-perylentetracarboxylic dianhydride). (e) Other conjugated carbonyl molecules: DCA (dichloroisocyanuric acid), AP (N,N′-diallyl-2,3,5,6-tetraketopiperazine), indigo carmine (5,5′-indigodisulphonic acid sodium salt). The theoretical specific capacities are calculated according to the carbonyl group number except for the dianhydrides and AP.[154]

2.3.4 Functional separators for Li-organic batteries

The development of new separators for Li-organic batteries has been rare, although the organic electrode shares a similar dissolution problem with the Li-S batteries. The dissolution of electroactive organic species into the electrolyte causes active material loss and quick capacity decay. Also, the shuttling of the electroactive organic species to the lithium metal anode results in the destabilization of the anode and low Coulombic efficiency. In this regard, the separator located between the electrodes is expected to improve the battery performance by ion-selectively allowing lithium ion transport and blocking the electroactive organic species. An excellent example is shown below.

Song et al. described a sandwich-structured polypropylene/Li-Nafion/polypropylene separator for Li-organic batteries (Figure 2.40).[161] First, Nafion was put between two layers of porous polypropylene separator to form a polypropylene/Nafion/polypropylene sandwich, which was then put into an organic solution of lithium salt for ion exchange from protons to lithium ions. The successful loading of Li-Nafion was characterized by FTIR. A series of samples with different Li-Nafion loading were prepared. Their ionic conductivity was measured by electrochemical impedance spectroscopy (EIS). It was found that the resistance increases with increasing Li-Nafion loading, although the higher loading of Li-Nafion can be expected to provide better blocking against the electroactive organic molecules/anions. Hence, an optimal loading of 0.5 mg cm^{-1} was determined according to the battery performance. With 1,1′-iminodianthraquinone (IDAQ) as the electroactive organic molecule, a long life of 400 cycles with capacity retention of 76% was obtained, along with high Coulombic efficiencies above 99.6%. In terms of the blocking effect

for the electroactive organic molecules/anions, a visual experiment gave direct evidence that the polypropylene/Li-Nafion/polypropylene separator completely prohibits the diffusion of $IDAQ^{n-}$.

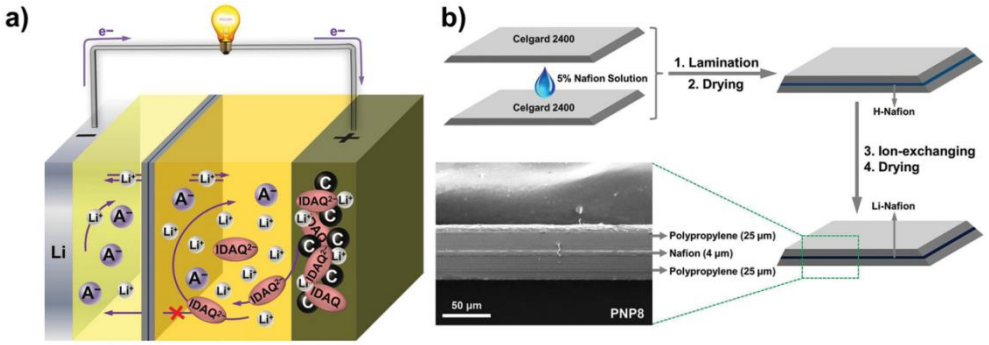

Figure 2.40 (a) Working mechanism of the ion-selective separator composed of sandwiched Nafion and (b) the preparation procedure.[161]

CHAPTER 3 EXPERIMENTAL

3.1 List of Materials

The list of materials and chemicals used during my study for the synthesis and characterization of materials is summarized in Table 3-1.

Table 3-1 Description of chemicals and materials used in this study.

Materials/Chemicals	Formula	Purity	Supplier
Sulphonic acid	H_2SO_4	98%	J&K Chemical
Poly(ether ether ketone), (PEEK)	$(C_{19}SO_3H_{12})_n$	N/A	Jilin University
lithium bis (trifluoromethanesulphonyl) imide (LiTFSI)	$CF_3SO_2NLiSO_2CF_3$	99%	J&K Chemical
1,3-dioxolane (DOL)	$C_3H_6O_2$	99.9%	J&K Chemical
1,2-dimethoxyethane (DME)	$C_4H_{10}O_2$	99.9%	J&K Chemical
Lithium nitrate	$LiNO_3$	98%	J&K Chemical
Lithium foil	Li	BG	Ganfeng
Ethanol	C_2H_5OH	Reagent	Q-Store Australia
Carbon black	C	Super P	Timcal Belgium
Poly(vinylidene fluoride)	$(CH_2CF_2)_n$	n/a	Sigma-Aldrich

Separator	PP/PE/PP	Celgard 2325	Hoechst Celanese
Sodium hydroxide	NaOH	98%+	Sigma-Aldrich
Potassium hydroxide	KOH	90%+	Sigma-Aldrich
Sodium nitrate	$NaNO_3$	99%	Sigma-Aldrich
Anthraquinone	$C_{14}H_8O_2$	99%	J&K Chemical
Perylene-3,4,9,10-tetracarboxylic dianhydride	$C_{24}H_8O_6$	99%	J&K Chemical
graphene	C	99%	J&K Chemical
CMK-3	C	99%	XFNANO
Graphene oxide	C_xO_y	99%	J&K Chemical

3.2 Experimental Procedures

The experimental procedures are presented in Figure 3.1. Materials were synthesized through varied chemical approaches with different chemicals and applied as varied components of the lithium-sulphur or lithium-organic batteries. Before the application, a series of characterizations were used to identify the material. Then, the material was used in the electrode or as another component of the battery (e.g., the separator). After the electrode preparation and the cell assembly, electrochemical methods were applied for testing in the batteries, to see how the material performed. Ex-situ characterizations were used to investigate the mechanism.

Figure 3.1 Outline of the experimental procedures.

3.3 Materials Preparation

3.3.1 Sulphonate reaction

The sulphonation reaction is applied in Chapter 4. The polymer poly(ether ether ketone) (PEEK) was sulphonated by sulphonic acid to produce sulphonated poly(ether ether ketone) (SPEEK). In a typical experiment, 2 grams of poly(ether ether ketone) and 40 mL of sulphonic acid were added into a three-neck flask. The mixture was vigorously mechanically stirred in a water bath at 40°C for varied lengths of time to obtain SPEEK with different degrees of sulphonation (DS). Then, the solutions were filtered and washed with deionized water until pH = 7, and finally dried to obtain the products.

3.3.2 Hydrothermal Method

The hydrothermal method is applied in Chapter 5. Graphite films were ultrasonically treated in acetone and then put into a 100 mL Teflon-lined stainless-steel autoclave. 50 mL of deionized water were added and heated at 120°C for 10 h. After the hydrothermal treatment, the films were sonicated in acetone and dried at 100°C for 4 h, and then put

into a glove box filled with argon. Before the cells were assembled, the graphite films were soaked in the electrolyte for 24 h.

3.3.3 Vacuum filtration

The hydrothermal method is applied in Chapter 6. A mixture of graphene oxide and Super P (or graphene) was suspended in deionized water (1 mg ml^{-1}) with the help of sonication. 1 ml of the suspension was re-dispersed in ethanol (10 ml) and vacuum filtrated to obtain a coating layer with areal density of around 0.1 mg cm^{-2} on the pristine Celgard 2325 separator.

3.3.4 Melt diffusion Method

The melt-diffusion method is a widely applied approach for infiltrating sulphur into mesoporous carbon materials. The mechanism depends on the properties of sulphur. At the temperature of 155°C, the melted sulphur achieves its lowest point of viscosity. Under capillary forces, the melted sulphur is infiltrated into the mesopores of the carbon material.

The melt-diffusion method is applied in Chapter 4. A mixture of mesoporous carbon (CMK-3) and sulphur with a certain weight ratio was ground together and put into a 5 mL glass bottle, which was put into a Teflon autoclave and heated at 155°C in a drying oven for 12 h. The obtained product was the sulphur/carbon composite with sulphur incorporated in the mesopores of the CMK-3.

3.3.5 Chemical Polymerization

A visual experiment is an important method for characterizing the membrane permeability for colored solvents. Usually two half glass cells are used and the membrane is fixed between them. One side is filled with a colored solvent and the other side with a colorless solvent. At rest or with a certain current for a certain length of time, the diffusion of the colored solution can be observed with real-time photography.

In this work, the visual experiment was carried out using an H-type glass cell composed of two halves. The Li_2S_8 solution used in the experiment was produced by the reaction between Li_2S and S with a molar ratio of 1:7 in DOL/DME (v/v = 1:1).

3.3.6 *I-V* experiment

I-V tests were carried out using a home-made conductivity cell and monitored by a picoammeter (Keithley Instruments, mode 6487). An SPEEK membrane was mounted between two halves of a conductivity cell. (The SPEEK membrane was prepared through a solution-casting method. The SPEEK was dissolved in N-methyl-2-pyrrolidone (NMP) and then spread on glass. After heating to evaporate the solvent, an SPEEK membrane was formed.) When a transmembrane potential difference is applied across the membrane, ions flow through the electrolyte-filled nanochannels, generating a measurable ion current. The *I-V* curve of the membrane is plotted using the ion current as a function of potential.

3.4 Characterization methods

3.4.1 X-ray powder diffraction (XRD)

X-ray powder diffraction (XRD) is an analytical method for determining the crystalline phase of a material. It helps to identify whether the material is amorphous or crystalline, and provides information about the unit cell dimensions. XRD is a technique for determining the average bulk composition of a sample, which is normally ground to fine powder and pressed to a smooth thin layer on the sample holder.

In 1912, Max von Laue (1879-1960), a German physicist and Nobel laureate (Physics, 1914), discovered the phenomenon of X-ray diffraction by crystals. Max von Laue made contributions to a variety of scientific fields, including optics, crystallography, quantum theory, superconductivity and the theory of relativity. He had many administrative positions before and after World War II, in which his endeavors guided the German science community for decades.

Thanks to the important findings of Max von Laue, X-ray diffraction is now a very common technique studying the atomic spacing and crystal structures of a crystalline sample. X-ray diffraction originates from the interference of a crystalline sample and monochromatic X-rays, which are produced by a cathode ray tube and then filtered, collimated to concentrate them, and directed toward the sample. An interaction will be result when the conditions satisfy Bragg's Law ($n\lambda = 2d \sin \theta$), in which λ is the wave length of the incident X-ray, d is the crystal lattice planar spacing, and θ is the interaction angle of incidence.

When scanning a sample through a range of angles 2θ, all diffraction directions of the lattice should be obtained due to the random orientation of crystallites in the powdered sample. Based on Bragg's Law, the *d*-spacings could be calculated from the diffraction peaks, because for a specific crystalline material, there are only one set of unique d values. The identification of the material is carried out by comparison of the experimental *d*-spacings with standard reference patterns.

X-ray powder diffraction has many applications. It is mostly used for identifying unknown crystalline materials such as inorganic materials and minerals, which is critical in fields such as materials science, engineering, environmental science, geology, biology, chemistry, and physics. It can also be used to help determine the purity of a sample. It identifies fine-grained materials (e.g., clays, mixed layer clays) that are difficult to observe optically. It determines whether a material is amorphous, semicrystalline, or crystalline. The peak strengths also show how perfect the prepared crystalline sample is. Combined with Rietveld refinement, XRD can be utilized to acquire crystal structures and for quantitative analysis.

3.4.2 Scanning electron microscopy (SEM)

Scanning electron microscopy (SEM) is an electron microscopy technique revealing the external morphology and the orientation of the sample. SEM generates image signals at the specimen surface by irradiating a focused beam of high-energy electrons. The data collected is normally a two-dimensional image showing the spatial variation of a selected area of the sample. The selected area ranges from 1 cm to several micrometers in width, and the magnification ranges from 20 to tens of thousands. Using

energy-dispersive X-ray spectroscopy (EDS), the chemical composition can be quantitatively or semi-quantitatively determined.

The early history of the development of SEM can be briefly presented as follows. In 1931, Max Knoll (1897-1969), a German electrical engineer, together with his colleague Ernst Ruska, invented the electron microscope. Knoll used an electron beam scanner to produce a photograph showing channeling contrast of an object with 50 mm in size. In 1937, Manfred von Ardenne (1907-1997), a German physicist and inventor, invented the scanning electron microscope with high magnification. He successfully scanned a tiny raster pattern with a finely focused electron beam. Ardenne applied the scanning principle to improve the magnification and to eliminate chromatic aberration. He also studied the various detection modes and the theories of SEM. He constructed the first high-magnification SEM. In 1965, the first commercial SEM instrument was introduced by the Cambridge Scientific Instrument Company.

The SEM signal is produced through the dissipation of the accelerated high-energy electrons in the solid sample. The signals include secondary electrons that produce SEM images, backscattered electrons (BSE), diffracted backscattered electrons (EBSD), etc. Secondary electrons are used for imaging samples with their morphology and topography. Normally, SEM analysis is non-destructive to the sample, except for some very fragile samples which are very sensitive to the heat produced by the high-energy electrons.

The SEM is one of the most frequently used instruments for materials scientists, engineers, biologists, chemists, and environmental scientists. Elemental maps can be acquired using EDS. The SEM helps to identify phases based on the crystalline structure and qualitative chemical analysis. The SEM can identify small particles down to 50 nm in size. The BSE can be used for rapid discrimination of phases in multiphase

samples. An SEM equipped with EBSD can examine the microfabric and crystallographic orientation in a wide range of materials.

3.4.3 Transmission electron microscopy (TEM)

TEM is a microscopy technique using a beam of electrons transmitting through a thin specimen, in which electron-sample interactions take place as the electron beam passes through the sample. An image is formed by the electrons as they are transmitted and interact with the material, before it is magnified and presented on an imaging screen. The TEM is based on the same principle as the light microscope, but it uses high-energy accelerated electrons. The limitation of a optical microscope is the wavelength of light. The much lower "wavelength" of electrons enables the resolution to be improved by a thousand times compared to light microscopy. With the help of TEMs, objects on the order of a few angstroms (10^{-10} m) can be observed, which means that the details of materials down to near atomic levels can be obtained. The high magnification is the most important feature of TEM, making it widely applied in medical, materials, and biological research.

The first TEM machine was built by Max Knol and Ernst Ruska (1906-1988, German physicist) in 1931. They built a TEM with resolution greater than that of light in 1933 and the first commercial TEM machine in 1936. The Nobel Physics prize was awarded to Ernst Ruska in 1986 for his great contribution to the development of TEM.

TEM is a major analysis technique in a range of scientific fields and finds applications in materials science, semiconductors, nanotechnology, virology, cancer research, etc. At lower magnifications, the varied thicknesses and compositions of the materials result in

different TEM image contrasts, owing to varied levels of electron absorption by the material. At higher magnifications, the observed images need expert analysis because the intensity of the image is modulated by complex wave interactions. With different magnification levels and analysis modes, besides the regular absorption-based imaging, the TEM is a very useful tool to observe modulations in chemical identity, crystal orientation, electronic structure, and sample induced electron phase shifts.

3.4.4 Energy-dispersive X-ray spectroscopy (EDS)

Energy-dispersive X-ray spectroscopy (EDS) is an important technique used to obtain a localized chemical analysis by analyzing the X-ray spectrum emitted by a solid-state specimen bombarded by a beam of high-energy electrons. Principally elements with atomic numbers ranging from 4 (Beryllium) to 92 (Uranium) can be detected with both qualitative and quantitative analyses.

Element distribution images of a selected area can be produced by scanning the electron beam in a television-like raster pattern and then displaying the intensity of a specific X-ray line. Also, by focusing on a point or a line on the surface of the sample, the data from that point or line analysis can be obtained. The EDS “map” results reveal the surface topography or the mean atomic number dispersion according to the selected mode. Nowadays, however, there is considerable function overlap with the SEM, which is designed primarily for producing electron images but can also be used for element mapping or point analysis if an X-ray spectrometer is added.

The X-ray intensities are obtained by counting the photons. The analytical accuracy is around ± 2%, owing to the uncertainties of the compositions in the standards and the

errors in the corrections applied to the raw data. The detection limit when using EDS is normally 1000 ppm by weight but it can still be further reduced using longer counting times.

There is also a certain spatial resolution in the EDS measurement. The spatial resolution is affected by the penetration and spreading of the electron beam in the solid sample. Spatial resolution varies according to the density of the material; the higher density the sample possesses, the more difficult it is for the electrons to penetrate the specimen. For instance, the nominal resolution is approximately 2 μm for silicates (3 g/mL), but for obtaining quantitative results, a minimum grain size of several micrometers is needed. In order to get better spatial resolution, ultra-thin specimens on the order of approximately 100 nm are needed so that the beam will not spread out too much. These ultra-thin samples can be measured in a TEM with an installed X-ray spectrometer, which is also called an analytical electron microscope (AEM).

3.4.5 Thermogravimetric analysis (TGA)

Thermogravimetric analysis (TGA) is an analytical method for measuring the weight change of a sample being heated in an inert or oxidizing atmosphere. TGA analysis is normally based on constant heating rates or as a function of time (e.g., constant temperature or constant mass loss). Over a specific temperature range, the weight change indicates the thermal stability and the composition of the sample. In detail, TGA provides information about vaporization, sublimation, adsorption, absorption, desorption, chemisorption, dehydration, decomposition, oxidation, reduction, etc.

TGA can used to analyze some specific characteristics (e.g., decomposition, oxidation, or vaporization) of materials exhibiting mass loss or gain. TGA can be used to determine the decomposition patterns of some materials. TGA can analyze the organic content in a sample. TGA can also be applied for studying the degradation mechanisms and reaction kinetics. TGA can be used to investigate a wide range of polymer materials, including thermoplastics, thermosets, composites, elastomers, fibers, plastic films, coatings, paints, etc.

3.4.6 Brunauer-Emmett-Teller (BET)

The Brunauer-Emmett-Teller (BET) technique is an important analysis technique for the measurement of the specific surface area of a material. BET can also refer to the theory published by Stephen Brunauer, Paul Hugh Emmett, and Edward Teller in 1938. The BET theory involves multi-layer adsorption of non-corrosive gases as adsorbates to determine the surface area of a sample.

3.4.7 Raman spectroscopy

Raman spectroscopy is a spectroscopic technique measuring molecular vibrations for sample identification and quantification. A monochromatic light (e.g., a laser) is directed onto a sample, and the scattered light is detected. The majority of the scattered light possesses the same frequency as the excitation light source, and this is known as Rayleigh or elastic scattering. A small proportion (around 10^{-5} % of the incident light intensity) of the scattered light is shifted in energy from the laser frequency owing to the

interaction between the incident electromagnetic waves and the vibrational energy levels of the sample molecules. The plot of intensity of the “shifted” light against the frequency is the Raman spectrum of the sample. The band positions will be located at frequencies corresponding to the energy levels of the different vibrations of various functional groups. Hence, the Raman spectrum can be interpreted in a similar way to the infrared absorption spectrum.

The inelastic scattering of light was predicted by Adolf Smekal (1895-1959, Austrian theoretical physicist) in 1923, but the observation in practice took place 5 years later. The Indian scientist Sir C. V. Raman (together with his student named K. S. Krishman) observed the effect by means of sunlight in 1928 and was awarded the Nobel Prize in Physics in 1930. He found that by using a narrow band photographic filter to create monochromatic light and a “crossed filter” to block the as-produced monochromatic light, a small amount of light changed in frequency and passed through the filter. It is worth mentioning that Grigory Samuilovich Landsberg (1890-1957, Soviet physicist) and Leonid Isaakovich Mandelstam (1879-1944, Soviet physicist) also independently discovered the Raman effect. Also, between 1930 and 1934, an important pioneering theory of the Raman effect was developed by George Placzek (1905-1955, Czech physicist). After 3 decades, the advent of the laser led to simplified Raman spectroscopy instruments and revived this technology as a widely-used analytical tool.

Raman spectroscopy can be used for both qualitative and quantitative analyses. Chemical identifications can be performed by using search algorithms acting on digital databases for the spectra, which are very specific. Raman is complementary to infrared absorption spectroscopy and offers several advantages over mid-IR and near-IR spectroscopy. For instance, Raman spectroscopy can be used to analyze bands of

symmetric linkages, which are weak in an infrared spectrum, such as -S-S-, -C-S- and -C=C-. Raman spectra are “cleaner” than mid-IR spectra, that is, Raman bands are narrower and combination bands are generally weak. The standard Raman spectral range reaches below 400 cm^{-1}, making the technique ideal for both organic and inorganic species.

3.4.8 Fourier Transform Infrared spectroscopy (FTIR)

Fourier Transform Infrared spectroscopy (FTIR) is a technique for identifying chemical bonds by obtaining an infrared absorption spectrum of the object of analysis, which is a solid, liquid, or gas. For any absorption spectroscopy (e.g., ultraviolet-visible (UV-Vis) spectroscopy), the mechanism depends on how well the light at each wavelength is absorbed by the sample. Unlike Raman spectroscopy, which uses a monochromatic beam of light to shine on the sample and test the frequency change of the scattered light, infrared spectroscopy shines a beam with a range of frequencies of light and measures how much is absorbed by the sample at each wavenumber.

A typical FTIR spectrometer includes several important components: the IR source, the detector, the beam splitter, and the Fourier transform software. The first spectrophotometer that was able to record an infrared spectrum was built by an American corporation called PerkinElmer in 1957. This first instrument covered the wavenumber range from 4000 cm^{-1} to 660 cm^{-1}. The lowest wavenumber of 660 cm^{-1} was limited by the dispersing material, single crystal sodium chloride. Later, the lower limit was extended to 400 cm^{-1} and even to 200 cm^{-1} by using prisms of potassium bromide and cesium iodide, respectively. The region beyond 200 cm^{-1} belongs to the

far-infrared region and then merges into the microwave range. The typical resolution is 4 cm^{-1} for typical cheaper FTIR instruments, and nowadays a high resolution of 0.001 cm^{-1} has already been commercialized.

FTIR spectrometers have been widely applied in areas where dispersive spectrometers are used and areas where dispersive spectrometers cannot be used owing to their improved sensitivity and detecting speed. FTIR can be used in microscopy and imaging. An infrared microscope enables samples absorbing IR light to be observed. Combined with a microscope with linear or two-dimensional array detectors, images revealing a map of the intensity at any wavenumber or range of wavenumbers being absorbed by the sample can be collected. This approach determines the distribution of different species in the sample, e.g., tissue sections, pharmaceutical tablets. Moreover, FTIR can be coupled with other instruments for real-time detection of gaseous species and monitoring reaction processes involving the formation of gases. Typical coupled instruments include gas-chromatography-infrared spectrometry (GC-IR) and thermogravimetric analysis-infrared spectrometry (TG-IR).

3.4.9 X-ray photoelectron spectroscopy

X-ray photoelectron spectroscopy (XPS) is the most widely used surface analysis technique for measuring the elemental composition and determining the empirical formula, electronic states, and chemical states of the elements spreading on the surface of a sample. XPS spectra are measured by irradiating the sample with a beam of X-rays and meanwhile recording the number of electrons with certain kinetic energies that escape from the top 10 nm of the sample being analyzed. As the energy of the particular

incident X-ray is known and the kinetic energy of the emitted electrons are measured, the electron binding energy of the emitted electrons can be calculated. In this way, the electronic and chemical states of the chemical species in the surface layer can be detected.

The history of the photoelectric effect and the development of photoemission as an analytical tool can be briefly stated as follows. In 1887, Heinrich Rudolf Hertz (1857-1894, German physicist) discovered the photoelectric effect but could not explain this phenomenon. In1905, Albert Einstein (1879-1955, German-born theoretical physicist) successfully resolved this problem and because of this contribution won the Nobel Prize in Physics 1921. Two years later, the first XPS spectrum was recorded experimentally. After continuous improvement of the equipment, in 1954, the first high-energy-resolution XPS spectrum was recorded, indicating the great potential of XPS. In 1967, Kai Siegbahn (1918-2007, Swedish physicist) carried out a comprehensive study of XPS and together with a groups of engineers, successfully built the first commercial monochromatic XPS instrument in 1969. The Nobel Prize in Physics in 1981 was awarded to Siegbahn for his key contribution to the development of XPS into a useful analytical tool.

XPS is a widely-used technique in a wide range of fields and has many applications. XPS determines the elements and the composition of those elements at the surface (1-12 nm) of a sample. XPS can be used to detect impurities, if there are any, at the surface of a bulk sample. XPS distinguishes between the different electronic states of a specific element. By applying ion beam stripping depth analysis, XPS can examine the change in the element compositions and the corresponding chemical states from the outermost layer to the interior.

3.4.10 Gel Permeation Chromatography (GPC)

Gel permeation chromatography (GPC) is a type of size exclusion chromatography (SEC) that separates macromolecules by allowing them to pass through a column filled with porous gel. SEC was first developed in 1955, and GPC was first reported in 1964 by John C. Moore at the Dow Chemical Company. GPC normally is used to analyze polymer materials or to purify the desired product. GPC is used to provide information on a variety of definitions of molecular weight, including the number average molecular weight (M_n), the weight average molecular weight (M_w), the size average molecular weight (M_z), or the viscosity molecular weight (M_v).

3.4.11 Nuclear Magnetic Resonance (NMR) Spectroscopy

Over the past fifty years nuclear magnetic resonance (NMR) spectroscopy has become the major technique for analyzing the structure of organic molecules. Among all the spectroscopic methods, NMR is the only one that is capable of complete analysis and interpretation of an analyte. NMR spectroscopy is based on the finding that the nuclei of many elemental isotopes have a characteristic spin, whether it is integral spin, fractional spin, or no spin. A spinning charge generates a magnetic field (unit, Tesla, T). In the presence of an external magnetic field, there will be two spin states: the magnetic moment of the lower energy spin state is aligned with the external field and that of the higher energy spin state is opposed to the external field. The energy difference (given as a frequency in units of MHz) between the two spin states depends on the strength of the external magnetic field. Therefore, in order to enlarge the energy difference (for NMR

purpose, 20 to 900 MHz is needed) between the spin states, a strong magnetic field is normally applied.

When placed in a magnetic field, the NMR active nuclei (e.g. ^{1}H, ^{13}C) absorb electromagnetic radiation at a frequency characteristic of the isotope and show a specific nuclear magnetic resonance response. For protons in different electronic environments, the local field "shields" the proton from the applied magnetic field, which must be increased in order to achieve resonance, or the absorption of energy at the reference frequency. The increment is small, on the level of parts per million (ppm). A reference signal (that of tetramethylsilane) is used to normalize the reported data.

NMR is one of the most important techniques to be developed in the 20^{th} century, and the related discoveries have already won 5 Nobel Prizes. The first one was the 1952 Nobel Prize in Physics, awarded to Edward Mills Purcell (1912-1997, American physicist) and Felix Bloch (1905-1983, Swiss physicist) for the independent development of NMR spectroscopy.

NMR has been widely applied in a wide range of field, particularly organic chemistry and biology. Typically, the sample needs to be dissolved in a solvent for the NMR analysis. In some particular cases, the physical environment does not allow the use of a solvent, so solid-state NMR has been developed. For molecules that are too complicated to analyze, two-dimensional NMR can be used to provide more detailed information on the molecule. Moreover, other types of NMR techniques, including protein NMR, nucleic acid NMR, and carbohydrate NMR, have been developed for measuring the corresponding specific kinds of complicated molecules.

3.4.12 Small-angle X-ray scattering (SAXS)

Small-angle X-ray scattering (SAXS) is a technique in which the signal from the elastic scattering of X-rays by a sample with nm-level inhomogeneities is recorded at very low angles. SAXS provides information about the shape and size of macromolecules or colloids, as well as the characteristic distances of partially ordered materials or pore sizes. SAXS reveals structural information on macromolecules from 5 nm to 25 nm in size, or characteristic repeated distances up to 150 nm.

SAXS, together with small angle neutron scattering (SANS), belongs to the family of small-angle scattering (SAS) techniques. SAXS also belongs to the family of X-ray scattering techniques, along with ultra-small angle X-ray scattering (USAXS).

SAXS is widely applied in nanoscience for determining the microscale or nanoscale structure of particle systems in terms of particle size, shape, distribution, etc. The analyzed material can be a solid or a liquid, which contains nanoscale repeated solid, liquid, or gaseous domains. Also, ordered systems such as lamellae and fractal-like materials can be examined by SAXS. Other systems that can be examined include colloids, oils, polymers, cement, plastics, proteins, and pharmaceuticals.

3.5 Electrode fabrication and cell assembly

3.5.1 Electrode preparation

The electrodes were prepared by mixing the electroactive material (sulphur-based or organic molecules), conductive agent (Super P) and binder (poly(vinylidene fluoride, PVDF or SPEEK) and dispersing them in NMP solvent. The as-prepared slurry was cast on the current collector (carbon-coated or uncoated aluminum foil) using a doctor blade and then dried in a vacuum oven. The as-obtained electrodes were then cut into circles and put into a glove box for assembly of the cells.

3.5.2 Cell assembly

All the cell assembly processes were performed in a glove box. The standard devices for the half-cells were CR2032 coin cells. According to the procedure, the negative cap, the lithium metal anode, the separator (Celgard separator or the coated separator), the electrode (sulphur-based or organic electrode), the spacer, the spring, and the positive cap were sequentially stacked together. Before and after the stacking of the separator, one drop of ether-based electrolyte was dropped on the lithium metal and the separator, respectively. The assembled CR2032 coin cell was then pressed together using a sealing machine.

3.6 Electrochemical measurements

3.6.1 Cyclic voltammetry (CV)

Cyclic voltammetry (CV) is an electrochemical technique, which involves repeatedly ramping the working electrode potential linearly versus time between two set potentials. The current at the working electrode is plotted versus the applied voltage to give the CV data. Typically, a ramping rate of 0.1 mV/s was utilized for measuring the oxidation/reduction potentials of the active material in the cell.

3.6.2 Galvanostatic electrochemical testing

Land instruments were used for the galvanostatic testing of the assembled half-cells. For both the Li-S and the Li-organic batteries in this thesis, the first cycle begins with discharging for the reduction of sulphur or organic molecules. According to the theoretical capacities of sulphur and the organic molecules, certain C-rates (from 0.1 C to tens of C) were used for both the discharge and charge processes. All the C-rates were based on the weight of the active material in the electrode. The cut-off voltages were typically 1.7/2.6 V for Li-S batteries and 1.5/3.5 V for Li-organic batteries.

3.6.3 Electrochemical Impedance Spectroscopy (EIS)

Electrochemical impedance spectroscopy (EIS), or the so-called alternating current (AC) impedance method, studies the response to a periodic small amplitude AC signal

applied on an electrochemical system. EIS has been used to determine double-layer capacitance or AC polarography. Currently, EIS is mostly applied for characterization of electrode processes and complex interfaces. It reveals information on the structure of an interface and the electrochemical reactions that take place there. In testing the batteries, normally cells were characterized in their fully charged or discharged states. A voltage of 10 mV was used and frequencies from 100K Hz to 100 mHz were utilized.

CHAPTER 4 INTRODUCING ION-TRANSPORT-REGULATING NANOCHANNELS TO LITHIUM-SULPHUR BATTERIES

4.1 Preface

In nature, the phenomenon of ion regulation widely exists.[162] Ion channels across cell membrane control the communication of ions and charged substrates between inner cell and the extracellular environment.[163] The two distinctive features of ion channels are: channels mediate ion transport with high rate (10^6~10^8 ions per second); channels choose specific ions or molecules to pass through and reject other species.[164] For example, potassium channels allow rapid flow of K^+ (10^8 ions per second) while decline the translocation of Na^+ across the membrane.[71] Inspired by the interesting characteristics of ion channels, synthetic smart nanochannels have found wide applications ranging from nanofluidic to energy conversion devices.[165-169] This ion-regulating property of nanochannels is highly needed for the cathode of the lithium-sulphur battery to overcome the poor rate performance and quick capacity decay, which has been caused by the poor Li^+-ion transport through the cathode and the dissolution of the intermediate products of polysulphide anions.[7, 60, 63, 67, 74, 116, 131, 170-178]

To overcome the challenges of lithium-sulphur batteries, much progress has been achieved by developing varied sulphur-carbon composites, which greatly improve the electron transfer in the sulphur cathode.[61, 82, 179-184] For example, high rates of 10 C were obtained using unstacked double-layer graphene[76] and 3D hierarchical hollow carbon nanorods.[185] However, the ion transport through the sulphur cathode has been paid rare attention. Ion-selective separators have been reported alleviating the polysulphide

shuttling problem.[118, 127] However, the rate performance of the Li-S battery was hardly enhanced, since the separator almost has no effect on the lithium-ion transport of the electrode but mainly blocks the diffusion of polysulphide anions from the cathode side to the anode side. For a liquid electrolyte lithium-sulphur battery, the enhancement on both the rate performance and the cycling stability should be through developing new sulphur cathodes.

Here, an ion-containing polymer membrane with negatively charged nanochannels was prepared, which have a dimension of ca. 2 nm, comparable to the Debye length. The negatively charged nanochannels are capable of regulating ion transport by facilitating the transport of cations and rejecting anions. As a demonstration, the polymer membrane was integrated into a sulphur cathode and a high-performance lithium-sulphur battery was obtained. With the fast flow of lithium ions and the retaining of polysulphide anions, the novel sulphur cathode shows significantly improved rate and cycle properties compared to the cathode with the conventional polymer. Figure 4.1a presents the configuration of the integrated sulphur cathode with the ion-transport-regulating polymer membrane wrapping the sulphur/mesoporous carbon (CMK-3) composite. The polymer utilized is an ion-containing polymer, sulphonated poly (ether ether ketone) (Figure 4.1b). The polymer possesses excellent film-forming ability and the polymer film contains both hydrophobic domain of polymer backbone and hydrophilic domain of sulphonate groups. The ionic interactions of negative sulphonate groups form negatively charged nanochannels (Figure 4.1c). The sulphur was incorporated into the porous structure of CMK-3 (Figure 4.1d). Thus, the novel cathode integrated with the polymer membrane can regulate the ion transport by facilitating the transport of lithium ions and rejecting the polysulphide anions. Our novel design of the integrated cathode renders faster lithium-ion transport, which

significantly reduces the resistance. Besides, the polysulphide rejection alleviates the active material loss. Therefore, these merits together enable high-performance Li-S batteries. For instance, for the novel cathode, a high specific capacity of 1105 mA h g^{-1} is kept after 100 cycles at 0.2 C. Further, at a high rate of 18 C, a high specific capacity of 612 mA h g^{-1} is retained over 250 cycles, with excellent capacity retention of 91%.

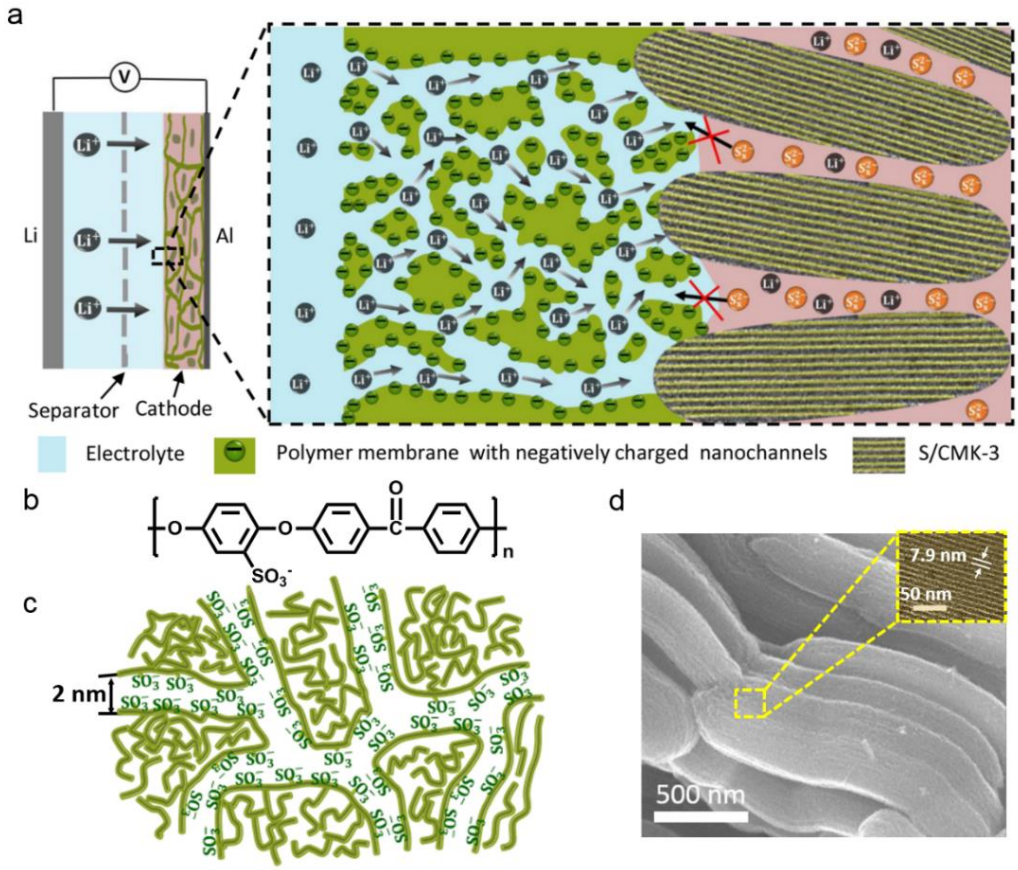

Figure 4.1 Design and working mechanism of the integrated sulphur cathode. a) Schematic illustration of the integrated sulphur cathode. SPEEK membrane wraps around S/CMK-3 composite and regulates the ion transport between the electrolyte and the cathode. b) Chemical structure of SPEEK. c) View of the nanochannels with a diameter of ca. 2 nm. d) Scanning electron microscopy image of CMK-3 and view of S/CMK-3 composite (inset) showing sulphur is encapsulated inside the nanochannels of CMK-3.

4.2 Experimental

4.2.1 Polymer synthesis and characterizations

The preparation was conducted according to the literature[186]. Poly (ether ether ketone) (PEEK) was kindly provided by Jilin University. At 40°C, SPEEK (2 gram) was added into sulphonic acid (40 mL). Under vigorous stirring, the mixture was stirred for 10 h. The as-prepared yellow solution was poured into ice water; then white solid product was observed. The solid product was collected and washed with deionized water thoroughly until pH reaches 7, then dried at 80°C in vacuum. The sulphonated product was named as sulphonated poly (ether ether ketone) (SPEEK). The reaction equation is expressed as Figure 4.2.

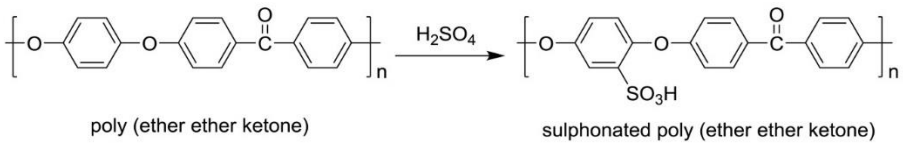

Figure 4.2 Equation of a sulphonation reaction to produce sulphonated poly (ether ether ketone) (SPEEK).

The Molecular Weight of SPEEK was measured on a Gel Permeation Chromatography (Waters1515, USA). The morphologies were observed using field-emission scanning electron microscopy (SEM, JEOL JSM7500F) and transmission electron microscopy (TEM, JEM 1200EX). ^{1}H NMR (400 MHz, d-DMSO) was carried out on a Varian NMR machine. The Fourier Transform Infrared (FTIR) spectra were recorded on an AVATAR 360 spectrometer (Nicolet Instrument Corp., USA) in the wavelength range of 400–4000 cm^{-1}. The TEM samples of SPEEK were prepared by spreading a low-concentration solution of SPEEK in NMP on carbon-coated copper grids. In order

to stain the ion channels, SPEEK was immersed in an aqueous solution of 0.5 M $AgNO_3$ overnight. The stained SPEEK was rinsed thoroughly by deionized water and dried at room temperature for 24 h. Then the dried stained SPEEK was dissolved in NMP and dripped on carbon-coated copper grids.

The specimen was imaged in a Talos™ F200C TEM (Transmission Electron Microscope), operated at 200 kV, in room temperature, and Ceta 4K*4K Camera was used for Images recorded. Total 61 images were acquired in a high magnification of 150 kx (pixel size of 0.069 nm) and low dose mode. Tilt angle range is from -60° to +60°, in increments of 2°. Defocus values for these tilt series ranged from 9.23 ± 0.10 μm. Serial-EM was used for data collection and all tilt series were denosing, alignment and reconstruction by Inspect3D (FEI Company). The final 3D structure was acquired by reconstruction algorithm "SIRT" (simultaneous iterative reconstruction technique) with 10 iterations. 3D rendering of this specimen was completed by Chimera after structure reconstruction of TEM tomography data (Talos™ F200C TEM), the dark region represents hydrophilic domain and the brighter region is hydrophobic domain.

1D small-angle X-ray scattering (SAXS) experiments were carried out with a SAXS instrument (SAXSess, AntonPaar) containing Kratky block-collimation system. An image plate was used to record the scattering patterns form between 0.06 and 29 nm^{-1}. The radius of gyration of SPEEK is 27.5 nm determined through Static light scattering by measuring the scattering intensity from 20° to 150° on a laser light scattering (LLS) spectrometer (ALV/DLS/SLS-5022F) equipped with a cylindrical 22 mW He—Ne laser (Uniphase, at $\lambda = 632.8$ nm). The spectrometer has a high coherence factor of $\beta \approx 0.95$ because of a novel single-mode fiber optics coupled to an efficient avalanche photodiode. The LLS cell was held in a thermostat refractive index matching vat filled with purified and dust-free toluene.

The visual experiment was carried out using an H-type glass cell composed of two halves. The Li2S8 solution used in the experiment was produced by the reaction between Li_2S and S with a molar ratio of 1:7 in DOL/DME (*v*/*v* = 1:1). *I-V* tests were carried out using a home-made conductivity cell and monitored by a picoammeter (Keithley Instruments, mode 6487). The schematic illustration of the home-made device is shown in Figure 4.3. An SPEEK membrane was mounted between two halves of a conductivity cell. (The SPEEK membrane was prepared through a solution-casting method. SPEEK was dissolved in NMP and then spread on glass. After heating to evaporate the solvent, an SPEEK membrane was formed.) When a transmembrane potential difference is applied across the membrane, ions flow through the electrolyte-filled nanochannels, generating a measurable ion current. *I-V* curve of the membrane is plotted using the ion currents as a function of potential.

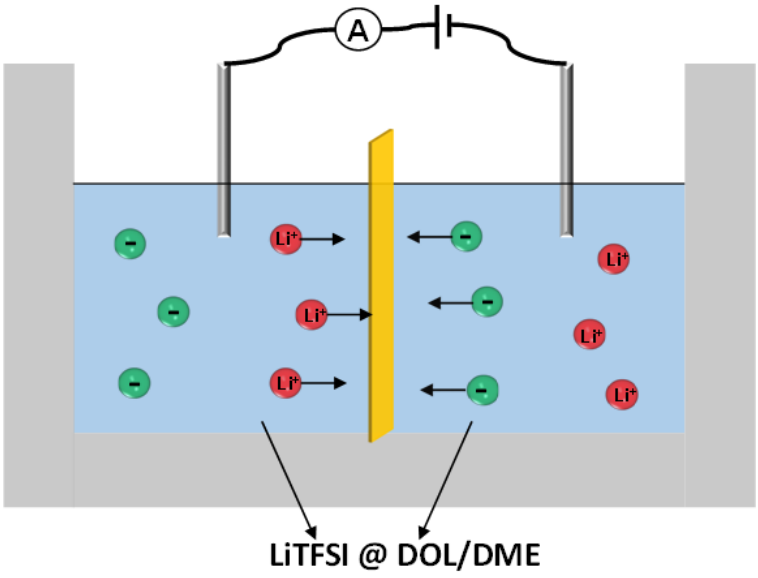

Figure 4.3 Depiction of home-made conductivity cell measuring the I-V property of the nanoporous SPEEK membrane. The test was monitored by a picoammeter (Keythley Instruments, mode 6487).

4.2.2 Electrode preparation

CMK-3 was purchased from Nanjing XF-nano, China. The Brunauer-Emmett-Teller (BET) data of CMK-3 (pore volume 1.32 cm^3 g^{-1}, average pore diameter 3.7 nm and specific surface area of 1188 m^2 g^{-1}) were measured through the N_2 adsorption-desorption isotherm at 77 K on a BELSORP-mini instrument. S/CMK-3 composite was synthesized by melt-diffusion method. Sulphur and CMK-3 with weight ratio of 1:1 was mixed and heated at 155°C for 24 h under argon. The sulphur content in the S/CMK-3 composite was measured by Thermogravametric analysis on a NETZSCH STA 409PC instrument under nitrogen gas. Powder X-ray diffraction was performed in the 2θ range of 10–80° (Rigaku MiniFlex600, Cu Kα radiation). The integrated cathode of SPEEK and S/CMK-3 was constructed by a dispersion-evaporation process. SPEEK was dissolved in N-methyl-2-pyrrolidone (NMP) and then S/CMK-3 composite was added to form the dispersion; which was coated on aluminium foil using a doctor blade and heated at 50ºC to eliminate the NMP solvent. Circular disks with diameter of 1.0 cm were cut out for use in the batteries. During this process, SPEEK film was formed to wrap the sulphur/carbon composite owing to the strong thermodynamic driving force in reducing hydrophobic interface and the excellent film-forming ability of SPEEK. The integrated sulphur cathodes were constructed with weight ratios of 8:1:1 and 6:2:2 (S/CMK-3: Super P: SPEEK). The electrode laminate weight ranges from 1.0 to 1.5 mg. A control cathode with formulation of 8:1:1 (S/CMK-3: Super P: PVDF) and similar electrode laminate weight was used for comparison.

4.2.3 Electrochemical Measurements

CR2032 coin cells were assembled in an argon-filled glove box by pairing sulphur cathodes and lithium anodes, and the electrolyte was 1.0 M lithium bis (trifluoromethanesulphonyl) imide (LiTFSI) with 1% LiNO3 in a binary mixture of 1,3-dioxolane (DOL) and 1,2-dimethoxyethane (DME) (1:1 by volume). Galvanostatic charge/discharge was performed on a LAND battery testing machine (Wuhan, China) and a voltage window between 1.7 and 2.6 V was applied. The current density and the specific capacity of an electrode were calculated based on the mass of sulphur, if not specified. Both Cyclic Voltammograms (CV) and Electrochemical impedance spectroscopy (EIS) were recorded with a PARSTAT electrochemical workstation. The sweeping rate of CV was 0.1 mV s^{-1}. The EIS was recorded in the frequency range from 100 kHz to 100 mHz with a perturbation amplitude of 5 mV. The electrodes with 10 wt% of polymer were measured at charged state (current density: 1 C) from the 1st to the 200th cycle. The obtained EIS data were fitted using ZView software.

4.3 Results and Discussion

Nanochannels with surface charge can regulate the ion transport across the membrane.[165] There are two major factors that determine the ion-transport property of nanochannles: (1) the dimension of the channels and (2) the surface charge density of the channels. For battery applications, polymer material containing nanochannels is more desirable for its controlled charge density and excellent stability. Particularly, polymer with negatively charged nanochannels can be expected to enhance the Li^+-ion transport and reject the diffusion of S_x^{2-} (x = 4~8) anions, simultaneously solving the

two most important problems for Li-S batteries. In this work, a typical sulphonated aromatic polymer, sulphonated poly (ether ether ketone) (SPEEK), [186] is introduced into the sulphur cathode.

The molecular structure of SPEEK is shown in Figure 1b. SPEEK was prepared through a sulphonation reaction of the precursor aromatic polymer poly (ether ether ketone). Sulphonate groups are introduced through an electrophilic substitution reaction into the hydroquinone segment of the polymer backbone, for the hydroquinone part has been activated by the ether linkage. The existence of sulphonate groups in SPEEK is evidenced by FTIR (Figure S4.4). The peak at 1490 cm^{-1} (ascribed to aromatic C=C stretching) for PEEK is split into two peaks at 1473 and 1505 cm^{-1} for SPEEK due to the effect of sulphonate groups. Meanwhile, compared to the spectra of PEEK, three new peaks appear for SPEEK: 1253 cm^{-1} for O=S=O asymmetric stretch, 1080 cm^{-1} for O=S=O symmetric stretch and 710 cm^{-1} for S-O symmetric stretch.

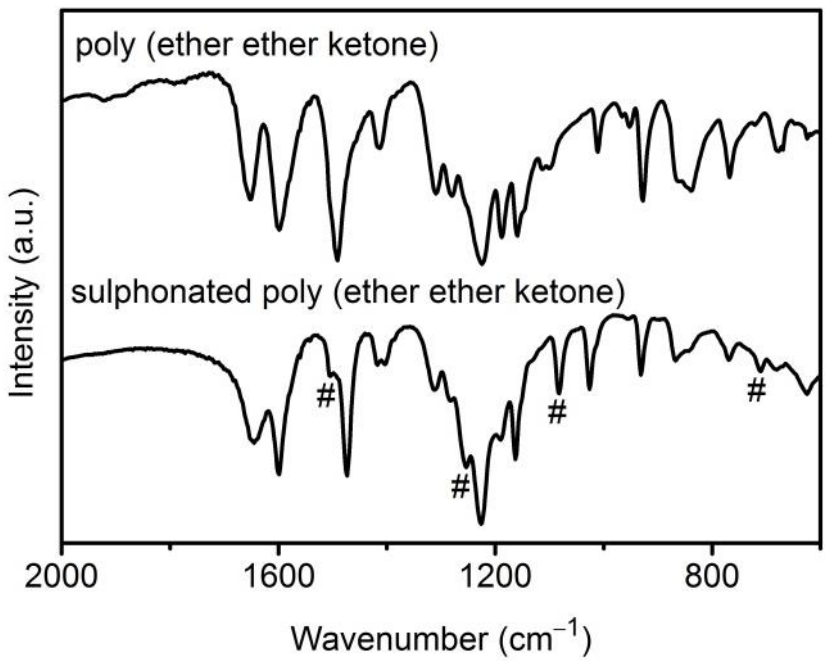

Figure 4.4 FTIR spectra of PEEK and SPEEK.

The structure of SPEEK was further analyzed by the ^{1}H NMR spectra. The molecular structure is shown in Figure 4.5a with each hydrogen atom numbered. The percentage of the x part in the polymer structure composed of x and y indicates the degree of sulphonation (DS), which refers to the percent of monomers that have been substituted by sulphonate groups. The chemical shift assignment of SPEEK is shown in Figure 4.5b. Under the effect of the sulphonate group, the chemical shift of the adjacent hydrogen atom moves toward the lower field by 0.25 ppm. Based on the relative integration of the H10' peak from the ^{1}H NMR, The DS is calculated to be 89% according to the literature. It is assumed that the area of H10' is 1, then the area of all the peaks of the numbered hydrogen atoms is integrated to be 12.5. DS/ (12-DS) = A (H10')/ A (all the numbered H) = 1/12.5. Thus, DS is calculated to be 89%.

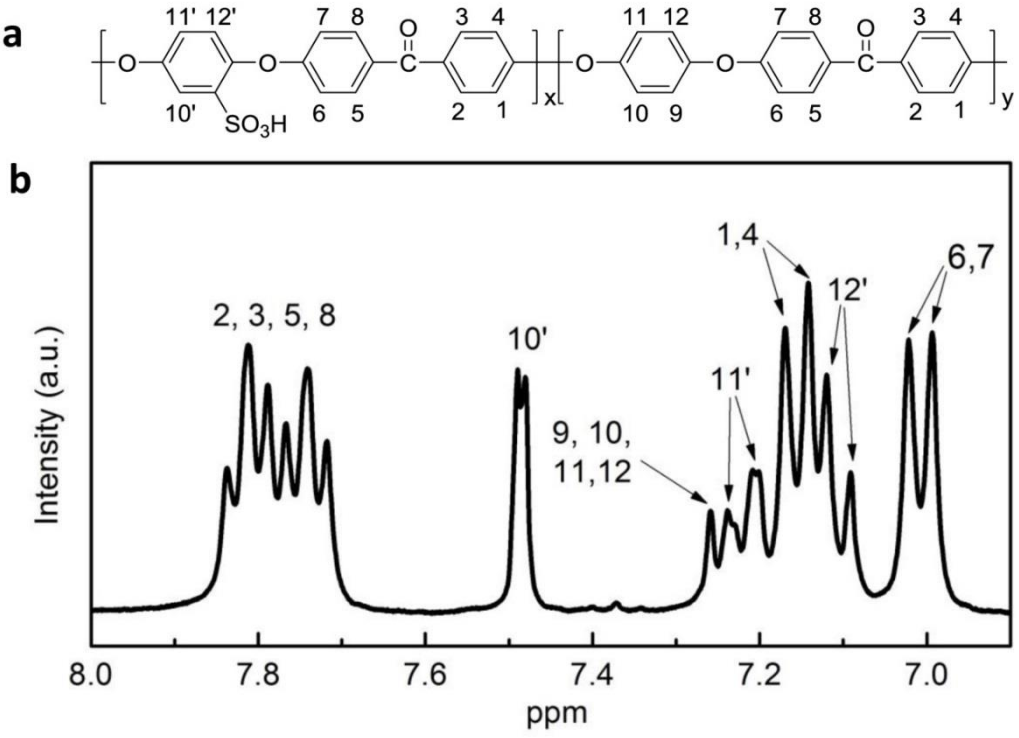

Figure 4.5 The molecular formula (a) and ^{1}H NMR spectra (b) of SPEEK in DMSO-d_6.

Owing to the introduction of sulphonate groups, SPEEK is composed of two separated domains: hydrophobic backbone and hydrophilic ionic groups. The ionic interactions of

the negative sulphonate groups produce nanochannels, which are negatively charged by the sulphonate groups at the surface. The charge density and diameter of the channels could be adjusted with the degrees of sulphonation (DS). the SPEEK with a high DS of 89% was used, owing to the high charge density of the sample and the excellent film-forming ability at nanometer levels. Furthermore, the digital photo of a 50 μm thick SPEEK membrane (Inset, Figure 4.6a) demonstrates that the polymer can form films with thickness at micrometre levels.

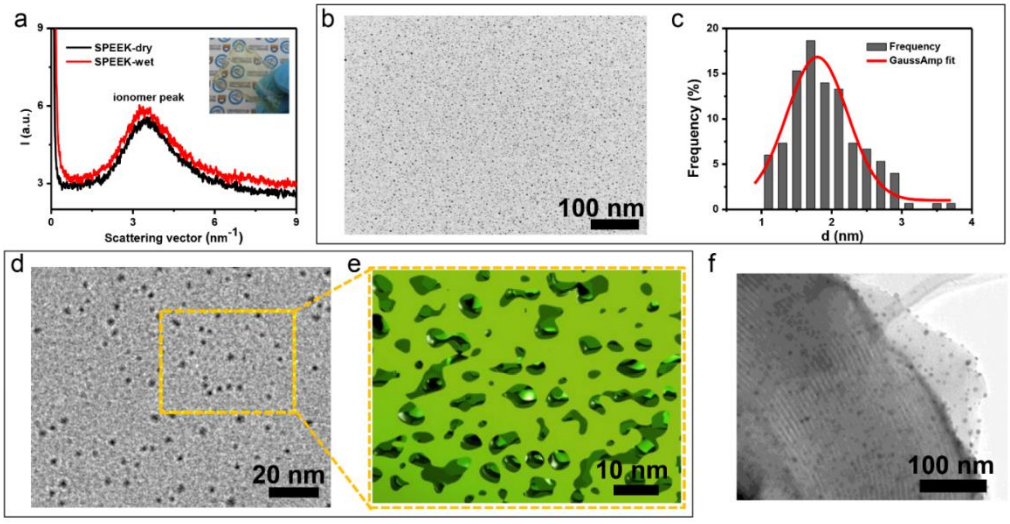

Figure 4.6 Characterizations of SPEEK membrane. a) SAXS data of the polymer membrane before and after soaking in the electrolyte for 24 h. (Inset) Digital photo of solution-casted SPEEK membrane with thickness of approximately 50 μm. b) TEM image of SPEEK membrane stained with silver ions. The darker areas represent hydrophilic domains and the lighter arears represent hydrophobic domains. c) Statistics of the dimension of the hydrophilic domains and the Gauss fitting profile. d) 2D raw image and e) the corresponding 3D reconstruction of Ag+-stained SPEEK membrane. f) TEM image of Ag+-stained SPEEK membrane wrapping CMK-3 particles.

The nanoscale structure of the polymer, particularly the inherent negatively charged nanochannels, was characterized by small-angle X-ray scattering (SAXS) and Transmission Electron Microscopy (TEM). The average diameter of the channels was determined to be 1.8 nm, calculated ($d = 2\pi/q$) using the $q = 3.5$ nm^{-1} of the ionomer

peak (Figure 4.6a).[187, 188] To evaluate the maintenance of the nanochannels structure of SPEEK in electrolyte, a piece of the SPEEK membrane after being immersed in the electrolyte for 24 h was characterized by SAXS. The ionomer peaks of the two samples overlapped with each other, demonstrating that the nanochannels structure would remain the same even in the electrolyte. Besides, the robustness of the SPEEK membrane was also proved, for the physical shape of the membrane was maintained in the electrolyte without evident swelling or dissolution.

In order to clearly observe the hydrophilic nanochannels, SPEEK was stained with Ag^+, as the staining with heavy metal enlarged the contrast between the hydrophilic domain and the hydrophobic domain of the polymer (Figure 4.6b).[189] The spreading dark areas refer to the hydrophilic nanochannels and the brighter region represents the hydrophobic domain. The size distribution of darker domains indicates the average diameter of 1.8 nm (Figure 4.6c), which agrees well with the result of SAXS analysis.

3D structure reconstruction of SPEEK was also obtained by TEM tomography data with tilt angle range of ±60°, in increments of 2°. A raw image of the SPEEK specimen can be seen in Figure 4.6d. 3D rendering of this specimen was completed by Chimera[190] after structure reconstruction of TEM tomography, which is a technique broadly applied in biological field.[191, 192] The corresponding 3D image of the square region marked by yellow imaginary frame is shown in Figure 4.6e. In contrast to the 2D image, the nanochannels formed by the hydrophilic domain (transparent region) are observed to be networked and across the membrane. This 3D reconstruction tomography gives us direct evidence about the networked-channel structure and paves the way for analysis of similar polymers comprised of separated hydrophilic and hydrophobic microphases.

The proposed structure of the integrated cathode with SPEEK membrane and S/CMK-3 composite, as revealed in Figure 4.1, was proved by TEM observation. It has been demonstrated that SPEEK possesses excellent film-forming ability, at thickness levels ranging between nanometer and micrometer. However, because of the similar contrast between the polymer material and the carbon material, it was difficult to distinguish them in TEM images. Besides, the main elements are the same (i.e. carbon) for the two materials, hence the tool of Energy dispersive spectrometry (EDS) can hardly be utilized for the characterization. Therefore, in order to clearly identify the polymer membrane, the Ag^+-stained SPEEK was used to replace the bare SPEEK polymer. In result, the SPEEK membrane with both darker and lighter nanosized domains was obviously seen wrapping the carbon material of CMK-3 with ordered structure (Figure 4.6f).

SPEEK is a sulphonated aromatic polymer with bulk region of the aromatic polymer skeleton and networked nanochannels with a diameter of ~ 2 nm. The sulphonate groups uniformly distribute at the surface of the nanochannels for ionic interaction with a surface charge density σ_0. According to the solution theory by de Gennes[193], in semidilute solution, polymer coils are densely packed and the surface charge density of sulphonate groups is calculated as follows: $\sigma = f / r^2$, where f is the divided number of sulphonate groups and r is the radius of gyration. Based on reptation model[194], considering that f/r^2 is just about the densely packed polymer coils with size of radius of gyration applying to solution of polymer at overlap concentration, and the polymer film was prepared using larger concentration of polymer solution, so here a rectified factor A (A > 1) is introduced to make the model approach to the experiment. Then the area density of sulphonate groups should be: $\sigma_0 = A * f/r^2$. According to the experimental data and the theoretical value, the σ_0 is assumed to be approximately 0.16 C/m^2.

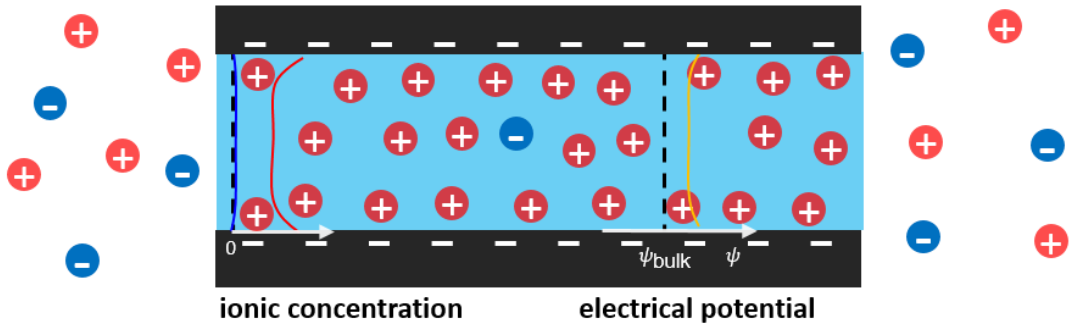

Figure 4.7 Surface charge governs the ion transport behavior in nanochannels. When the radius of the channel is comparable to Debye length, the electric potential (yellow) in the nanochannels is not equal to the bulk potential. And the counter-ion concentration (red) is much higher than the co-ion concentration (blue).

For simplicity, the networked nanochannels in SPEEK is considered as a cylindrical shape with a diameter of 2 nm with a surface charge density σ_0 generating a surface potential φ_0 and a length L (100 nm) as shown in Figure 4.7.

A two-dimensional symmetric model was used to calculate the ion transport along the nanochannels COMSOL:

(1) Ionic charge distribution in the liquid inside the nanochannels is obtained by Poission-Boltzman equation:

$$\nabla^2\varphi = -\frac{\rho(r)}{\epsilon_r} = -\frac{e\sum_i z_i n_i}{\epsilon_r} \quad (4.1)$$

Where φ is the electrical potential, $\rho(x)$ is the net charge density in the nanochannel, ϵ_r is permittivity of the fluid, n_i is the concentration of the ith ionic species, and z_i is the valence.

(2) Steady-state Nerest-Plank equation for ion motion:

$$\nabla \cdot \overrightarrow{N_i} = \nabla \cdot (n_i\vec{v} - D_i\nabla n_i - \mu_i n_i \nabla U) = 0 \quad (4.2)$$

Where $\overrightarrow{N_i}$ is the ionic flux density of *i*th ionic species, D_i is the diffusivity and is μ_i the mobility.

The net charge density inside pore, *ρ(r)* is obtained by the Poisson-Boltzmann equation, Boltzmann distribution, and Debye-Hückel theory (*r* is the radial position (*0≤r≤R/2*))[195], as a function of the wall potential *φ0*.

$$\rho(\mathrm{r}) = -\epsilon\kappa^2\varphi_0 \frac{I_0(\kappa r)}{I_0(\kappa R)}$$

(4.3)

where ϵ is the permittivity of the electrolyte solution, and I_0 is the zero-order modified Bessel function of the first kind.

The negative charge on the surface governs the ion transport behaviour in the nanochannels (Figure 4.7). The charge induces an electrical double layer (EDL) containing an excess of cations of which the thickness is comparable to the Debye screening length κ^{-1} (Debye length ($\kappa^{-1} = \epsilon_r\epsilon_0 kT/2z^2e^2N_a c$), where ϵ_0 is the permittivity of free space, ϵ_r is the dielectric constant of solvent DOL and DME, *k* is the Boltzman constant, N_a is the Avogadro number, *T* is the absolute temperature, e is the charge of an electron, *c* is ionic strength of the electrolyte in moles per m^3). And the Debye screening length κ^{-1} is about 1 nm (lowest concentration 10 mM). So the radius of the nanochannels is comparable to the Debye length which determines the ideal cation permselectivity[165].

Consider the concentration of the LiTFSI solution to be 0.1 mol L^{-1} in DOL and DME, and the surface charge density is 0.16 C m^{-2}. Figure 4.8 shows the concentration of ions in SPEEK nanochannels in *x* direction along the axis of symmetry, from which the concentration difference between Li^+ and $TFSI^-$ can be read to be about 1000 mM which is larger than the bulk concentration. So there is a large potential barrier for anions pass through the channels. In this case, the channels become essentially a unipolar solution

of cations which agree to the visual experiment in Figure 3a very well. With such high surface charge density in SPEEK membrane, the nanochannels are unipolar solution of lithium ions and the anions (polysulphides) are essentially repelled from the channels, thus keep the loss of sulphur from dissolved into the electrolyte.

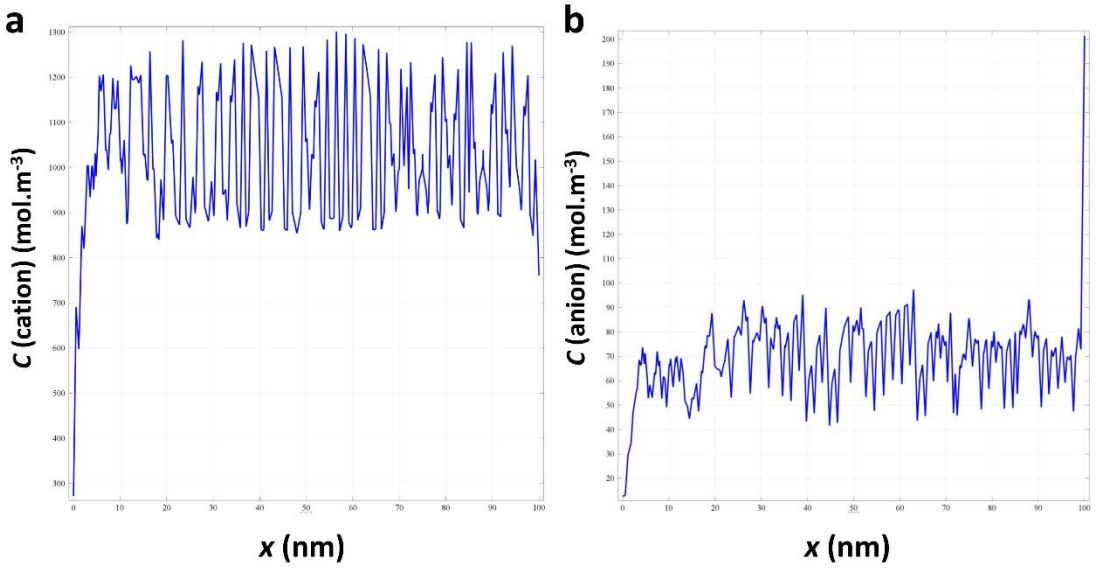

Figure 4.8 The concentration of ions in negatively charged nanochannels along the *x* direciton. The surface charge is considered to be 0.16 C m^{-2}. The bulk concentration of LiTFSI solution is 0.1 mol L^{-1} in DOL and DME.

As discussed above, the concentration of counter-ion (lithium ion) are enhanced in the negatively charged nanochannels. When an external potential *E* is applied across the SPEEK membrane, the net lithium ions will produce an electroosmotic flow (EOF). This EOF increases the drag force on the enriched lithium ions in the channels which enhance the translocation speed of lithium ions through the cathode/electrolyte interface as shown in Figure 3d.

In the nanochannels, surface charge will affect both ion permselectivity[165] and translocation speed.[196] In this work, the SPEEK polymer possesses negatively charged nanochannels with diameter of ca. 2 nm. To verify the ion permselectivity of SPEEK membrane, a visual experiment was conducted by mounting the SPEEK

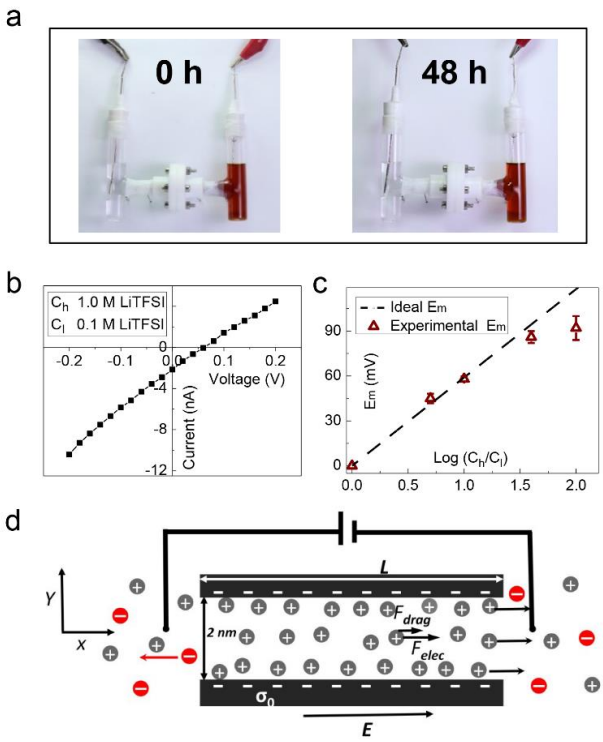

Figure 4.9 Ion-regulation property of SPEEK membrane. a) Visual evidence of SPEEK membrane regulating ion transport. The left side is LiTFSI (0.1 M) and the right side is Li2S8 (0.1 M) in 1,3-dioxolane (DOL) / 1,2-dimethoxyethane (DME) (*v*/*v* = 1:1). b) I-V curve in the case of a concentration ratio of 10 for the electrolyte solution with 1 M in one side and 0.1 M in the other side. The solution is LiTFSI in DOL/DME (*v*/*v* = 1:1). c) Comparison of membrane potentials obtained for the SPEEK membrane and the values showing ideal cation permselectivity (the dashed line); each experimental data point is the average of five replicate measurements. d) Schematic depiction of the negatively charged nanochannels in SPEEK membrane facilitating the transport of lithium ions and rejecting anions. Inside the nanochannels, it is almost a unipolar solution of lithium ions without the presence of anions.

membrane between two half-cells of an H-type glass cell (Figure 4.9a) with one side containing lithium bis(trifluoromethanesulphonyl) imide (LiTFSI, 0.1 M) as an electrolyte and the other side a colored lithium polysulphide solution (Li_2S_8, 0.1 M). The electrolyte solution still remained colorless even after voltage sweeping between -0.5 V and 0.5 V for 48 h at a rate of 0.05 V s^{-1}. The corresponding *I-V* curve is shown in Figure 4.10 in the Supporting Information. In spite the high

current produced, no colour change on the LiTFSI side of the glass cell was observed, showing that the SPEEK membrane can reject the polysulphide anions to migrate through the nanochannels but allow the transport of lithium ions with the observed current flow. This important experimental phenomenon leads us to hypothesize that inside the channels it is a unipolar solution of lithium ions without the presence of polysulphide anions.

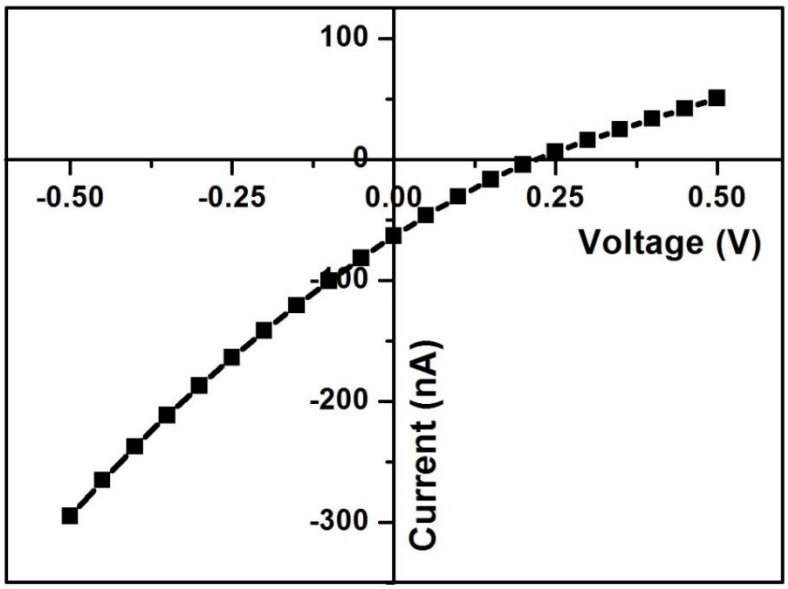

Figure 4.10 *I-V* curve of an SPEEK membrane set in an H-type glass cell with one side containing LiTFSI (0.1 M) and the other side with coloured lithium polysulphide solution (0.1 M).

The cation permeability was quantitatively studied by mounting the SPEEK membrane between asymmetric chambers with different concentrations of LiTFSI solution (one with a lower concentration (C_l) and the other with a higher concentration (C_h)). The *I-V* curve collected when the concentration ratio was 10 (Figure 4.9b) indicates a three-order preference for Li^+ over $TFSI^-$ according to equation 1, the Goldman-Hodgkin-Katz (GHK) equation [162]:

$$P_{Li^+}/P_{LTFSI^-} = \frac{(C_{LTFSI^-})_h * e^{\frac{V_r F}{RT}} - (C_{LTFSI^-})_l}{(C_{Li^+})_h - (C_{Li^+})_l * e^{\frac{V_r F}{RT}}}$$

(4.4)

Where V_r is the reversal potential which can be read from the intercept of the current-voltage curve with the X axis, C_x is the concentration of ion x, F is the Faraday constant, R is the gas constant, T is the absolute temperature, subscripts h and l represent the high and low compartments, respectively.

The reversal potential was compared with the membrane Em, which is calculated by the Nernst equation: $E_m = (t_+ - t_-)\ln(C_h/C_l)RT/zF$, where z is the charge of the ions, t_+ and t_- are the transference numbers for cations and anions, respectively. As shown in Figure 4.9c, the reversal potential is comparable to the ideal membrane potential, reflecting the ideal cation permeability property of SPEEK, which agrees well with the theoretical analysis result.[165]

For the negatively charged nanochannels in SPEEK, not only lithium ions are permeably transported and the polysulphide anions are rejected, but also the translocation speed of lithium ions is enhanced. The negative sulphonate groups of SPEEK uniformly distribute at the surface of networked channels with a diameter of ca. 2 nm. The surface charge induces an electrical double layer (EDL), which possesses a thickness comparable to the Debye length (Figure 4.7). The EDL contains an excess of cations to compensate the fixed surface charge. According to the theoretical analysis, it is assumed that inside the channels, it is almost a unipolar solution of lithium ions (Figure 4.8). With a high surface charge density in SPEEK membrane, the nanochannels are unipolar solution of lithium ions and the anions (including polysulphide ions) are essentially repelled from the channels. These properties of the negatively charged

nanochannels in SPEEK membrane lead to an ideal cation permselectivity. Moreover, when an external potential is applied across the SPEEK membrane, the net lithium ions will produce an electroosmotic flow (EOF). This EOF increases the drag force on the enriched lithium ions in the channels, enhancing the translocation speed of lithium ions and rejecting the anions to pass through (Figure 4.9d).

Based on the experimental and theoretical results, the negatively charged nanochannels in SPEEK membrane enable rapid transport of cations (e.g., lithium ions) and reject anions (e.g., polysulphides), which holds a great potential in application in the cathode of the Li-S battery. In order to demonstrate this key property of the SPEEK polymer, the SPEEK polymer membrane was integrated in the sulphur cathode with significantly enhanced electrochemical performance.

The SPEEK and the S/CMK-3 composite was integrated to form sulphur cathode through a dispersion-evaporation strategy. Sulphur was filled into the channels of CMK-3 by melt-diffusion method and an S/CMK-3 sample with sulphur contents of 48 wt% was produced. In the process of electrode preparation, SPEEK was dissolved in N-methyl-2-pyrrolidone (NMP) and then S/CMK-3 composite was added to form the dispersion, which was coated on aluminium foil using a doctor blade and heated at 50ºC to eliminate the NMP solvent. During this process, SPEEK film was formed to wrap the sulphur/carbon composite because of (1) the excellent film-forming ability of SPEEK and (2) the strong thermodynamic driving force in eliminating hydrophobic interface.[197, 198] In this novel integrated sulphur cathode, SPEEK membrane locates between the sulphur and the liquid electrolyte; the negatively charged nanochannels across the SPEEK membrane regulate the ion transport of both Li^+ and S_x^{2-} ions[165], hence mediate the electrochemical performance of the novel cathode.

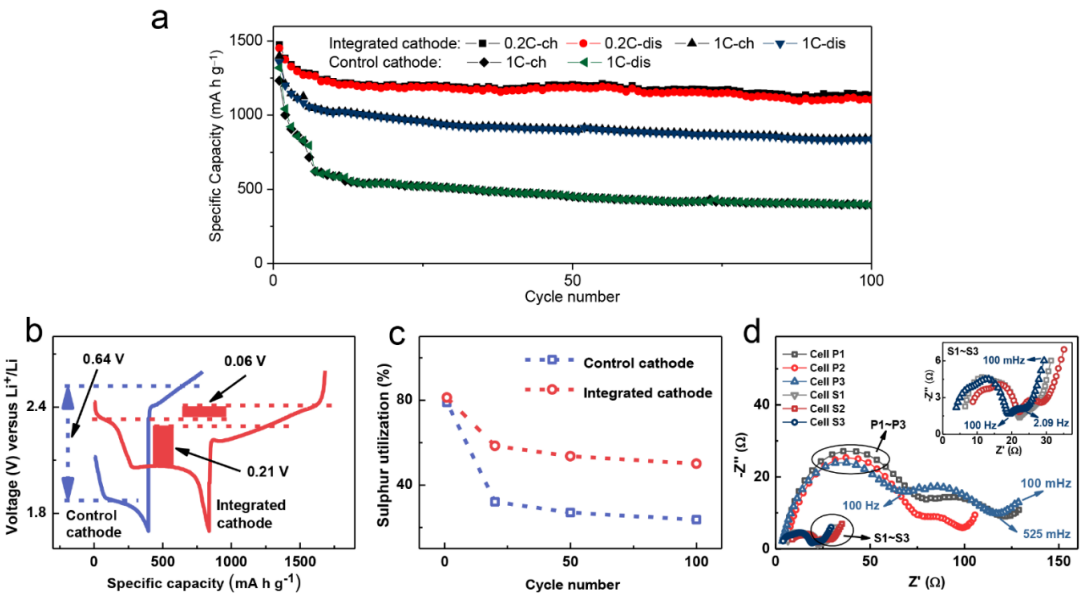

Figure 4.11 Comparison of electrochemical performances between the integrated cathode and the control cathode. a) The cycling profiles of the integrated cathode at 0.2 C and 1 C and that of the control cathode at 1 C. b) Galvanostatic charge/discharge profiles at the 100th cycle for the integrated cathode and the control cathode at 1C. c) Plot of sulphur utilization versus cycle number for the integrated cathode and the control cathode. d) Nyquist plots of the cells for the Integrated cathode (S1~S3) and the control cathode (P1~P3) at charged state after 100 cycles.3 cells were tested for each cathode. The integrated cathode contains 10 wt% of SPEEK (S/CMK-3: Super P: SPEEK = 8:1:1).

The integrated cathode, which possesses the ion-regulation property of the involved SPEEK polymer membrane, was demonstrated in Li-S batteries. It is well-known that the diffusion of the dissolvable polysulphide anions into the electrolyte from a sulphur cathode could cause quick capacity decay. For the integrated cathode, the polysulphide-rejecting ability of the polymer membrane will significantly improve the cycling stability. As shown in Figure 4.11a, the integrated cathode shows high capacities and stable cycling at 0.2 C and 1 C. The initial specific capacities are 1452 and 1358 mA h g^{-1}, respectively. Moreover, high capacities of 1105 and 838 mA h g^{-1} are retained after 100 cycles at 0.2 C and 1 C,

respectively. In comparison, at 1 C, the 100th-cycle capacity of the control cathode is 395 mA h g^{-1}, much lower than that of the integrated cathode. Besides, the integrated cathode shows markedly lower hysteresis. The charge/discharge voltage profile (Figure 4.11b) of the integrated cathode presents two discharge plateaus at 2.3 and 2.1 V and two charge plateaus at 2.3 and 2.4 V, in accordance with the CV results (Figure 4.12). In contrast, the charge/discharge voltage profile of the control cathode exhibits one discharge voltage platform at a much lower voltage (1.9V) and one sloping curve centered at 2.5 V, much higher than that of the charge process for the integrated cathode. The significantly higher capacity and lower hysteresis together make the specific energy density of the integrated cathode much higher than that of the control cathode. The higher sulphur utilization of the integrated cathode also indicates the polysulphide-retaining property of the SPEEK polymer membrane (Figure 4.11c). The integrated cathode has a sulphur utilization (50%) more than twofold that for the control cathode (23.6%) after 100 cycles, though the utilizations for the initial cycle are similar (approximately 80%) for the two cathodes. The greatly improved capacity, enhanced cycling stability and the increased sulphur utilization of the integrated cathode indicates that the SPEEK polymer membrane greatly blocks the diffusion of the polysulphide anions into the electrolyte, as demonstrated by the visual experiment.

Additionally, the electrochemical kinetics of the integrated cathode is significantly enhanced, as evidenced by the electrochemical impedance spectroscopy (EIS) results. EIS is a useful tool in evaluating the reaction mechanism and kinetics of an electrochemical system. As have been stated, the negatively charged nanochannels across SPEEK membrane enhance the transport of lithium ions and reject the diffusion of negative polysulphide anions. Therefore, the sulphur cathode integrated with the SPEEK membrane holds the potential to

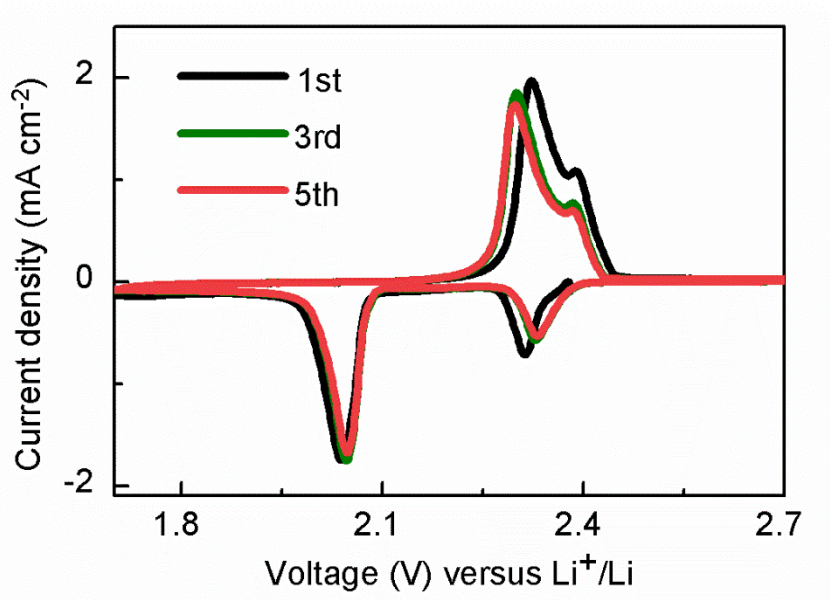

Figure 4.12 CV curves of the integrated sulphur cathode. The two reduction peaks at approximately 2.05 and 2.3 V imply that two discernible discharging processes exist, that is, sulphur is reduced to form polysulphide intermediates and then the end products of Li_2S_2/Li_2S. Two overlapping oxidation peaks at 2.3 and 2.4 V indicate two stages of the charge procedure with close reactive potentials.

improve the electrochemical kinetics of the corresponding Li-S cell. Besides, for the conventional sulphur cathode, the polysulphides diffuse out of the carbon nanochannels of CMK-3 and transform into sulphur at the charged state and Li_2S/Li_2S_2 at the discharged state. The insulating products of sulphur or Li_2S/Li_2S_2 accumulate on the carbon surface and can be a barrier for both the Li^+-ion transport and the electron transfer. In this regard, the polysulphides-rejecting property of the SPEEK membrane can greatly reduce the impedance resulted from the solid product accumulation. Furthermore, the Li^+-facilitating ability of the polymer membrane also enhances the electrochemical kinetics and lowers the impedance. These important properties are revealed by the significantly decreased two depressed semicircles (Figure 4.11d). Integrated cathodes and control cathodes, each with 3 samples, were

examined. All the six curves are composed of two depressed semicircles and one sloping line. One of the semicircles locates in the high frequency (HF) region (100 kHz – 100 Hz) and the other in the middle frequency (MF) region (100 Hz – 1 Hz), while the sloping line in the low frequency (LF) region (1 Hz – 0.1 Hz) (Table 4.1).

Table 4-1 Frequency regions of the Nyquist plots of the six cells with the integrated cathodes and control cathodes after 100 cycles.

Cells		HF region (Hz)	MF region (Hz)	LF region (Hz)
Integrated cathodes	S1	100 k ~ 100	100 ~ 2.089	2.089 ~ 0.1
	S2	100 k ~ 229	229 ~ 2.754	2.754 ~ 0.1
	S3	100 k ~ 100	100 ~ 2.754	2.754 ~ 0.1
Control cathodes	P1	100 k ~ 174	174 ~ 0.692	0.692 ~ 0.1
	P2	100 k ~ 76	76 ~ 0.692	0.692 ~ 0.1
	P3	100 k ~ 100	100 ~ 0.525	0.525 ~ 0.1

The equivalent electrical circuit for the Nyquist plots is presented in Figure 4.13a. Re represents the electrolyte resistance. R_{sei}//CPE1 corresponds to the HF semicircle, representing the resistance and capacitance in the HF region. Rsei represents the impedance of the solid-electrolyte interface, which refers to both the cathode/electrolyte and anode/electrolyte interfaces. The circuit element of CPE (constant phase element) is used here to replace Capacitance in order to take into account the non-ideal property of the real electrode, the surface of which to some extent is porous and rough. R_{ct}//CPE2 is attributed to the MF semicircle, representing the charge-transfer resistance and capacitance in the MF region.

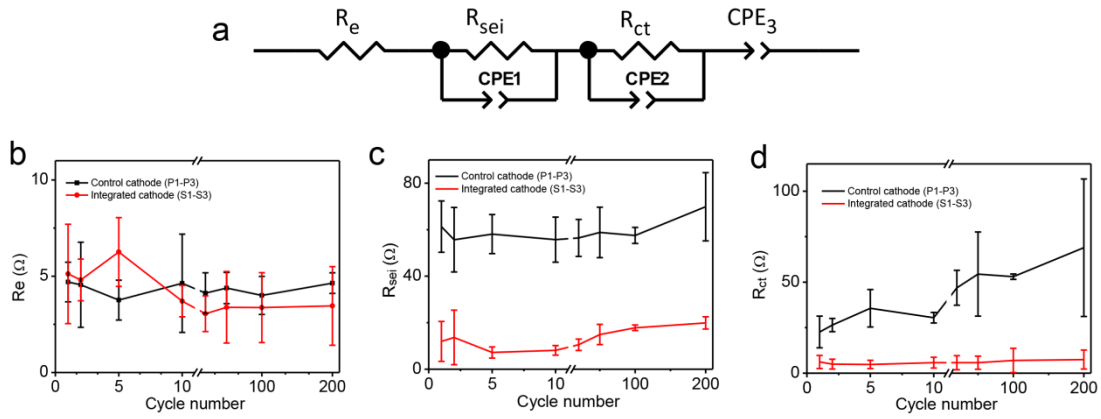

Figure 4.13 Analysis of the resistance parameters of Li-S batteries. (a) Equivalent electrical circuit for the Nyquist plots of the Li-S batteries at charged state for both the integrated cathode and the control cathode. (b) Plots of Re versus cycle number for the integrated cathodes (S1~S3) and the control cathodes (P1~P3). (c) the same as in b, but for R_{sei}. (d) the same as in b, but for Rct. Error bars are added in (b-d) to indicate the measurement uncertainty.

As for the inclined line in the LF region, although in the literature, Warburg impedance (W_o) is used for modelling the ion diffusion in the electrode. However, it is found that either the W_o-R or W_o-T needs to be "fixed", otherwise the fitting would fail. Therefore, CPE3 is used for the LF region to represent an infinite length Warburg element.

All the Nyquist plots are fitted and the resistance values are plotted against cycle number. As shown in Figure 4.13b, R_e is similar and stable for both the integrated and control cathodes. In Figure 4.13c, R_{sei} for the integrated cathodes is much smaller than the control ones. With the cells cycled, polysulphides diffuse out of the channels and are oxidized to solid sulphur. For the integrated cathode, the polysulphides are blocked inside the carbon nanochannels by the negatively-charged nanochannels across SPEEK membrane, hence less sulphur accumulated on the carbon surface and the R_{sei} is much smaller. Meanwhile, the accumulation of the polysulphides on the lithium anode has also been greatly decreased, which leads to lower impedance compared to that of the

control cells. Both the cathodes have a trend of decreasing in the initial 10 cycles and then increasing in the following cycles. This phenomenon might be caused by the "activation" process in the initial several charge/discharge cycles. However, with the cycles increasing, the accumulation of inactive solid sulphur species on the carbon surface becomes more severe and the impedance grows. As for R_{ct}, the values for the

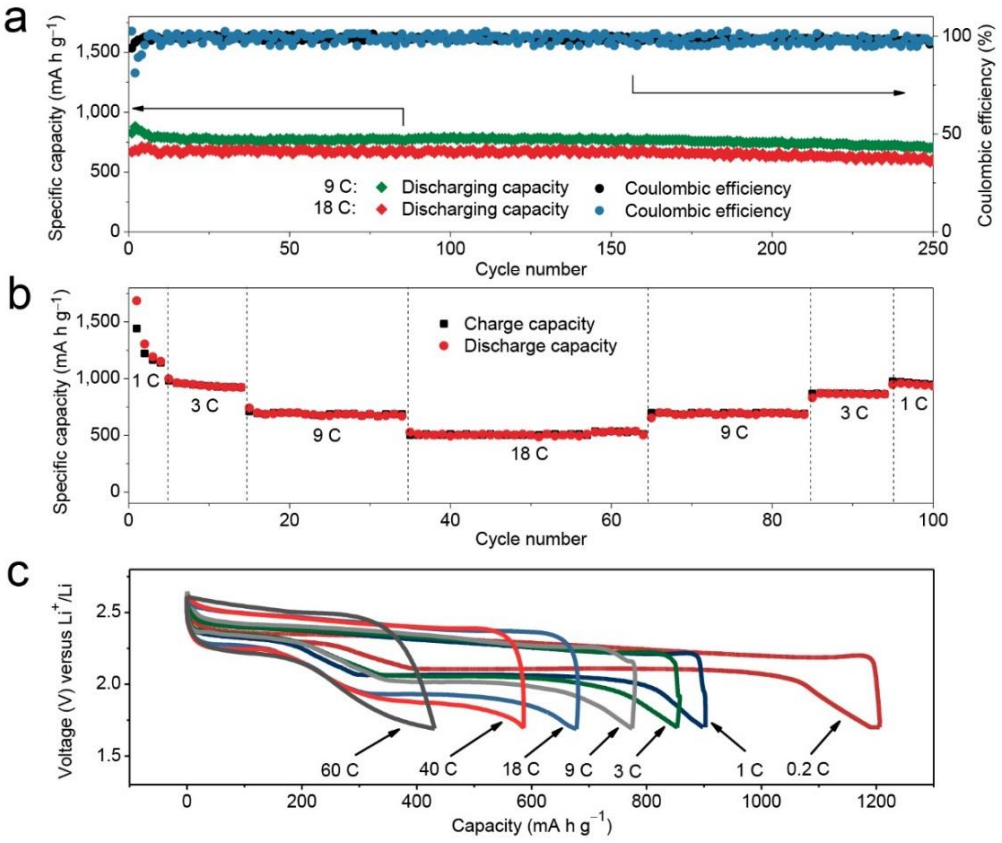

Figure 4.14 High-rate properties of the integrated cathode. a) Discharge capacity and Coulombic efficiency over 250 cycles at current densities of 9 C and 18 C, respectively. b) Cycling stability of a Li-S cell at different rates ranging from 1 C to 18 C. c) Charge and discharge voltage profiles at different rates of 0.2 C, 1 C, 3 C, 9 C, 18 C, 40 C and 60 C. The cathode contains 20 wt% of SPEEK (S/CMK-3: Super P: SPEEK = 6:2:2).

integrated cathodes are much smaller than those for the control cathodes for the Li^+-ion enhancing property of negatively charged nanochannels in the integrated SPEEK membrane. Also should be noted is that R_{ct} for the integrated cathodes keeps almost

stable with cycling, while for the control cathodes R_{ct} becomes larger. The smaller and more stable R_{ct} for the integrated cathodes demonstrates that the integrated SPEEK membrane has the potential of evidently improving the electrochemical kinetics and stabilizing the electrode in operation.

The low impedance of the integrated cathode, together with the strong retaining ability for the polysulphide anions, results in stable high-rate battery performance. At 9 C, the capacity retains at 708 mA h g^{-1} over 250 cycles with a small capacity decay of 0.059% per cycle (Figure 4.14). At such high rate, the Coulombic efficiency stays at a high level above 96.5%. At 18 C, the initial capacity is 670 mA h g^{-1} and he capacity retention is 91% over 250 cycles. Both the high capacity and excellent Coulombic efficiency prove the high-rate capability and high stability of the integrated cathode. Further, undervaried charge/discharge rates from 1 C to 18 C, a high capacity of 947 mA h g^{-1} is maintained after 100 cycles (Figure 4.14b). The charge/discharge profiles of the integrated cathode at varied rates from 0.2 C to 60 C are presented in Figure 4.14c, demonstrating high capacities and High stabilities in a wide range of rates. Even at extremely high rates of 40 C and 60 C, the cycling stabilities are excellent (Figure 4.15). The high-rate performance of the integrated cathode indicates the Li^+-facilitating property of the SPEEK polymer membrane, the other of the two important aspects of the ion-transport-regulation.

4.4 Conclusions

In summary, the ion-transport-regulating property of the SPEEK membrane was theoretically and experimentally characterized and successfully demonstrated it in lithium-sulphur batteries. The polymer membrane bares negatively charged

nanochannels with a dimension (ca. 2 nm) comparable to the Debye length, which facilitate the transport of the cations (e.g., lithium ions) and reject the anions

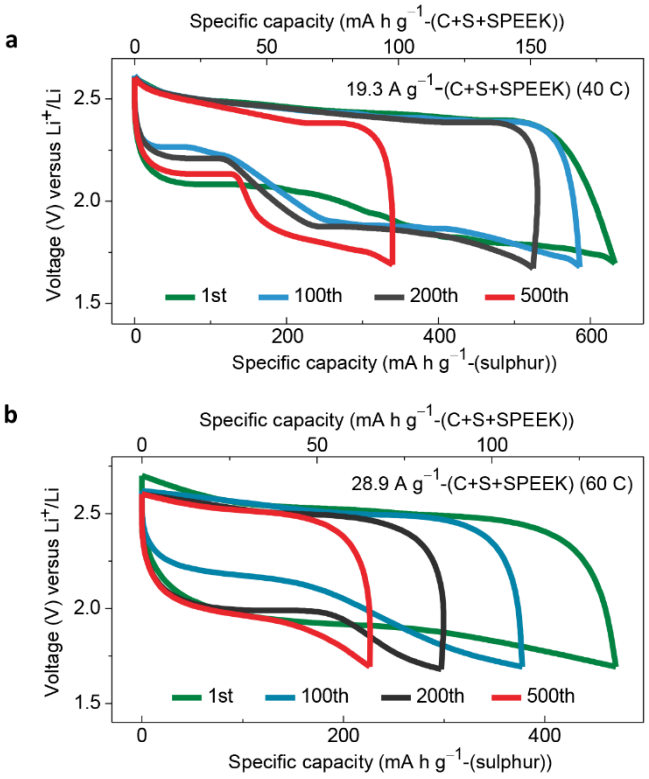

Figure 4.15 Charge and discharge voltage profiles for the 1st, 100th, 200th and 500th cycles at rates of (a) 40 C and (b) 60 C respectively. Based on the total weight of the electrode laminate, the current densities are 19.3 and 28.9 A g^{-1}, respectively. At such high current densities, the capacities reach high level comparable to the best results for conventional intercalation cathode materials at similar high rates. The capacities for the first and 500th cycles are 633 and 340 mA h g^{-1}, respectively. Similarly, at 60 C, the initial capacity is ca. 470 mA h g^{-1} with capacity retention of 48% over 500 cycles.

(polysulphides). The novel integrated sulphur cathode shows stable long-life high-rate cycling. At 0.2 C, the capacity is kept at 1105 mA h g^{-1} after 100 cycles. At a high rate of 18 C, a high capacity of 612 mA h g^{-1} can be kept after 250 cycles. It is believed this novel design of the integrated sulphur cathode with polymer membrane regulating ion transport could open up new opportunities for revolutionizing the traditional ways of advancing battery systems.

CHAPTER 5 IMPROVED CYCLING STABILITY OF LITHIUM-SULPHUR BATTERIES BY ENHANCING THE RETENTION OF ACTIVE MATERIAL WITH A SANDWICHED HYDROTHERMALLY TREATED GRAPHITE FILM

5.1 Preface

Li-S batteries have been considered as promising next-generation batteries owing to their high theoretical specific capacity of 1675 mA h g^{-1} and energy density of 2500 W h kg^{-1}, the abundance and low price of sulphur[7, 199-201]. The theoretical energy density of Li-S batteries is 3~5 times higher than that of conventional lithium ion batteries[116, 175, 202]. These attractive advantages make Li-S batteries an important candidate of energy storage systems for wide applications in electric vehicles and back-up energy storage applicants for renewable and intermittent energies like solar and wind. However, compared to conventional electrode materials ($LiCoO_2$, $LiFePO_4$, etc.), a unique problem for sulphur as the cathode material is the low utilization of the active material sulphur[67, 172, 203]. First, the intrinsic high electrical resistivity of sulphur makes the active material utilization very low, particularly at high rates[204]. Because of the poor transport of both lithium ions and electrons, a certain percentage of the sulphur in the cathode is not able to be participating in the electrochemical reactions. This is one main reason that for a long time, the reported capacity of Li-S batteries was low until Nazar et al. reported a high-capacity Li-S cathode of S/CMK-3 composite, prepared by a melt-diffusion method[74]. Second, apart from the low utilization of

sulphur in the cathode, sulphur is lost in the form of polysulphides, which are the solvable intermediate products in the transformation between the two end products of sulphur and Li_2S. The intermediate polysulphides are dissolved in the ether-based liquid electrolyte and shuttle between the sulphur cathode and the lithium anode, causing quickly decay of the capacity[181, 205-207]. To increase the active material utilization, varied approaches have been applied. For example, sulphur has been incorporated with different carbon materials[76, 82, 174, 180, 208], conductive polymer[93, 171, 183] and metal oxides[85, 100]. Also, the interlayer strategy proves effective in decreasing the polysulphide shuttling problem[134, 209].

Here, we report a new configuration of Li-S batteries using a graphite film sandwiched between the sulphur cathode and the separator (Figure 5.1). The cathode material is sulphur/Super P composite (S/SP). The graphite film was hydrothermally treated in order to anchor functional groups of carbonyl and carboxyl, which have strong affinity with the polysulphides. The graphite film suppresses the polysulphide shuttling problem and provides extra reaction sites for the sulphur species, thereby improves the active material utilization, the capacity and the cycling stability of the Li-S battery.

5.2 Experimental

5.2.1 Hydrothermal treatment of the graphite film

Graphite films were ultrasonically treated in acetone, and then put into a 100 mL Teflon-lined stainless-steel autoclave. 50 mL of deionized water was added and heated at 120°C for 10 h. After the hydrothermal treatment, the films were ultrasonicated in

acetone and dried at 100 for 4 h and then put into a glove box filled with argon. Before the cells were assembled, the graphite films were soaked in the electrolyte for 24 h.

5.2.2 Material characterizations

S/SP composite was prepared through the reaction between sodium thiosulphate and oxalic acid. Raman scattering experiments were performed on a JOBIN YVON HR800 Confocal Raman system with a 632.8 nm He-Ne laser. The morphology and structure of the samples were investigated by X-ray diffraction (XRD) (GBC MMA), field emission scanning electron microscopy (FE-SEM; JEOL JSM-7500FA) with an energy dispersive X-ray spectroscopy (EDS) detector and transmission electron microscopy (TEM, JEM 1200EX). X-ray photoelectron spectroscopy (XPS) was conducted with a SPECS PHOIBOS 100 Analyser installed in a high-vacuum chamber with the base pressure below 10^{-8} mbar, with X-ray excitation provided by Al Kα radiation with photon energy hυ = 1486.6 eV at the voltage of 12 kV and power of 120 W. XPS spectra were recorded with a 20 eV constant pass energy. The binding energy scale was calibrated using the C1s peak at 284.6 eV.

5.2.3 Electrochemical Measurements

The S/SP composite was mixed with super P and poly (vinylidene fluoride) (PVDF) with a weight ratio of 80:10:10 in N-methyl-2-pyrrolidone (NMP) to form slurry, which was pasted on aluminium foil and then dried in a vacuum oven at 50°C for 24 h. Sulphur content in a typical electrode is around 0.8 mg cm^{-1}. CR 2032 coin-type cells were assembled in an Ar-filled glove box (Mbraun, Unilab, Germany) using lithium

metal foil as the counter electrode. For the new configuration, a piece of graphite film was placed between the sulphur cathode and the separator. The electrolyte was 1 M bis (trifluoromethane) sulphonimide lithium salt (LiTFSI) in a 1:1 vol/vol mixture of 1, 3-dioxolane (DOL)/dimethoxyethane (DME). Cell disassemble was carried out in the glove box; the sandwiched graphite film and the cathode were washed with DOL and dried at room temperature. The cells were charged/discharged at 168 mA g^{-1} using a charger system manufactured by Land Battery Testers. Cyclic voltammetry (CV) was conducted on a Biologic VMP3 electrochemistry workstation at a scanning rate of 0.1 mV s^{-1}.

5.3 Results and Discussion

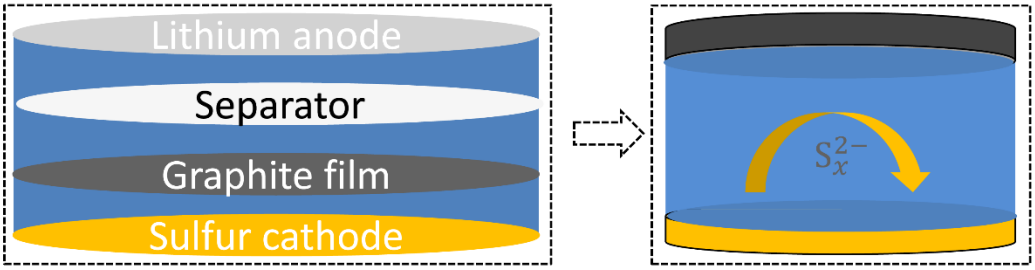

Figure 5.1 A new cell configuration with a graphite film sandwiched between the sulphur cathode and the separator. A lithium metal foil as the anode and a core-shell structured S@SP is used as the cathode material. A hydrothermally treated graphite film is sandwiched between the sulphur cathode and the Celgard 2500 separator.

For the cathode material, a new structure of S/SP composite was prepared. The sulphur in the S/SP composite was confirmed by X-ray diffraction (Figure 5.2a) and Raman spectra (Figure 5.2b). The two peaks at 1345 and 1604 nm-1 are assigned to Super P. As determined by Thermogravimetric analysis, the content of sulphur in the composite is

75 wt%. The core-shell morphology of the composite can be seen from the scanning electron microscopy (SEM) images. The size of the composite is around 10 μm (Figure 5.2c), at the surface of which are linked nanoparticles of Super P (Figure 5.2d). The linked nanoparticles have a diameter of around 40 nm (Inset). The S/SP composite is composed of the micrometer-sized sulphur particle as the core and the linked nanoparticle (~ 50 nm) of Super P as the wrapping layer. We assume the contact coating of Super P improves the conductivity of the micrometer-sized sulphur particles.

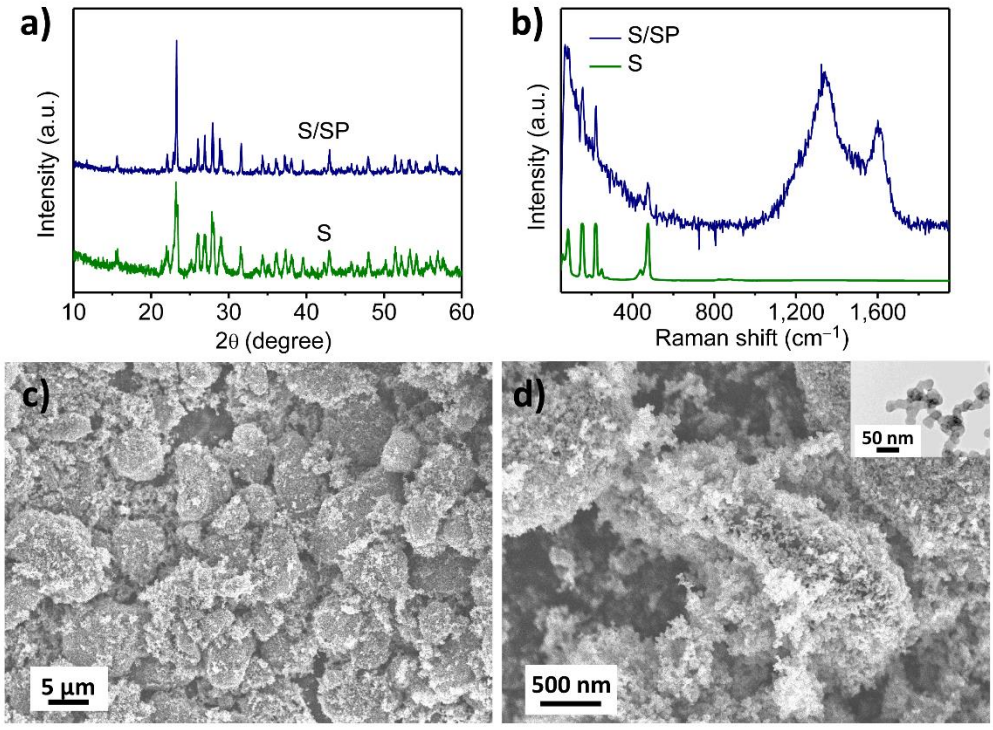

Figure 5.2 Composition, structure and morphology analysis of the as-prepared core-shell structured S@SP composite. (a) XRD patterns and (b) Raman spectra of S@SP and sulphur. SEM images of S@SP composite at magnifications of (c) × 2,000 and (d) × 30,000. The dark areas marked by red dotted circles represent sulphur as the core and the brighter linked nanoparticles are Super P as coating layer.

The graphite film after hydrothermally treated was analysed by XPS and SEM. The XPS C1s spectrum of graphite is presented in Figure 5.3a. The main peak at 284.6 eV

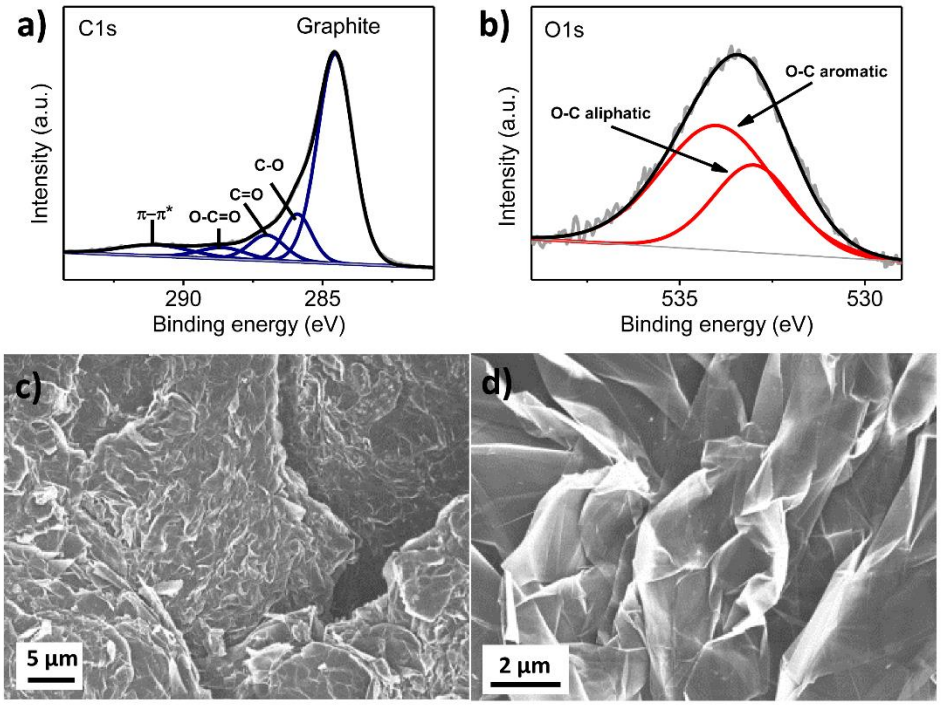

Figure 5.3 Structure and morphology characterization of hydrothermally treated graphite film. XPS spectra for (a) C1s and (b) O1s peaks and fitting curves. SEM images of the inside of the graphite film at magnifications of (c) × 2,000 and (d) × 10,000.

can be assigned to aromatic C-C bonds, and the broad low-intensity peak centred at 291.0 eV corresponds to the π-π* shake up satellite[210]. Between them are the other three peaks, which are at 285.9, 287.0 and 288.6, respectively. It was reported[211] that compared to the graphite C1s peak, single-bonded C-O, double-bonded C=O and carboxylic O-C=O are shifted by ~1.5 eV, 3.0 eV and4.5 eV, respectively. It can be seen that the shifts for these three components match very well with these values. These organic functional groups are also reflected by the XPS O1s spectrum in Figure 5.3b. The peaks at 533 and 534 eV are assigned to O-C sp^3 and O-C sp^2 species, respectively[212]. These oxygen species might have been introduced into the graphite

under the hydrothermal treatment. It is noteworthy that, during the charging and discharging of the modified cell, the organic functional groups on the graphite film might play a glue-like role in retaining sulphur and polysulphides[114]. Moreover, in the graphite film, there are evident cracks (Figure 5.3c), which might have been introduced by the hydrothermal treatment. In the closed environment of the autoclave at 120°C, a temperature above the boiling point of water, the water vapour might strongly interact with the graphite film and produce some channels in it. In another work[213], a certain ratio of carbon black was mixed with reduced graphene oxide to form a free-standing paper for a new Li-S battery configuration, and the function of the carbon black was to produce channels, which enabled the transportation of electrolyte and lithium ions. As can be seen from Figure 5.3d, the graphite film is composed of carbon nanosheets stacking with each other. The nanosheets behave as the reaction sites for the active sulphur species.

The electrochemical performances of cells with and without a graphite film are presented in Figure 5.4. Typical electrochemical reactions are revealed by the CV results (Figure 5.4a). The cathodic peaks at 2.00 V and 2.23 V correspond to the two-step reaction from elemental sulphur to insoluble Li_2S_2 or Li_2S through intermediate soluble polysulphides (e.g., Li_2S_8, Li_2S_6 and Li_2S_4). The overlapping anodic peaks at 2.45 V relates to the inverse reactions, i.e., lithium sulphides are oxidized to lithium polysulphides and elemental sulphur. Initial discharge/charge voltage profiles for the first cycles present one discharge plateau at ~ 2.0 V, followed by a long slope (Figure 5.4b). While for the following two cycles, there are two discharge plateaus: the first at ~ 2.3 V and the second at 2.1 V. The two cycles show high discharge capacities of 1008 and 942 mA h g^{-1}, respectively.

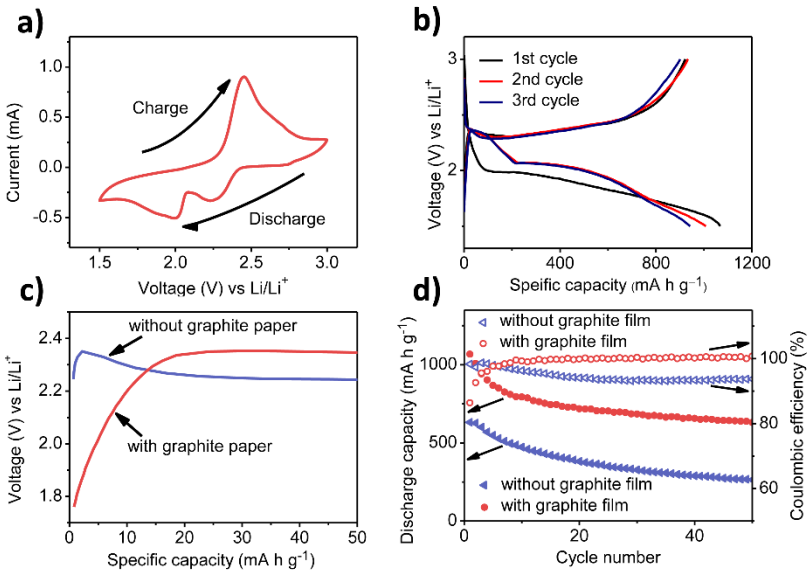

Figure 5.4 Electrochemical performance of the Li-S battery with cathode material of core-shelled sulphur@Super P and graphite film between the separator and the cathode. (a) A typical CV curve of the Li-S battery with new configuratioin. (b) charge/discharge voltage profiles for the first and second cycles of the Li-S battery with new configuration. (c) Charge voltage profiles at the beginning stage of the initial cycles for the cells without and with sandwiched graphite film. (d) Capacity retention and the corresponding coulombic efficiency of the cells without and with sandwiched graphite film.

It is noted that for the first cycle, the discharge voltage plateau is more negative than the following cycles. This phenomenon can be attributed to the affected electrochemical reactions between lithium ion and sulphur owing to the addition of the graphite film[95]. Further investigation is needed to unveil the exact mechanism. Moreover, compared to the cell without the graphite film, the beginning stage of the charge process exhibits a much lower polarization, demonstrating that the graphite film functions as a pseudo-substrate for the sulphur cathode (Figure 5.4c). The graphite film enables much higher capacity, markedly decreased capacity decay and higher electrochemical stability (Figure 5.4d). The cell with the graphite film exhibits a high initial capacity of 1068 mA

h g^{-1}. After 50 cycles, the retained capacity is 631 mA h g^{-1}, triple that of the 203 mA h g^{-1} for the cell without the graphite film.

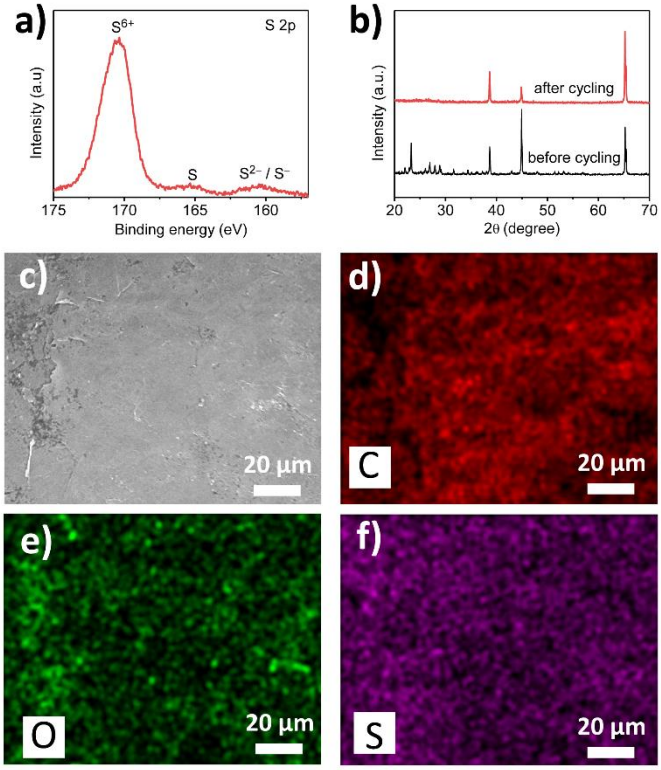

Figure 5.5 Characterization of the cathode and the graphite film after charge/discharge. (a) XRD patterns of the cathode before and after charge/discharge. (b) Raman spectra of the graphite film before and after charge/discharge. (c) The SEM image of the graphite film after charge/discharge and the corresponding XEDS elemental maps for (d) C, (e) O, and (f) S.

In order to exclude the capacity contributed by the graphite film, a Li/graphite film battery was assembled. The contribution from the graphite/Li+ intercalation process was 36 mA h per gram of sulphur, which takes place only ten percent of the whole improvement of capacity. It can be revealed that the graphite film only functions as a polysulphide blocking layer instead of an electrode. It is noted that the graphite/Li+ intercalation happens at a voltage below 0.2 V, while the voltage window here applied is from 1.7 V to 2.6 V. Also, the Coulombic efficiency of the Li-S battery with the new

configuration stabilizes at near 100%, compared to the 94% for the conventional cell configuration. The improved Coulombic efficiency indicates that the sandwiched graphite film plays an important role in suppressing the polysulphide shuttling.

The function of the graphite film was further studied by disassembling the cell and examining the cathode and the graphite film using XRD, XPS, SEM and EDS (Figure 5.5). After 10 cycles, the XRD peaks for sulphur disappear, with only peaks for the aluminium substrate remained, showing that the sulphur in the cathode has turned amorphous (Figure 5.5a). Moreover, the XPS S2p spectrum shows three peaks centred at around 170, 165 and 160 eV (Figure 5.5b). The values of these three peaks match very well with the literature[214], from which they can be assigned to S^{6+}, elemental S, and S^{2-}/S^{-}, respectively. The S^{6+} species could be assigned to residue lithium salt from the electrolyte, while S, S^{-} and S^{2-} are ascribed to the products of the electrochemical reactions that take place on the graphite film. This observation proves that the graphite film locating between the separator and the cathode provides extra place for the electrochemical reactions in the Li-S battery. The sulphur species on the graphite film originate from the solvable polysulphides, that is, the intermediate products in the transformation between the end products of sulphur and Li_2S (Figure 5c-5f). The polysulphides are retained by the functional groups in the graphite film. Hence, they can stay on the graphite film and be oxidized or reduced in the charge/discharge process. In this way, the graphite film functions as a pseudo-substrate, greatly enhancing the retention of active material, improving the capacity, electrochemical stability and cycling capability.

5.4 Conclusions

A hydrothermally treated graphite film was sandwiched between the sulphur cathode and the separator. The functional groups on the graphite film play an important role in retaining the solvable sulphur species. Owing to the improved utilization of active material, the specific capacity was significantly improved for the new configuration. The graphite film in the Li-S cell acts as a blocking layer against soluble polysulphides and provides additional reaction sites for the sulphur species. After 50 cycles, the cell with the graphite film retained a capacity which was almost triple that of the cell without the graphite film. Also, the Coulombic efficiency was increased from around 94% to near 100%, indicating a much more stable Li-S battery.

CHAPTER 6 AN ION SELECTIVE SEPARATOR FOR LITHIUM-ORGANIC BATTERIES

6.1 Preface

Electroactive organic molecules as cathode materials have regained researchers' interest in recent years, after being overwhelmed by $LiCoO_2$ and similar intercalation cathode materials for decades.[14, 16, 28, 145-149] With the intensive research and development that have been conducted both in the academy and in industry, the conventional insertion cathode materials have gradually reached their intrinsic limits in terms of capacity and energy density. In addition, the associated pressure on the environment and resources has become increasingly greater, due to the great demand for the metal oxide ores. Therefore, greater attention has been paid to next-generation cathode materials with high energy density and a low ecological footprint.

Organic molecules, owing to their merits, such as cost-effectiveness, sustainability, chemical tunability, and environmental-friendliness,[150-153] have been considered as a promising alternative to the conventional intercalation cathode materials. The organic electrode molecules and their corresponding semidischarge and discharge products, however, are normally easily dissolved in the organic liquid electrolyte, which causes serious problems, including serious self-discharge and unstable cycling. Taking organic carbonyl electrode materials as an example, the carbonyl groups are reduced at discharge and oxidized to the original state at charge. After being dissolved in the electrolyte, the electroactive organic species accumulate and become inactive at the cathode/separator interface and inside the micropores of the polymer separator, and they

also migrate to the lithium anode to form an unstable solid electrolyte interphase on the anode surface. This irreversible loss of the electroactive species results in unstable batteries. In addition, the organic carbonyl anions shuttle between the cathode and the anode, as in the case of the "polysulphide shuttling problem" in lithium-sulphur batteries, leading to unstable cycling and poor Coulombic efficiency. [116, 173, 215, 216] In this regard, strategies such as polymerization[217, 218] of electroactive small molecules or the use of polymer electrolytes[219, 220] (e.g., polyethylene glycol (PEG) or polyethylene (PEO) based ones) are applied to reduce the solubility, although the polymerization reactions or the preparation of the polymer electrolytes could be complicated or involve tedious processing steps.

The separator[221] in a battery system plays an important role in physically and electronically separating the cathode and anode to prevent short circuits, while allowing wetting by the electrolyte and the transport of lithium ions between the electrodes. Whether at charge or discharge, the lithium ions flow inside the cell, and the electron transfer along the external electrical circuit involves binary cooperative complementary particle movements in the lithium battery system.[222] The separator is hence a key component that is needed to make the battery function as a energy storage system, transforming chemical energy into electric energy at discharge, and vice versa at charge. Actually, besides this fundamental role, the separator can be endowed with additional serviceable functions by applying new configurations or materials, in order to overcome some specific practical problems. For example, to improve its safety and endurance, commercial polymer separator was coated by ceramic particles (e.g., nanosized Al_2O_3 powder).[223] The resulting better wettability of the separator by the electrolyte significantly improves the lithium anode stability and the long-term cycling performance.[224, 225]

For cathodes (e.g., sulphur) with the problem of dissolution of the electroactive species, there have been mainly two directions towards the functionalization of the separator. One strategy is applying ion-selective materials (e.g., Nafion®,[119, 226] lithium superionic conductor,[131, 132] V_2O_5,[125] and reconstructed graphene oxide membrane[127]) to block the electroactive anions (e.g., polysulphides in lithium-sulphur batteries) on the cathode side but not affect the lithium ion transport. The other strategy is coating a layer of conductive carbon on the polymer substrate, so that the coated carbon layer acts as an upper current collector to improve the active material utilization.[227] In contrast, although the lithium-organic battery is also plagued by similar dissolution problems to the lithium-sulphur battery, related studies on the separator are rare.[161]

Herein, we demonstrate a thin bicomponent laminate composed of graphene oxide (GO) and nanoscale conductive carbon, integrating the dual functions of ion-selectivity and upper current collector, which is constructed on a polymer substrate as a novel-configured separator for stable lithium-organic batteries. Taking carbonyl organic electrode materials as an example, the organic molecules and the organic anion discharge products are soluble in the electrolyte (Figure 6.1a). With the application of the bicomponent-laminate-coated separator, the electroactive species are kept on the cathode side, and the utilization is significantly improved (Figure 6.1b).The bicomponent laminate is constructed on the polymer substrate through a simple vacuum filtration approach (Figure 6.1c). The GO sheets are reconstructed into a film with numerous channels between the two-dimensional sheets, which bear negative charge originating from the the carboxylic acid and phenolic hydroxyl groups. The negatively charged nanochannels selectively allow the fast transport of the counterions (e.g., lithium ions) and reject co-ions (e.g., electroactive organic anions). In addition, the conductive carbon layer functions as an upper current collector for reactivating the

inactive electroactive species. With anthraquinone (AQ) and perylene-3,4,9,10-tetracarboxylic dianhydride (PTCDA) as two examples of organic electrode materials, the open circuit voltage (OCV) is effectively stabilized, and the cycling stability is greatly improved compared to the electrodes with the pristine polymer separator.

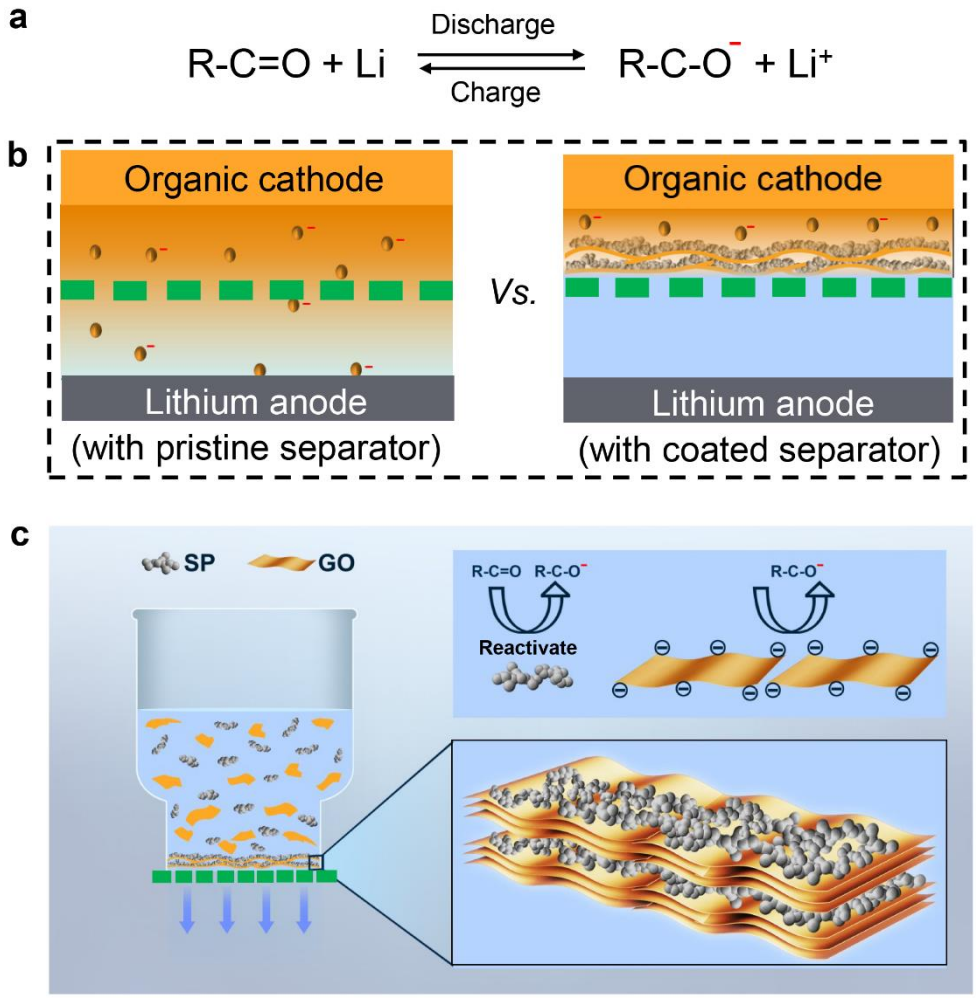

Figure 6.1 Schematic illustrations of the dissolution problem for the organic cathode and the bicomponent laminate structure on the polymer substrate. (a) The electrochemical reaction of an electroactive organic molecule with conjugated carbonyl groups. (b) The blocking of the dissolved electroactive organic molecules and anions by the bicomponent laminate in a lithium-organic battery. (c) Schematic illustration of the preparation of the bicomponent-laminate-coated separator and its functioning mechanism in a lithium-organic battery.

6.2 Experimental

6.2.1 Materials

Anthraquinone (AQ) and perylene-3,4,9,10-tetracarboxylic dianhydride (PTCDA) were purchased from J&K Chemical Co. Graphene and graphene oxide were purchased from the Nanjing XFNANO Co. Celgard 2325 with a layered structure of PP/PE/PP and thickness of 25 μm was purchased from Celgard Corp.

6.2.2 Separator coating

A mixture of graphene oxide and Super P (or graphene) was suspended in deionized water (1 mg ml^{-1}) with the help of sonication. 1 ml of the suspension was re-dispersed in ethanol (10 ml) and vacuum filtrated to yield a coating layer with areal density of around 0.1 mg cm^{-2} on pristine Celgard 2325 separator.

6.2.3 Measurements

The morphologies were observed using field-emission scanning electron microscopy (SEM, Hitachi S4800) and transmission electron microscopy (TEM, JEM 1200EX). A visual experiment was carried out using an H-type glass cell composed of two halves. The electrode was prepared by coating the slurry with AQ onto a nickel foam current collector. A constant potential of 2.2 V was applied with lithium as the counter electrode.

6.2.4 Electrode preparation and battery testing

The AQ or PTCDA was mixed with Super P and the poly(vinylidene difluoride) (PVDF) binder with a weight ratio of 6:3:1, respectively, to form a homogenous slurry, which was coated on carbon-coated aluminum foil to form an organic electrode with active material loading of 1.6 mg cm^{-2}). CR2032 coin cells were assembled in an argon-filled glove box by pairing sulphur cathodes and lithium anodes, and the electrolyte was 1.0 M lithium bis (trifluoromethanesulphonyl) imide (LiTFSI) in a binary mixture of 1,3-dioxolane (DOL) and 1,2-dimethoxyethane (DME) (v/v, 1:1). Galvanostatic charge/discharge was performed on a LAND battery testing machine (Wuhan, China), and a voltage window between 1.7 and 3.5 V was applied. Cyclic voltammetry (CV) curves were recorded with a VSP-300 electrochemical workstation with a sweep rate of 0.1 mV s^{-1}.

6.3 Results and Discussion

To obtain the GO/Super-P (SP)-coated or the GO/graphene (G)-coated separators (denoted as GO/SP-P or GO/G-P), a mixture of GO/SP (w/w, 1:2) or GO/G (w/w, 1:1) was dispersed in deionized water (1 mg ml^{-1}) with the help of an ultrasonic probe. The GO/SP or GO/G mixture was well-dispersed (Figure 6.2a), which might have been resulted from the electrostatic repulsion between the GO nanosheets with high negative charge at the surface, which originates from the carboxylic acid and phenolic hydroxyl groups. The zeta potential was determined to be –34 mV, more negative than –30 mV, which is commonly considered to indicate a mutual repulsion strong enough to ensure a stable dispersion.[228] In contrast, the SP or G particles easily precipitate in the

corresponding aqueous suspensions due to their low surface charge densities (9 and –11 mV, respectively). (Figure 6.2b and 6.2c)

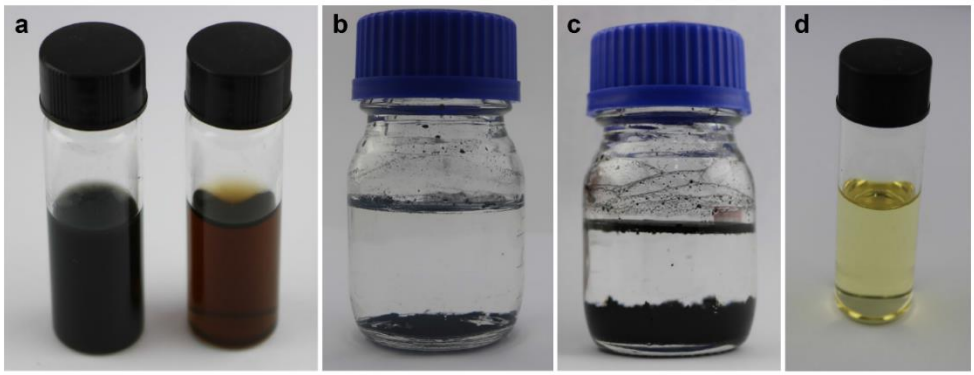

Figure 6.2 Digital photographs of suspensions of (a) GO/SP (left) and GO (right), (b) aqueous suspension of SP (0.1 mg ml^{-1}) after ultrasonication for 1 h and resting for 1 h, (c) aqueous suspension of graphene (0.1 mg ml^{-1}) after ultrasonication for 1 h and resting for 1 h, and (d) concentrated AQ solution in the electrolyte.

The structures of the Celgard triple-layered polypropylene/polyethylene/polypropylene (PP/PE/PP) separator (denoted as pristine P) and the coated bicomponent laminate were characterized by electron microscopy (Figure 6.3). The pristine P is composed of three layers with PE sandwiched between two outer layers of PP, with a total thickness of 25.8 μm and each layer of PP or PE possessing a similar thickness of 8−9 μm (Figure 6.3a). The top-view scanning electron microscope SEM image presents the microporous structure of the polymer separator (Figure 6.3b). The coated bicomponent GO/SP laminate shows a layered structure with SP particles between and on top of the crumpled GO films, with a total thickness of 905 nm (Figure 6.3c). The sub-laminate structure of the reconstructed GO sheets possesses numerous negatively-charged nanochannels; both the thickness of the GO sheets and the width dimension of the thus-formed nanochannels are approximately 1 nm.[129] The negatively charged nanochannels selectively allow the fast transport of lithium ions while rejecting the electroactive organic anions. An examination of the top-view image indicates that there

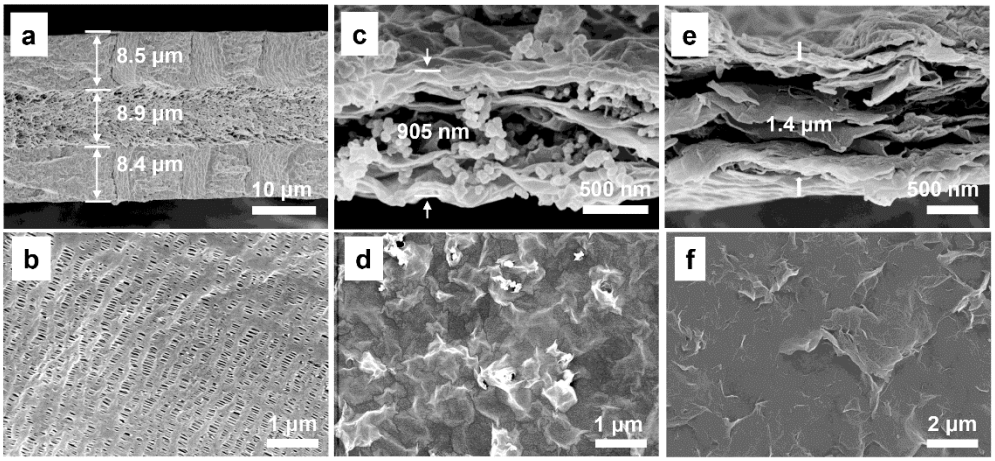

Figure 6.3 Electron microscopy characterization of the pristine and the coated separators. (a) Cross-sectional SEM image of the pristine Celgard 2325 separator with the triple-layered structure of polypropylene/polyethylene/polypropylene (PP/PE/PP). (b) Top-view SEM image of the pristine separator. (c) Cross-sectional and (d) top-view SEM images of the graphene oxide/Super P (GO/SP) bicomponent laminate. (e) Cross-sectional and (f) top-view SEM images of the graphene oxide/graphene (GO/G) bicomponent laminate.

are scattered SP particles (Figure 6.3d) on top of the bicomponent laminate, which would have intimate contact with the organic cathode, acting as an upper current collector. The cross-sectional and top-view SEM images of the other GO/G bicomponent laminate can be seen in Figure 6.3e and 6.3f, respectively. The thickness of the GO/G coating layer is ~ 1.4 µm. The surface of the GO/G bicomponent laminate is crumpled, owing to the overlapping of the GO nanosheets and the G nanosheets, both of which have similar dimensions of several hundred nanometers. Similar to GO/SP, the electronic conductivity of the G and the cation selectivity of the layered GO nanosheets synergistically improve the active material utilization and the cycling stability.

To characterize the coated separators, two typical carbonyl organic molecules, i.e., anthraquinone (AQ) and perylene-3,4,9,10-tetracarboxylic dianhydride (PTCDA), were applied as cathode materials in lithium-organic batteries[154]. AQ (yellow color) and

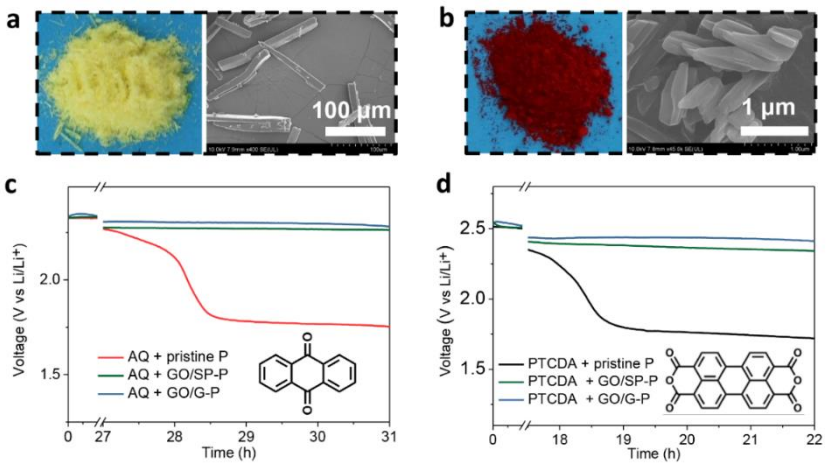

Figure 6.4 Digital photograph (left) and SEM image (right) of the organic molecules of (a) anthraquinone (AQ) and (b) perylene-3,4,9,10-tetracarboxylic dianhydride (PTCDA). Retention of the open-circuit voltage (OCV) of (c) the AQ electrode and (d) the PTCDA electrode with the pristine separator and the coated separators with the dual components GO/SP and GO/G. Insets: the molecular structures of (c) AQ and (d) PTCDA.

PTCDA (red color), both of which are rod-shaped particles, possess 2 and 4 carbonyl groups in each molecule, respectively (Figure 6.4a and 6.4b). As cathode materials, both the AQ and the PTCDA support a two-electron reversible reaction process, which make their theoretical capacities 257 and 132 mA h g^{-1}, respectively (Figure 6.5). The other two carbonyl groups in the PTCDA molecule can be further reduced only at voltages lower than 1.3 V (versus Li^+/Li), so they do not contribute to the capacity when PTCDA is charged/discharged in the range above ~ 2 V (versus Li^+/Li)[229]. The reduction/oxidation potentials of the two organic cathodes are revealed by their cyclic voltammetry (CV) curves. The CV curve for the AQ electrode presents a reduction peak at ~ 2.2 V and an oxidation peak at ~ 2.4 V (Figure 6.6a). In this ether-based electrolyte system, the two steps of the reduction or oxidation reaction cannot be distinguished, but are expressed by only one peak[230]. For the CV curve of the PTCDA electrode (Figure 6.6b), there are two reduction peaks (at ~ 2.4 V and 2.5 V) and one oxidation peak (at ~

2.7 V). The voltage profiles of the electrodes under galvanostatic charge/discharge agree well with the corresponding CV curves (Figure 6.6c and 6.6d).

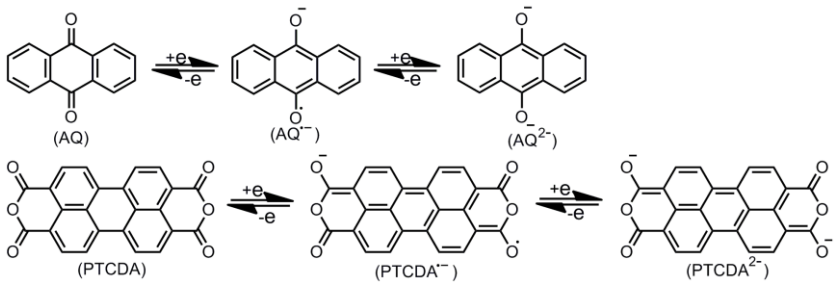

Figure 6.5 Electrochemical redox mechanism for the two molecules: AQ and PTCDA.

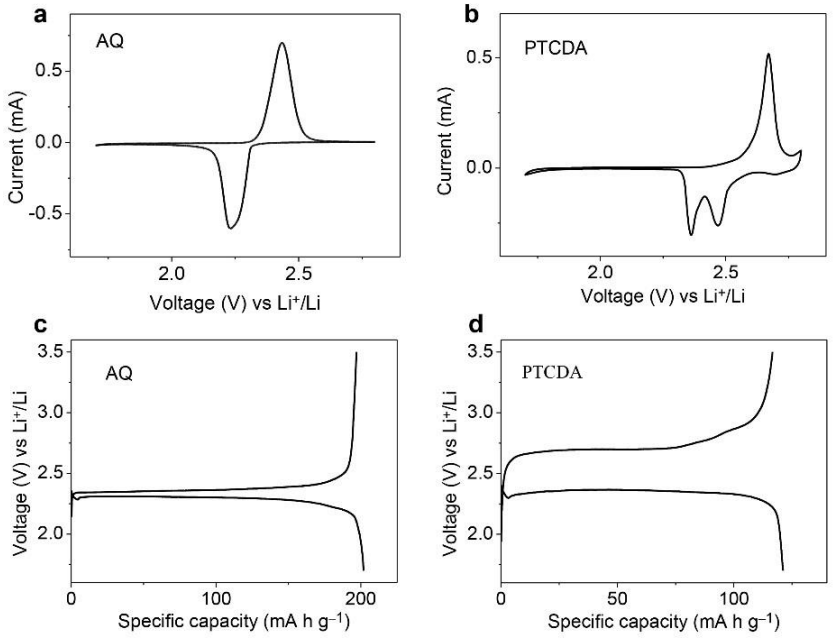

Figure 6.6 Typical cyclic voltammetry (CV) curves and charge/discharge voltage profiles of the AQ electrode (a and c, respectively) and the PTCDA electrode (b and d, respectively).

The open-circuit voltages (OCVs) of the AQ and the PTCDA electrodes with the coated separators remain significantly more stable than those with the pristine P, as shown in Figure 6.4c and 6.4d. The OCVs of the AQ and the PTCDA electrodes with the pristine P drop to approximately 1.7 V after resting for 31 and 22 h, respectively, far below the discharge voltage plateaus, while those with the coated separators are retained very well.

When the battery with the pristine P was rested, the ongoing process of organic molecule dissolution inevitably resulted in the OCV drop, which seriously shortens the shelf-life of the batteries. In contrast, for the bicomponent-laminate-coated separators, the coating layer of GO/SP or GO/G functions as a buffering zone to mitigate the migration process of the soluble organic materials, which greatly stabilizes the OCV and alleviates the self-discharge of the electrodes.

The GO/SP or GO/G bicomponent laminate improves not only the OCV stability of the AQ or the PTCDA electrode, but also the capacity and the cycling stability (Figure 6.7). At 100 mA g^{-1}, the AQ electrode with GO/SP-P or GO/G-P shows higher capacities at the initial cycle, and the GO/SP-P in particular exhibits an initial capacity of 233.3 mA h g^{-1}, compared to 201.9 mA h g^{-1} for the pristine P (Figure 6.7a). After 150 cycles, both the coated separators show similar capacities twofold that of the 50 mA h g^{-1} for the pristine separator. The greatly improved capacities can also be observed from the comparison of the charge/discharge voltage profiles. For instance, the voltage profiles for the cells with the GO/SP-P and the pristine P after 100 cycles show similar charge/discharge plateau voltages (Figure 6.7b), although the discharge capacity for the coated separator is much higher than that for the pristine separator (104 *vs.* 64 mA h g^{-1}). As can be seen from the results, for the AQ electrode, both the GO/SP-P and the GO/G-P coated separators have similar effects on the battery performance in terms of capacity and cycling stability.

The effects of the coated separators were also demonstrated using another carbonyl organic electrode material, i.e., PTCDA. The GO/SP-P and GO/G-P show greatly improved cycling stability compared to the pristine P. In particular, the capacity at the 200^{th} cycle for the GO/SP-P is 104 mA h g^{-1}, almost triple the 36 mA h g^{-1} with the

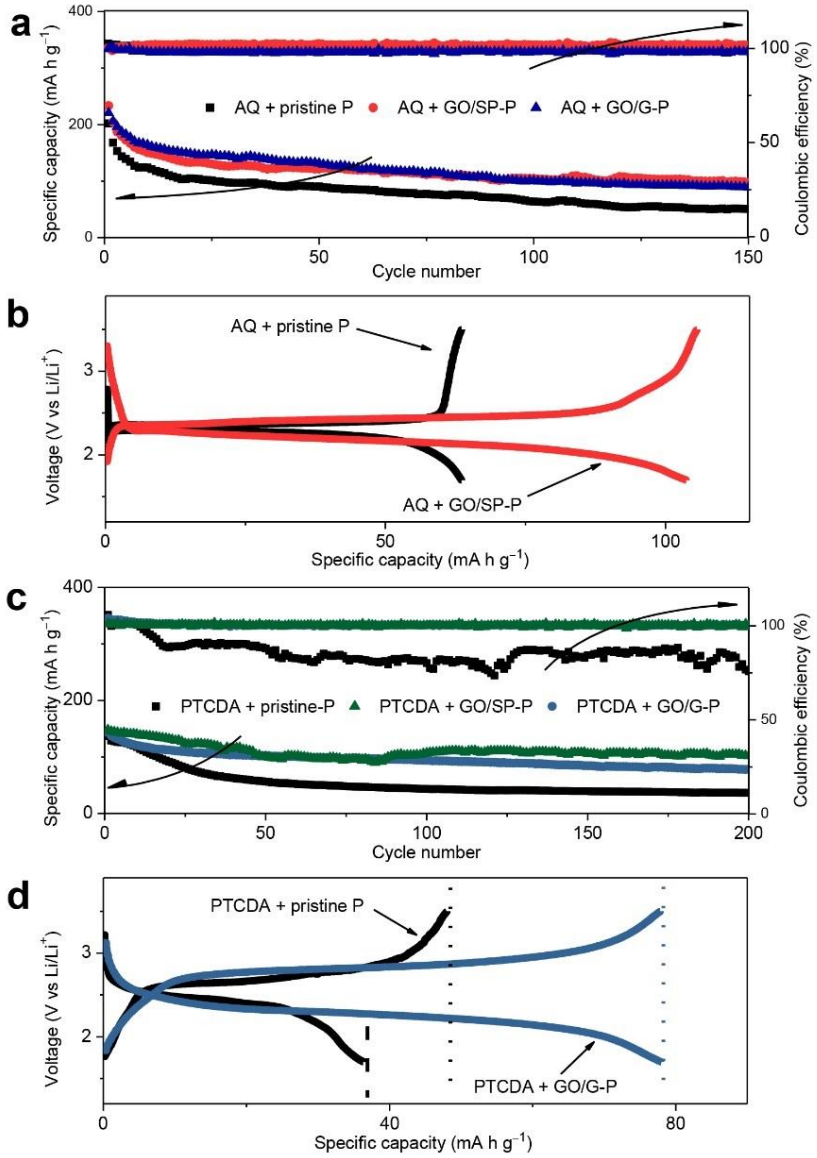

Figure 6.7 Electrochemical performances of the anthraquinone (AQ) and the perylene-3,4,9,10-tetracarboxylic dianhydride (PTCDA) electrodes with different separators. (a) Cycling behavior of the AQ electrode with the pristine separator and the coated separators with the GO/SP and GO/G dual components. (b) Charge/discharge voltage profiles of the AQ electrode with the pristine P and the GO/SP-P separators at the 100th cycle. (c) Cycling behavior and Coulombic efficiency of the PTCDA electrode with the pristine separator and the coated separators with GO/SP and GO/G dual components. (d) Charge/discharge voltage profiles of the PTCDA electrode with the pristine P and the GO/G-P separators at the 200th cycle. All the current densities are 100 mA g^{-1}.

pristine P. Moreover, the Coulombic efficiency is significantly improved. For the pristine P, the Coulombic efficiency gradually drops to around 90% and remains lower than 90% for the rest of the charge/discharge cycling. In contrast, both the GO/G-P and the GO/SP-P present Coulombic efficiency of nearly 100% (Figure 6.7c). The charge/discharge voltage profiles at the 200th-cycle for the GO/G-P and pristine P are presented in Figure 6.7d. The results indicate significantly improved capacity and similar plateau voltages. Moreover, the superior Coulombic efficiency for the cell with the GO/G-P can be observed from the same charge and discharge capacities, compared to the inferior Coulombic efficiency for the cell with the pristine P, which shows much lower discharge capacity than charge capacity. The demonstration with the PTCDA

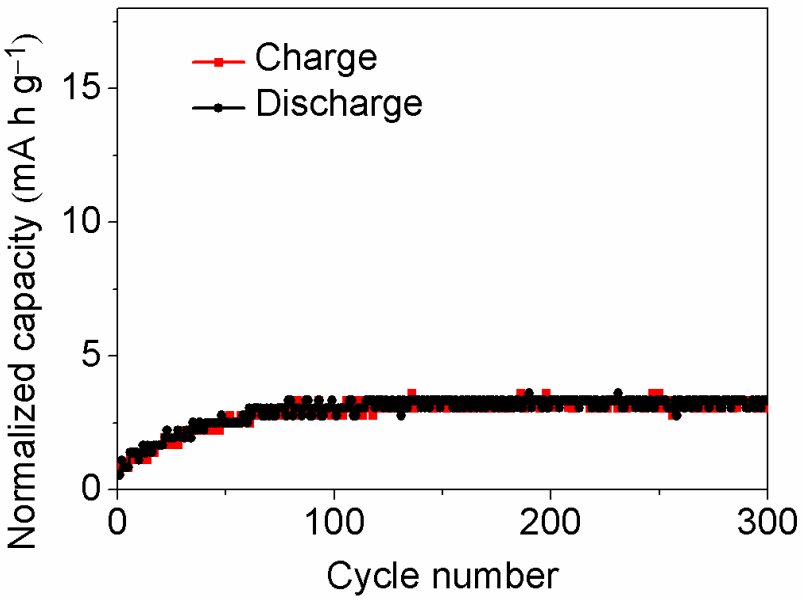

Figure 6.8 Cycling performance of the GO/SP-P without an organic cathode.

electrode reveals that both the coated separators, GO/SP-P and GO/G-P, exhibit significant positive effects on the battery performance in terms of capacity, Coulombic efficiency, and cycling stability. The GO/SP-P in particular shows the best behavior among the three separators.

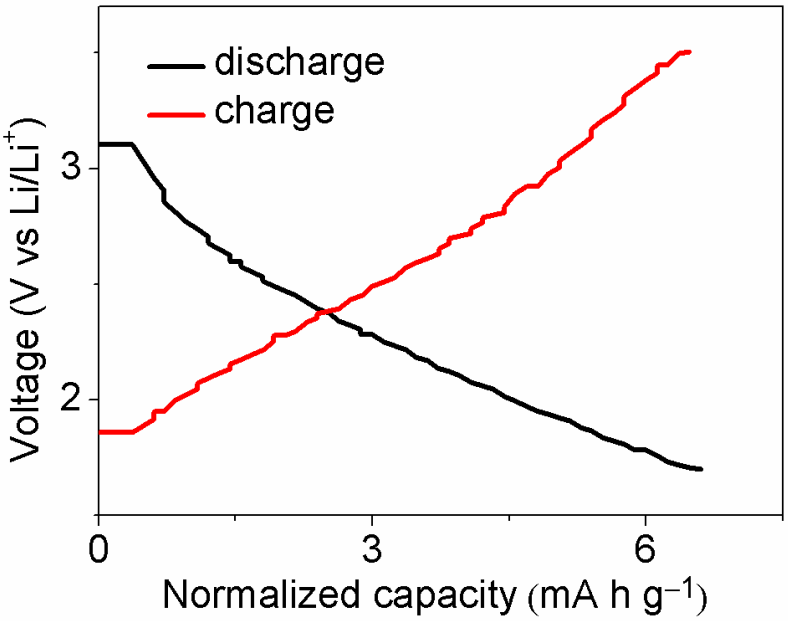

Figure 6.9 Typical voltage profile of the GO/G-P without an organic cathode.

The significantly improved battery performance from several important aspects such as the cycling stability and the self-discharge property is ascribed to the thin coating layer with dual components of GO and a nanoscale conductive carbon material (SP or G). The normalized capacity contributions of the two bicomponent laminates are minor (3 mA h g^{-1} for the GO/SP and 7 mA h g^{-1} for the GO/G, Figure 6.8 and 6.9), and therefore most of the enhanced capacity is from the improved utilization of the electroactive organic materials due to the separator functionalization. In a bicomponent laminate, the GO sub-laminate is composed of reconstructed GO nanosheets, which form nanochannels, with negative charge carried by the functional groups of carboxylic acid and phenolic hydroxyl. The width dimension of the negatively charged nanochannels (~ 1 nm) is comparable to the Debye length, so that they reject the transport of anions but allow fast migration of lithium ions.[231] Because of this, the electroactive organic anions are retained on the cathode side of the lithium-organic cell. Moreover, the other sub-laminate composed of nanoscale conductive carbon (SP or G) acts as an upper current collector, reactivating the inactive electroactive organic

molecules/anions at the cathode/separator interface. Both the GO and the SP (or G) components synergistically increase the utilization of the active material and hence improve the capacity, the cycling stability, the Coulombic efficiency, and the anti-self-discharge capability of the cell.

To understand the functioning mechanism of the bicomponent laminate on the separator, ex-situ characterizations were carried out. Similar to the solubility problem arising from the intermediate products of "polysulphides" in lithium-sulphur batteries, the small organic molecules, the intermediate products, and the discharged anions are easily soluble in the ether-based electrolyte. For example, AQ molecules are easily soluble in the electrolyte, and the concentrated solution presents a yellow color (Figure 6.2d). With the AQ electrode, two cells containing the pristine P and GO/SP-P separators were rested for 10 h and then disassembled. For the cell with the pristine P, both the separator and the lithium anode (Figure 6.10a) were contaminated by AQ-related organic species. In contrast, the lithium anode which was coupled with the GO/SP-P was uncontaminated (Figure 6.10b). Moreover, the much smoother surface of the lithium anode which was coupled with the GO/SP-P indicates lighter contamination than that with the pristine P (Figure 6.10c, 6.10d). The inhibited contamination of the lithium anode coupled with the GO/SP-P suggests that the GO/SP bicomponent laminate on the polymer membrane substrate accommodates and blocks the dissolved AQ-related organic species very well, which is the reason for the more stable OCV and much higher initial capacity when using the modified GO/SP-P or GO/G-P separators.

Furthermore, the permselectivity of the bicomponent laminate of GO/SP was demonstrated by a visual diffusion experiment conducted with an H-type glass cell. It can be seen that, in the case of the pristine P after 24 h, the organic molecules and

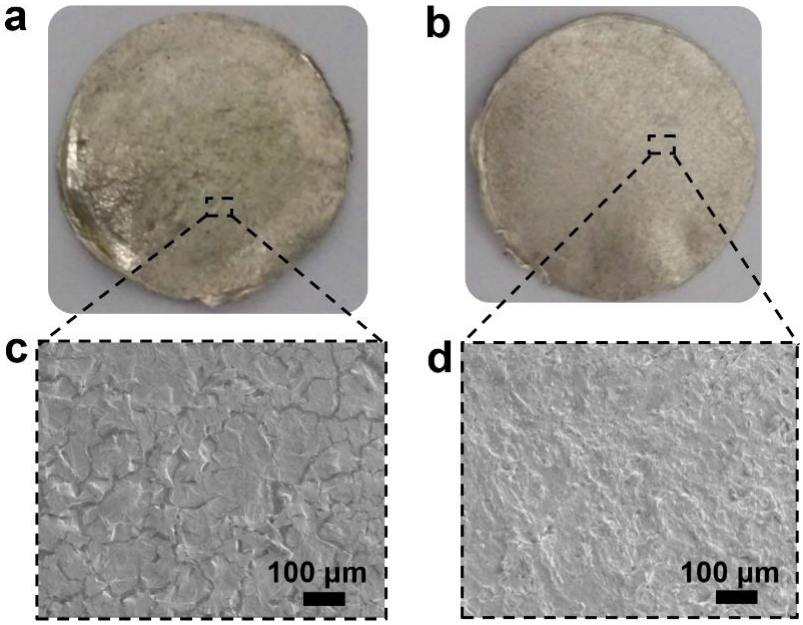

Figure 6.10 Digital photographs and SEM images of the lithium anodes after the cells were rested for 10 h and disassembled. Digital photographs of the lithium anode with pristine P (a) and GO/SP-P (b) separators. (c) SEM images of the lithium anode with pristine P (c) and GO/SP-P (d) separators.

anions dissolved on the left side have diffused to the right side (Figure 6.11a, 6.11b). In contrast, with the GO/SP-P, the active materials have been blocked, and the right side remains colorless after the same length of time (Figure 6.11c, 6.11d). The cation permselectivity of the GO/SP laminate originates from the GO sub-laminate, which possesses abundant negatively charged nanochannels between the reconstructed GO sheets. Actually, the reconstructed GO sheets are the basic configuration of the bicomponent laminate and are needed for forming a dependent membrane and accommodating the SP particles. The GO sheets overlap with each other and produce negatively charged nanochannels with a width dimension comparable to the Debye length, thereby regulating the ion transport by allowing the fast migration of lithium ions and rejecting the electroactive organic anions[129, 232]

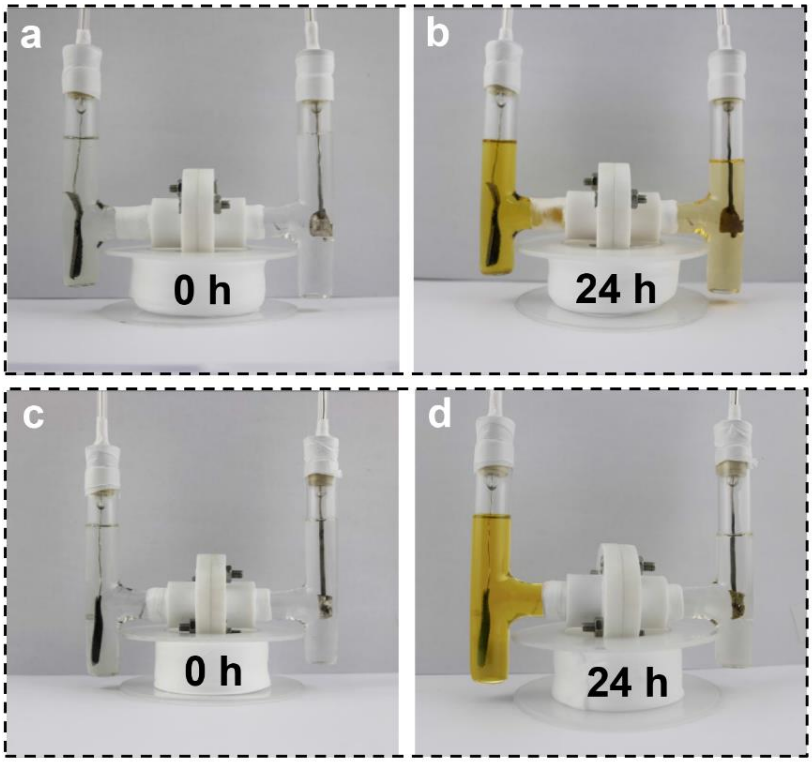

Figure 6.11 Visual demonstration of the retention of the electroactive organic species by a bicomponent-laminate-coated separator. (a, b) The diffusion of colored AQ-related species in an H-type glass cell with AQ cathode, pristine PP/PE/PP separator, and lithium anode at a potential of 2.2 V. (c, d) The diffusion of AQ-related species in an H-type glass cell with AQ cathode, GO/SP-PP/PE/PP separator, and lithium anode at a potential of 2.2 V.

6.4 Conclusions

In summary, we have demonstrated a new strategy involving separator modification in lithium-organic batteries with carbonyl organic cathode materials, AQ or PTCDA in this work, by coating a bicomponent laminate (GO/SP or GO/G) on commerical Celgard 2325 separator. Both the bicomponent laminates have a thickness of ~ 1 μm and areal density of ~ 0.1 mg cm^{-2}. For both cathodes, the OCV stability and the cycling stability were greatly improved by using the bicomponent-laminate-coated separators,

compared to the pristine separator. For instance, the cell with the GO/SP-P has almost triple the capacity of the cell with the pristine P (104 *vs.* 36 mA h g^{-1}) after 200 cycles at 100 mA g^{-1}. The advanced performance of these lithium-organic batteries is attributed to the synergetic functions of the dual components in the coating laminate: the rejection of the electroactive organic anions by the negatively charged nanochannels between the reconstructed GO sheets and the reactivation of the dissolved electroactive organic species by the nanoscale conductive carbon as upper current collector. This novel strategy of separator coating with a bicomponent laminate can be extended to lithium-sulphur batteries and other similar electrochemical energy storage systems with the problem of dissolution of the electroactive materials.

CHAPTER 7 CONCLUSIONS AND OUTLOOK

7.1 Conclusions

In my thesis, two types of lithium-based batteries, including Li-S and Li-organic batteries, have been investigated. In these two promising battery systems, a common problem is the dissolution and shuttling of the electroactive species, which results in quick capacity decay, unstable solid-electrolyte interface at the anode and poor Coulombic efficiency. Targeting at this common issue, varied membrane strategies have been applied for obtaining stable Li-S and Li-organic batteries. An ion-transport-regulating membrane has been applied on the sulphur/carbon cathode to facilitate the transport of lithium ions and suppress the dissolution of polysulphide anions, leading to long-cycle high-rate Li-S batteries. A commercial carbon film, after hydrothermal treatment, has been used as an interlayer between the cathode and the separator, resulting in improved active material retention, capacity, cycle life and Coulombic efficiency. With respect to the Li-organic battery, a novel ion-selective separator prepared by coating a thin layer of graphene oxide/conductive carbon on a porous polyolefin substrate has been exploited and highly stable batteries with enhanced Coulombic efficiency has been obtained.

A sulphonated aromatic polymer, SPEEK, has been prepared and integrated into sulphur cathodes for high-rate Li-S batteries. SPEEK contains both hydrophobic domain of polymer backbone and hydrophilic domain of sulphonate groups. The ion interactions of negative sulphonate groups form negatively charged nanochannels, which facilitate the transport of the Li^+ ions and reject the anions (including the S_x^{2-} ions), resulting in

high-performance Li-S batteries. For instance, at an ultrahigh rate of 18 C, a high capacity of 612 mA h g^{-1} can be kept for 250 cycles. Furthermore, at a high current density of 28.9 A g^{-1}-(C+S+SPEEK), the specific capacity reaches a high level of 135 mA h g^{-1}, comparable to the best results of conventional lithium-ion batteries. It is believed that this novel design of the integrated sulphur cathode with polymer membrane regulating ion transport and porous carbon enhancing electron transfer could open up new opportunities for revolutionizing the traditional ways of advancing battery systems.

A hydrothermally treated graphite film was sandwiched between the sulphur cathode and the separator. The functional groups on the graphite film play an important role in retaining the solvable sulphur species. Owing to the improved utilization of active material, the specific capacity was significantly improved for the new configuration. The graphite film in the Li-S cell acts as a blocking layer against soluble polysulphides and provides additional reaction sites for the sulphur species. After 50 cycles, the cell with the graphite film retained a capacity which was almost triple that of the cell without the graphite film. Also, the Coulombic efficiency was increased from around 94% to near 100%, indicating a much more stable Li-S battery.

A new strategy involving separator modification in lithium-organic batteries with carbonyl organic cathode materials of AQ or PTCDA by coating a bicomponent laminate (GO/SP or GO/G) on the commerical Celgard 2325 separator has been reported. Both the bicomponent laminates have a thickness of ca.~ 1 μm and areal density of ca.~ 0.1 mg cm–2. For both the cathodes, the OCV stability and the cycling stability have beenwere greatly improved by using the bicomponent- laminate-coated separators, compared to the pristine separator. For instance, the cell with the GO/SP-P has almost triples the capacity of the cell with the pristine P (104 vs. 36 mA h g–1) after

200 cycles at 100 mA g–1. The advanced performance of these lithium-organic batteries are is attributed to the synergetic functions of the dual components in the coating laminate: the rejection of the electroactive organic anions by the negatively charged nanochannels between the reconstructed GO sheets and the reactivation of the dissolved electroactive organic species by the nanoscale conductive carbon as upper current collector. This novel strategy of separator coating with a bicomponent laminate can be extended to lithium-sulphur batteries and other similar electrochemical energy storage systems with the dissolution problem of dissolution of the electroactive materials.

7.2 Outlook

This thesis focuses on two promising next-generation battery systems, i.e., Li-S and Li-organic batteries, which are prospective energy storage systems in the future for building up a sustainable and economy-effective society. However, both the sulphur and the organic cathodes are plagued by the similar problems of (1) poor conductivity and (2) electroactive material dissolution and shuttling.

To improve the conductivity of the sulphur and the organic cathodes, porous carbon materials with high surface area are highly desired. Microporous or mesoporous carbon materials incorporating nano-sized sulphur or organics are expected to exhibit stable cycling. The carbon materials can be modified with certain polymers to construct chemical gradient, which might further retard the dissolution of the electroactive species. Other species like metal elements can be used for doping the carbon materials to create a favored environment for the electrochemical reactions. The design of the porosity of the carbon materials needs further attention, considering the different chemistries that may happen in the pores with dimensions less than 1 nm. Besides carbon materials,

metal oxides with inherent polarity are also expected to form composites with sulphur or organics for high-performance batteries. Conductive polymers are another appealing candidate to coat the sulphur or organics for high capacity and long cycle life. In short, developing new host materials of carbon materials, metal oxides or conductive polymers is a universal strategy for the advance of the sulphur or organic cathodes.

Polymer binders as a small portion of electrodes, however, might greatly affect the performance. Polymers with high adhering ability can tightly bind the active materials and the conductive agent on the current collector. Also, good compatibility with the other components in the electrode is an important requirement for the polymer binder. Polymers with functional groups like carboxylic or sulphonate might enhance the ionic conductivity of the electrode for the hopping mechanism of the functional groups. The type of material and the amount of the binder need careful adjusting to achieve the optimal electrochemical performance.

The advance of electrolytes can also be expected to play an important role in constructing stable Li-S and Li-organic batteries. New Li salts and solvents are to be developed for further improvement of the batteries. Also, different solvent mixtures need further investigation, for varied solvents have different solubility for the Li salts and might have different effects on the formation of the SEI layers. Additives are also critical for stable SEI films, which is key for the electrochemical performance. Ionic liquids can also be explored as the solvent for mediating the self-discharge properties of the Li-S or Li-organic batteries.

The separator, which locates between the cathode and the anode, is an important component in the Li-S or Li-organic battery. Typically, the separator is a porous polyolefin membrane allowing the transport of lithium ions and preventing physical

contact between the cathode and the anode. In order to prevent the diffusion problem of the dissolved electroactive species, functional separators that are capable of selectively permeating ions are highly desired. Independent or dependent ion-selective membranes that are capable of transporting lithium ions but rejecting negative ions are expected to improve the active material utilization and achieve long cycle life. Besides, separator coating with conductive carbon on the side facing the cathode is an effective way, because the conductive coating acts as upper current collector to improve the utilization of the active material.

Both Li-S and Li-organic batteries are promising candidates for next-generation high-energy batteries. However, to achieve successful commercialization, further improvement in terms of the cathode, the binder material, the electrolyte and the separator is needed. Moreover, the study of the lithium metal anode will be critical for the practical implementation of these two battery systems. New chapters for the energy storage technology surely will be opened when these cost-effective and environmental-friendly batteries can be successfully commercialized, before which intense efforts should be made on the scientific and technological investigation.

REFERENCES

1. R. Marom, S. F. Amalraj, N. Leifer, D. Jacob, D. Aurbach, A review of advanced and practical lithium battery materials. *Journal of Materials Chemistry* **21**, 9938 (2011).

2. J. B. Goodenough, Y. Kim, Challenges for rechargeable batteries. *Journal of Power Sources* **196**, 6688 (2011).

3. B. Dunn, H. Kamath, J. M. Tarascon, Electrical Energy Storage for the Grid: A Battery of Choices. *Science* **334**, 928 (2011).

4. F. Y. Cheng, J. Liang, Z. L. Tao, J. Chen, Functional Materials for Rechargeable Batteries. *Advanced Materials* **23**, 1695 (2011).

5. J. M. Tarascon, M. Armand, Issues and challenges facing rechargeable lithium batteries. *Nature* **414**, 359 (2001).

6. W. H. Meyer, Polymer electrolytes for lithium-ion batteries. *Advanced Materials* **10**, 439 (1998).

7. J. B. Goodenough, Y. Kim, Challenges for Rechargeable Li Batteries. *Chemistry of Materials* **22**, 587 (2010).

8. J. B. Goodenough, K. S. Park, The Li-Ion Rechargeable Battery: A Perspective. *Journal of the American Chemical Society* **135**, 1167 (2013).

9. Z. G. Yang, J. L. Zhang, M. C. W. Kintner-Meyer, X. C. Lu, D. W. Choi, J. P. Lemmon, J. Liu, Electrochemical Energy Storage for Green Grid. *Chemical Reviews* **111**, 3577 (2011).

10. Bruno Scrosati, Jusef Hassoun, Yang-Kook Sun, Lithium-ion batteries. A look into the future. *Energy & Environmental Science* **4**, 3287 (2011).

11. V. Etacheri, R. Marom, R. Elazari, G. Salitra, D. Aurbach, Challenges in the development of advanced Li-ion batteries: a review. *Energy & Environmental Science* **4**, 3243 (2011).

12. M. G. Kim, J. Cho, Reversible and High-Capacity Nanostructured Electrode Materials for Li-Ion Batteries. *Advanced Functional Materials* **19**, 1497 (2009).

13. H. Li, Z. X. Wang, L. Q. Chen, X. J. Huang, Research on Advanced Materials for Li-ion Batteries. *Advanced Materials* **21**, 4593 (2009).

14. J. B. Goodenough, Rechargeable batteries: challenges old and new. *Journal of Solid State Electrochemistry* **16**, 2019 (2012).

15. S. Flandrois, B. Simon, Carbon materials for lithium-ion rechargeable batteries. *Carbon* **37**, 165 (1999).

16. M. Armand, J. M. Tarascon, Building better batteries. *Nature* **451**, 652 (2008).

17. B. Scrosati, History of lithium batteries. *Journal of Solid State Electrochemistry* **15**, 1623 (2011).

18. J. Akimoto, Y. Gotoh, Y. Oosawa, Synthesis and structure refinement of LiCoO2 single crystals. *Journal of Solid State Chemistry* **141**, 298 (1998).

19. E. Antolini, LiCoO2: formation, structure, lithium and oxygen nonstoichiometry, electrochemical behaviour and transport properties. *Solid State Ionics* **170**, 159 (2004).

20. M. S. Whittingham, Lithium batteries and cathode materials. *Chemical Reviews* **104**, 4271 (2004).

21. Dmitry Belov, Mo-Hua Yang, Investigation of the kinetic mechanism in overcharge process for Li-ion battery. *Solid State Ionics* **179**, 1816 (2008).

22. D. Belov, Mo-Hua Yang, Failure mechanism of Li-ion battery at overcharge conditions. *Journal of Solid State Electrochemistry* **12**, 885 (2008).

23. Y. Takahashi, S. Tode, A. Kinoshita, H. Fujimoto, I. Nakane, S. Fujitani, Development of lithium-ion batteries with a LiCoO(2) cathode toward high capacity by elevating charging potential. *Journal of the Electrochemical Society* **155**, A537 (2008).

24. G. G. Amatucci, J. M. Tarascon, L. C. Klein, Cobalt dissolution in LiCoO2-based non-aqueous rechargeable batteries. *Solid State Ionics* **83**, 167 (1996).

25. G. G. Amatucci, J. M. Tarascon, L. C. Klein, CoO2, the end member of the LixCoO2 solid solution. *Journal of the Electrochemical Society* **143**, 1114 (1996).

26. J. Zhou, P. H. L. Notten, Studies on the degradation of Li-ion batteries by the use of microreference electrodes. *Journal of Power Sources* **177**, 553 (2008).

27. Li Wang, Jiangang Li, Xiangming He, Weihua Pu, Chunrong Wan, Changyin Jiang, Recent advances in layered $LiNi_xCo_yMn_{1-x-y}O_2$ cathode materials for lithium ion batteries. *Journal of Solid State Electrochemistry* **13**, 1157 (2009).

28. Brian L. Ellis, Kyu Tae Lee, Linda F. Nazar, Positive Electrode Materials for Li-Ion and Li-Batteries. *Chemistry of Materials* **22**, 691 (2010).

29. J. Belt, V. Utgikar, I. Bloom, Calendar and PHEV cycle life aging of high-energy, lithium-ion cells containing blended spinel and layered-oxide cathodes. *Journal of Power Sources* **196**, 10213 (2011).

30. F. Y. Cheng, J. A. Shen, B. Peng, Y. D. Pan, Z. L. Tao, J. Chen, Rapid room-temperature synthesis of nanocrystalline spinels as oxygen reduction and evolution electrocatalysts. *Nature Chemistry* **3**, 79 (2011).

31. D. K. Kim, P. Muralidharan, H. W. Lee, R. Ruffo, Y. Yang, C. K. Chan, H. Peng, R. A. Huggins, Y. Cui, Spinel LiMn2O4 Nanorods as Lithium Ion Battery Cathodes. *Nano Letters* **8**, 3948 (2008).

32. H. W. Lee, P. Muralidharan, R. Ruffo, C. M. Mari, Y. Cui, D. K. Kim, Ultrathin Spinel $LiMn_2O_4$ Nanowires as High Power Cathode Materials for Li-Ion Batteries. *Nano Letters* **10**, 3852 (2010).

33. M. Kopec, D. Lisovytskiy, M. Marzantowicz, J. R. Dygas, F. Krok, Z. Kaszkur, J. Pielaszek, X-ray diffraction and impedance spectroscopy studies of lithium manganese oxide spinel. *Journal of Power Sources* **159**, 412 (2006).

34. F. A. Amaral, N. Bocchi, R. F. Brocenschi, S. R. Biaggio, R. C. Rocha, Structural and electrochemical properties of the doped spinels $Li_{1.05}M_{0.02}Mn_{1.98}O_{3.98}N_{0.02}$ (M = Ga^{3+}, Al^{3+}, or Co^{3+}; N = S^{2-} or F^{-}) for use as cathode material in lithium batteries. *Journal of Power Sources* **195**, 3293 (2010).

35. M. Aklalouch, J. M. Amarilla, I. Saadoune, J. M. Rojo, $LiCr_{0.2}Ni_{0.4}Mn_{1.4}O_4$ spinels exhibiting huge rate capability at 25 and 55 degrees C: Analysis of the effect of the particle size. *Journal of Power Sources* **196**, 10222 (2011).

36. K. M. Shaju, G. V. Subba Rao, B. V. R. Chowdari, Li ion kinetic studies on spinel cathodes, $Li(M_{1/6}Mn_{11/6})O_4$ (M = Mn, Co, CoAl) by GITT and EIS. *Journal of Materials Chemistry* **13**, 106 (2003).

37. Z. X. Chen, S. Qiu, Y. L. Cao, X. P. Ai, K. Xie, X. B. Hong, H. X. Yang, Surface-oriented and nanoflake-stacked $LiNi_{0.5}Mn_{1.5}O_4$ spinel for high-rate and long-cycle-life lithium ion batteries. *Journal of Materials Chemistry* **22**, 17768 (2012).

38. V. A. Agubra, J. W. Fergus, The formation and stability of the solid electrolyte interface on the graphite anode. *Journal of Power Sources* **268**, 153 (2014).

39. J. Yan, B. J. Xia, Y. C. Su, X. Z. Zhou, J. Zhang, X. G. Zhang, Phenomenologically modeling the formation and evolution of the solid electrolyte interface on the graphite electrode for lithium-ion batteries. *Electrochimica Acta* **53**, 7069 (2008).

40. J. Yan, Y. C. Su, B. J. Xia, J. Zhang, Thermodynamics in the formation of the solid electrolyte interface on the graphite electrode for lithium-ion batteries. *Electrochimica Acta* **54**, 3538 (2009).

41. B. Li, Y. Q. Wang, H. B. Rong, Y. T. Wang, J. S. Liu, L. D. Xing, M. Q. Xu, W. S. Li, A novel electrolyte with the ability to form a solid electrolyte interface on the anode and cathode of a $LiMn_2O_4$/graphite battery. *Journal of Materials Chemistry A* **1**, 12954 (2013).

42. K. Ui, D. Fujii, Y. Niwata, T. Karouji, Y. Shibata, Y. Kadoma, K. Shimada, N. Kumagai, Analysis of solid electrolyte interface formation reaction and surface deposit of natural graphite negative electrode employing polyacrylic acid as a binder. *Journal of Power Sources* **247**, 981 (2014).

43. S. H. Lee, I. S. Jo, J. Kim, Surface analysis of the solid electrolyte interface formed by additives on graphite electrodes in Li-ion batteries using XPS,

FE-AES, and XHR-SEM techniques. *Surface and Interface Analysis* **46**, 570 (2014).

44. H. Guk, D. Kim, S. H. Choi, D. H. Chung, S. S. Han, Thermostable Artificial Solid-Electrolyte Interface Layer Covalently Linked to Graphite for Lithium Ion Battery: Molecular Dynamics Simulations. *Journal of the Electrochemical Society* **163**, A917 (2016).

45. H. Y. Wang, F. M. Wang, Electrochemical investigation of an artificial solid electrolyte interface for improving the cycle-ability of lithium ion batteries using an atomic layer deposition on a graphite electrode. *Journal of Power Sources* **233**, 1 (2013).

46. Candace K. Chan, Hailin Peng, Gao Liu, Kevin McIlwrath, Xiao Feng Zhang, Robert A. Huggins, Yi Cui, High-performance lithium battery anodes using silicon nanowires. *Nature Nanotechnology* **3**, 31 (2008).

47. Mi-Hee Park, Min Gyu Kim, Jaebum Joo, Kitae Kim, Jeyoung Kim, Soonho Ahn, Yi Cui, Jaephil Cho, Silicon Nanotube Battery Anodes. *Nano Letters* **9**, 3844 (2009).

48. Hui Wu, Gerentt Chan, Jang Wook Choi, Ill Ryu, Yan Yao, Matthew T. McDowell, Seok Woo Lee, Ariel Jackson, Yuan Yang, Liangbing Hu, Yi Cui, Stable cycling of double-walled silicon nanotube battery anodes through solid-electrolyte interphase control. *Nature Nanotechnology* **7**, 309 (2012).

49. C. M. Park, J. H. Kim, H. Kim, H. J. Sohn, Li-alloy based anode materials for Li secondary batteries. *Chemical Society Reviews* **39**, 3115 (2010).

50. M. V. Reddy, G. V. S. Rao, B. V. R. Chowdari, Metal Oxides and Oxysalts as Anode Materials for Li Ion Batteries. *Chemical Reviews* **113**, 5364 (2013).

51. Guangyuan Zheng, Seok Woo Lee, Zheng Liang, Hyun-Wook Lee, Kai Yan, Hongbin Yao, Haotian Wang, Weiyang Li, Steven Chu, Yi Cui, Interconnected hollow carbon nanospheres for stable lithium metal anodes. *Nature Nanotechnology* **9**, 618 (2014).

52. Claudiu B. Bucur, Adrian Lita, Naoki Osada, John Muldoon, A soft, multilayered lithium-electrolyte interface. *Energy & Environmental Science* **9**, 112 (2016).

53. Kai Yan, Hyun-Wook Lee, Teng Gao, Guangyuan Zheng, Hongbin Yao, Haotian Wang, Zhenda Lu, Yu Zhou, Zheng Liang, Zhongfan Liu, Steven Chu, Yi Cui, Ultrathin Two-Dimensional Atomic Crystals as Stable Interfacial Layer for Improvement of Lithium Metal Anode. *Nano Letters* **14**, 6016 (2014).

54. Qing Chen, Ke Geng, K. Sieradzki, Prospects for Dendrite-Free Cycling of Li Metal Batteries. *Journal of the Electrochemical Society* **162**, A2004 (2015).

55. S. S. Zhang, A review on the separators of liquid electrolyte Li-ion batteries. *Journal of Power Sources* **164**, 351 (2007).

56. H. Lee, M. Yanilmaz, O. Toprakci, K. Fu, X. W. Zhang, A review of recent developments in membrane separators for rechargeable lithium-ion batteries. *Energy & Environmental Science* **7**, 3857 (2014).

57. X. S. Huang, Separator technologies for lithium-ion batteries. *Journal of Solid State Electrochemistry* **15**, 649 (2011).

58. Xin Fang, Huisheng Peng, A Revolution in Electrodes: Recent Progress in Rechargeable Lithium-Sulphur Batteries. *Small* **11**, 1488 (2015).

59. W. B. Wan, W. H. Pu, D. S. Ai, Research Progress in Lithium Sulphur Battery. *Progress in Chemistry* **25**, 1830 (2013).

60. Peter G. Bruce, Stefan A. Freunberger, Laurence J. Hardwick, Jean-Marie Tarascon, Li-O_2 and Li-S batteries with high energy storage. *Nature Materials* **11**, 19 (2012).

61. C. Y. Nan, Z. Lin, H. G. Liao, M. K. Song, Y. D. Li, E. J. Cairns, Durable Carbon-Coated Li_2S Core-Shell Spheres for High Performance Lithium/Sulphur Cells. *Journal of the American Chemical Society* **136**, 4659 (2014).

62. W. Zheng, X. G. Hu, C. F. Zhang, Research progress on high specific energy cathode materials for rechargeable lithium sulphur batteries. *Journal of Rare Earths* **23**, 593 (2005).

63. S. S. Zhang, Liquid electrolyte lithium/sulphur battery: Fundamental chemistry, problems, and solutions. *Journal of Power Sources* **231**, 153 (2013).

64. Johan Scheers, Sébastien Fantini, Patrik Johansson, A review of electrolytes for lithium–sulphur batteries. *Journal of Power Sources* **255**, 204 (2014).

65. J. J. Hu, G. R. Li, X. P. Gao, Current Status, Problems and Challenges in Lithium-sulphur Batteries. *Journal of Inorganic Materials* **28**, 1181 (2013).

66. A. Fedorkova, R. Orinakova, O. Cech, M. Sedlarikova, New Composite Cathode Materials for Li/S Batteries: A Review. *International Journal of Electrochemical Science* **8**, 10308 (2013).

67. Y. X. Yin, S. Xin, Y. G. Guo, L. J. Wan, Lithium-Sulphur Batteries: Electrochemistry, Materials, and Prospects. *Angewandte Chemie-International Edition* **52**, 13186 (2013).

68. Arumugam Manthiram, Sheng-Heng Chung, Chenxi Zu, Lithium-Sulphur Batteries: Progress and Prospects. *Advanced Materials* **27**, 1980 (2015).

69. J. Wang, Y. S. He, J. Yang, Sulphur-Based Composite Cathode Materials for High-Energy Rechargeable Lithium Batteries. *Adv Materials*, **27**, 569 (2014).

70. Z. D. Yao, W. Wei, J. L. Wang, J. Yang, Y. N. Nuli, Review of Sulphur-Based Cathodes for High Performance Lithium Rechargeable Batteries. *Acta Physico-Chimica Sinica* **27**, 1005 (2011).

71. X. Hou, L. Jiang, Learning from Nature: Building Bio-Inspired Smart Nanochannels. *ACS Nano* **3**, 3339 (2009).

72. A. Manthiram, Y. Z. Fu, Y. S. Su, Challenges and Prospects of Lithium-Sulphur Batteries. *Accounts of Chemical Research* **46**, 1125 (2013).

73. S. Evers, L. F. Nazar, New Approaches for High Energy Density Lithium-Sulphur Battery Cathodes. *Accounts of Chemical Research* **46**, 1135 (2013).

74. X. L. Ji, K. T. Lee, L. F. Nazar, A highly ordered nanostructured carbon-sulphur cathode for lithium-sulphur batteries. *Nature Materials* **8**, 500 (2009).

75. Kai Zhang, Lijiang Wang, Zhe Hu, Fangyi Cheng, Jun Chen, Ultrasmall Li_2S Nanoparticles Anchored in Graphene Nanosheets for High-Energy Lithium-Ion Batteries. *Scientific Reports* **4**, 6467 (2014).

76. Meng-Qiang Zhao, Qiang Zhang, Jia-Qi Huang, Gui-Li Tian, Jing-Qi Nie, Hong-Jie Peng, Fei Wei, Unstacked double-layer templated graphene for high-rate lithium-sulphur batteries. *Nature Communications* **5**, 3410 (2014).

77. Zhiyu Wang, Yanfeng Dong, Hongjiang Li, Zongbin Zhao, Hao Bin Wu, Ce Hao, Shaohong Liu, Jieshan Qiu, Xiong Wen Lou, Enhancing lithium-sulphur battery performance by strongly binding the discharge products on

amino-functionalized reduced graphene oxide. *Nature Communications* **5**, 5002 (2014).

78. Chao Wang, Xusheng Wang, Yuan Yang, Akihiro Kushima, Jitao Chen, Yunhui Huang, Ju Li, Slurryless Li2S/Reduced Graphene Oxide Cathode Paper for High-Performance Lithium Sulphur Battery. *Nano Letters* **15**, 1796 (2015).

79. Chao Wang, Xusheng Wang, Yanjie Wang, Jitao Chen, Henghui Zhou, Yunhui Huang, Macroporous free-standing nano-sulphur/reduced graphene oxide paper as stable cathode for lithium-sulphur battery. *Nano Energy* **11**, 678 (2015).

80. Kai Han, Jingmei Shen, Cary M. Hayner, Hongqi Ye, Mayfair C. Kung, Harold H. Kung, Li_2S-reduced graphene oxide nanocomposites as cathode material for lithium sulphur batteries. *Journal of Power Sources* **251**, 331 (2014).

81. Lan Zhou, Xiujing Lin, Tao Huang, Aishui Yu, Binder-free phenyl sulphonated graphene/sulphur electrodes with excellent cyclability for lithium sulphur batteries. *Journal of Materials Chemistry A* **2**, 5117 (2014).

82. Jiantie Xu, Jianglan Shui, Jianli Wang, Min Wang, Hua-Kun Liu, Shi Xue Dou, In-Yup Jeon, Jeong-Min Seo, Jong-Beom Baek, Liming Dai, Sulphur-Graphene Nanostructured Cathodes via Ball-Milling for High-Performance LithiumSulphur Batteries. *ACS Nano* **8**, 10920 (2014).

83. Y. G. Zhang, Y. Zhao, Z. Bakenov, M. R. Babaa, A. Konarov, C. Ding, P. Chen, Effect of Graphene on Sulphur/Polyacrylonitrile Nanocomposite Cathode in High Performance Lithium/Sulphur Batteries. *Journal of the Electrochemical Society* **160**, A1194 (2013).

84. L. C. Yin, J. L. Wang, F. J. Lin, J. Yang, Y. Nuli, Polyacrylonitrile/graphene composite as a precursor to a sulphur-based cathode material for high-rate rechargeable Li-S batteries. *Energy & Environmental Science* **5**, 6966 (2012).

85. Quan Pang, Dipan Kundu, Marine Cuisinier, L. F. Nazar, Surface-enhanced redox chemistry of polysulphides on a metallic and polar host for lithium-sulphur batteries. *Nature Communications* **5**, 4759 (2014).

86. X. Y. Tao, J. G. Wang, Z. G. Ying, Q. X. Cai, G. Y. Zheng, Y. P. Gan, H. Huang, Y. Xia, C. Liang, W. K. Zhang, Y. Cui, Strong Sulphur Binding with Conducting Magneli-Phase Ti_nO_{2n-1} Nanomaterials for Improving Lithium-Sulphur Batteries. *Nano Letters* **14**, 5288 (2014).

87. M. Oschatz, S. Thieme, L. Borchardt, M. R. Lohe, T. Biemelt, J. Bruckner, H. Althues, S. Kaskel, A new route for the preparation of mesoporous carbon materials with high performance in lithium-sulphur battery cathodes. *Chemical Communications* **49**, 5832 (2013).

88. K. Xi, S. Cao, X. Y. Peng, C. Ducati, R. V. Kumar, A. K. Cheetham, Carbon with hierarchical pores from carbonized metal-organic frameworks for lithium sulphur batteries. *Chemical Communications* **49**, 2192 (2013).

89. Y. X. Wang, L. Huang, L. C. Sun, S. Y. Xie, G. L. Xu, S. R. Chen, Y. F. Xu, J. T. Li, S. L. Chou, S. X. Dou, S. G. Sun, Facile synthesis of a interleaved expanded graphite-embedded sulphur nanocomposite as cathode of Li-S batteries with excellent lithium storage performance. *Journal of Materials Chemistry* **22**, 4744 (2012).

90. W. D. Zhou, Y. C. Yu, H. Chen, F. J. DiSalvo, H. D. Abruna, Yolk-Shell Structure of Polyaniline-Coated Sulphur for Lithium-Sulphur Batteries. *Journal of the American Chemical Society* **135**, 16736 (2013).

91. X. M. He, W. H. Pu, J. U. Ren, L. Wang, J. L. Wang, C. Y. Jiang, C. R. Wan, Charge/discharge characteristics of sulphur composite electrode at different temperature and current density in rechargeable lithium batteries. *Ionics* **14**, 335 (2008).

92. J. Wang, J. Chen, K. Konstantinov, L. Zhao, S. H. Ng, G. X. Wang, Z. P. Guo, H. K. Liu, Sulphur-polypyrrole composite positive electrode materials for rechargeable lithium batteries. *Electrochimica Acta* **51**, 4634 (2006).

93. X. M. He, W. H. Pu, J. G. Ren, L. Wang, J. L. Wang, C. Y. Jiang, C. R. Wan, Charge/discharge characteristics of sulphur composite cathode materials in rechargeable lithium batteries. *Electrochimica Acta* **52**, 7372 (2007).

94. J. L. Wang, J. Yang, J. Y. Xie, N. X. Xu, A novel conductive polymer-sulphur composite cathode material for rechargeable lithium batteries. *Advanced Materials* **14**, 963 (2002).

95. J. Wang, J. Yang, C. Wan, K. Du, J. Xie, N. Xu, Sulphur Composite Cathode Materials for Rechargeable Lithium Batteries. *Advanced Functional Materials* **13**, 487 (2003).

96. L. C. Yin, J. L. Wang, J. Yang, Y. N. Nuli, A novel pyrolyzed polyacrylonitrile-sulphur@MWCNT composite cathode material for high-rate rechargeable lithium/sulphur batteries. *Journal of Materials Chemistry* **21**, 6807 (2011).

97. W. Wei, J. L. Wang, L. J. Zhou, J. Yang, B. Schumann, Y. N. NuLi, CNT enhanced sulphur composite cathode material for high rate lithium battery. *Electrochemistry Communications* **13**, 399 (2011).

98. L. C. Yin, J. L. Wang, X. L. Yu, C. W. Monroe, Y. NuLi, J. Yang, Dual-mode sulphur-based cathode materials for rechargeable Li-S batteries. *Chemical Communications* **48**, 7868 (2012).

99. Y. Yang, G. H. Yu, J. J. Cha, H. Wu, M. Vosgueritchian, Y. Yao, Z. A. Bao, Y. Cui, Improving the Performance of Lithium-Sulphur Batteries by Conductive Polymer Coating. *ACS Nano* **5**, 9187 (2011).

100. Z. W. Seh, W. Y. Li, J. J. Cha, G. Y. Zheng, Y. Yang, M. T. McDowell, P. C. Hsu, Y. Cui, Sulphur-TiO2 yolk-shell nanoarchitecture with internal void space for long-cycle lithium-sulphur batteries. *Nature Communications* **4**, 1331 (2013).

101. J. W. Zhou, R. Li, X. X. Fan, Y. F. Chen, R. D. Han, W. Li, J. Zheng, B. Wang, X. G. Li, Rational design of a metal-organic framework host for sulphur storage in fast, long-cycle Li-S batteries. *Energy & Environmental Science* **7**, 2715 (2014).

102. S. E. Cheon, J. H. Cho, K. S. Ko, C. W. Kwon, D. R. Chang, H. T. Kim, S. W. Kim, Structural factors of sulphur cathodes with poly(ethylene oxide) binder for performance of rechargeable lithium sulphur batteries. *Journal of the Electrochemical Society* **149**, A1437 (2002).

103. Y. Q. Huang, J. Sun, W. K. Wang, Y. Wang, Z. B. Yu, H. Zhang, A. B. Wang, K. G. Yuan, Discharge process of the sulphur cathode with a gelatin binder. *Journal of the Electrochemical Society* **155**, A764 (2008).

104. J. Sun, Y. Q. Huang, W. K. Wang, Z. B. Yu, A. B. Wang, K. G. Yuan, Application of gelatin as a binder for the sulphur cathode in lithium-sulphur batteries. *Electrochimica Acta* **53**, 7084 (2008).

105. Q. Q. Wang, W. K. Wang, Y. Q. Huang, F. Wang, H. Zhang, Z. B. Yu, A. B. Wang, K. G. Yuan, Improve Rate Capability of the Sulphur Cathode Using a Gelatin Binder. *Journal of the Electrochemical Society* **158**, A775 (2011).

106. S. S. Zhang, Binder Based on Polyelectrolyte for High Capacity Density Lithium/Sulphur Battery. *Journal of the Electrochemical Society* **159**, A1226 (2012).

107. M. M. Rao, X. Y. Song, H. G. Liao, E. J. Cairns, Carbon nanofiber-sulphur composite cathode materials with different binders for secondary Li/S cells. *Electrochimica Acta* **65**, 228 (2012).

108. M. J. Lacey, F. Jeschull, K. Edstrom, D. Brandell, Why PEO as a binder or polymer coating increases capacity in the Li-S system. *Chemical Communications* **49**, 8531 (2013).

109. J. L. Wang, Z. D. Yao, C. W. Monroe, J. Yang, Y. Nuli, Carbonyl-beta-Cyclodextrin as a Novel Binder for Sulphur Composite Cathodes in Rechargeable Lithium Batteries. *Advanced Functional Materials* **23**, 1194 (2013).

110. M. He, L. X. Yuan, W. X. Zhang, X. L. Hu, Y. H. Huang, Enhanced Cyclability for Sulphur Cathode Achieved by a Water-Soluble Binder. *Journal of Physical Chemistry C* **115**, 15703 (2011).

111. Z. A. Zhang, W. Z. Bao, H. Lu, M. Jia, K. Y. Xie, Y. Q. Lai, J. Li, Water-Soluble Polyacrylic Acid as a Binder for Sulphur Cathode in Lithium-Sulphur Battery. *ECS Electrochemistry Letters* **1**, A34 (2012).

112. W. Z. Bao, Z. A. Zhang, Y. Q. Gan, X. W. Wang, J. Lia, Enhanced cyclability of sulphur cathodes in lithium-sulphur batteries with Na-alginate as a binder. *Journal of Energy Chemistry* **22**, 790 (2013).

113. Z. W. Seh, Q. F. Zhang, W. Y. Li, G. Y. Zheng, H. B. Yao, Y. Cui, Stable cycling of lithium sulphide cathodes through strong affinity with a bifunctional binder. *Chemical Science* **4**, 3673 (2013).

114. L. Wang, Z. H. Dong, D. Wang, F. X. Zhang, J. Jin, Covalent Bond Glued Sulphur Nanosheet-Based Cathode Integration for Long-Cycle-Life Li-S Batteries. *Nano Letters* **13**, 6244 (2013).

115. H. Schneider, A. Garsuch, A. Panchenko, O. Gronwald, N. Janssen, P. Novak, Influence of different electrode compositions and binder materials on the performance of lithium-sulphur batteries. *Journal of Power Sources* **205**, 420 (2012).

116. Arumugam Manthiram, Yongzhu Fu, Sheng-Heng Chung, Chenxi Zu, Yu-Sheng Su, Rechargeable Lithium–Sulphur Batteries. *Chemical Reviews* **114**, 11751 (2014).

117. I. Bauer, S. Thieme, J. Brückner, H. Althues, S. Kaskel, Reduced polysulphide shuttle in lithium–sulphur batteries using Nafion-based separators. *Journal of Power Sources* **251**, 417 (2014).

118. Z. Q. Jin, K. Xie, X. B. Hong, Z. Q. Hu, X. Liu, Application of lithiated Nafion ionomer film as functional separator for lithium sulphur cells. *Journal of Power Sources* **218**, 163 (2012).

119. Jia-Qi Huang, Qiang Zhang, Hong-Jie Peng, Xin-Yan Liu, Wei-Zhong Qian, Fei Wei, Ionic shield for polysulphides towards highly-stable lithium-sulphur batteries. *Energy & Environmental Science* **7**, 347 (2014).

120. Yongming Sun, Zhi Wei Seh, Weiyang Li, Hongbin Yao, Guangyuan Zheng, Yi Cui, In-operando optical imaging of temporal and spatial distribution of polysulphides in lithium-sulphur batteries. *Nano Energy* **11**, 579 (2015).

121. Zhaoqing Jin, Kai Xie, Xiaobin Hong, Electrochemical performance of lithium/sulphur batteries using perfluorinated ionomer electrolyte with lithium sulphonyl dicyanomethide functional groups as functional separator. *RSC Advances* **3**, 8889 (2013).

122. Zhaoqing Jin, Kai Xie, Xiaobin Hong, Synthesis and electrochemical properties of a perfluorinated ionomer with lithium sulphonyl dicyanomethide functional groups. *Journal of Materials Chemistry A* **1**, 342 (2013).

123. C. Y. Li, A. L. Ward, S. E. Doris, T. A. Pascal, D. Prendergast, B. A. Helms, Polysulphide-Blocking Microporous Polymer Membrane Tailored for Hybrid Li-Sulphur Flow Batteries. *Nano Letters* **15**, 5724 (2015).

124. Lin Ma, Pooja Nath, Zhengyuan Tu, Mukul Tikekar, Lynden A. Archer, Highly Conductive, Sulphonated, UV-Cross-Linked Separators for Li-S Batteries. *Chemistry of Materials* **28**, 5147 (2016).

125. Wen Li, Jocelyn Hicks-Garner, John Wang, Jun Liu, Adam F. Gross, Elena Sherman, Jason Graetz, John J. Vajo, Ping Liu, V_2O_5 Polysulphide Anion Barrier for Long-Lived Li–S Batteries. *Chemistry of Materials* **26**, 3403 (2014).

126. Songyan Bai, Xizheng Liu, Kai Zhu, Shichao Wu, Haoshen Zhou, Metal–organic framework-based separator for lithium–sulphur batteries. *Nature Energy* **1**, 16094 (2016).

127. Jia-Qi Huang, Ting-Zhou Zhuang, Qiang Zhang, Hong-Jie Peng, Cheng-Meng Chen, Fei Wei, Permselective Graphene Oxide Membrane for Highly Stable and Anti-Self-Discharge Lithium-Sulphur Batteries. *ACS Nano* **9**, 3002 (2015).

128. Wei Guo, Chi Cheng, Yanzhe Wu, Yanan Jiang, Jun Gao, Dan Li, Lei Jiang, Bio-Inspired Two-Dimensional Nanofluidic Generators Based on a Layered Graphene Hydrogel Membrane. *Advanced Materials* **25**, 6064 (2013).

129. Kalyan Raidongia, Jiaxing Huang, Nanofluidic Ion Transport through Reconstructed Layered Materials. *Journal of the American Chemical Society* **134**, 16528 (2012).

130. Ting-Zhou Zhuang, Jia-Qi Huang, Hong-Jie Peng, Lian-Yuan He, Xin-Bing Cheng, Cheng-Meng Chen, Qiang Zhang, Rational Integration of Polypropylene/Graphene Oxide/Nafion as Ternary-Layered Separator to Retard the Shuttle of Polysulphides for Lithium–Sulphur Batteries. *Small* **12**, 381 (2016).

131. Na Li, Zhe Weng, Yarong Wang, Feng Li, Hui-Ming Cheng, Haoshen Zhou, An aqueous dissolved polysulphide cathode for lithium-sulphur batteries. *Energy & Environmental Science* **7**, 3307 (2014).

132. Lina Wang, Yonggang Wang, Yongyao Xia, A high performance lithium-ion sulphur battery based on a Li2S cathode using a dual-phase electrolyte. *Energy & Environmental Science* **8**, 1551 (2015).

133. Lina Wang, Yu Zhao, Morgan L. Thomas, Arghya Dutta, Hye Ryung Byon, Sulphur-Based Catholyte Solution with a Glass-Ceramic Membrane for Li-S Batteries. *Chemelectrochem* **3**, 152 (2016).

134. Y. S. Su, A. Manthiram, Lithium-sulphur batteries with a microporous carbon paper as a bifunctional interlayer. *Nature Communications* **3**, 1166 (2012).

135. Y. S. Su, A. Manthiram, A new approach to improve cycle performance of rechargeable lithium-sulphur batteries by inserting a free-standing MWCNT interlayer. *Chemical Communications* **48**, 8817 (2012).

136. C. X. Zu, Y. S. Su, Y. Z. Fu, A. Manthiram, Improved lithium-sulphur cells with a treated carbon paper interlayer. *Physical Chemistry Chemical Physics* **15**, 2291 (2013).

137. Xingwen Yu, Jorphin Joseph, Arumugam Manthiram, Polymer lithium-sulphur batteries with a Nafion membrane and an advanced sulphur electrode. *Journal of Materials Chemistry A* **3**, 15683 (2015).

138. Liumin Suo, Yong-Sheng Hu, Hong Li, Michel Armand, Liquan Chen, A new class of Solvent-in-Salt electrolyte for high-energy rechargeable metallic lithium batteries. *Nature Communications* **4**, 1481 (2013).

139. F. J. Lin, J. L. Wang, H. Jia, C. W. Monroe, J. Yang, Y. N. NuLi, Nonflammable electrolyte for rechargeable lithium battery with sulphur based composite cathode materials. *Journal of Power Sources* **223**, 18 (2013).

140. Kazem Jeddi, Kaveh Sarikhani, Nader Taheri Qazvini, P. Chen, Stabilizing lithium/sulphur batteries by a composite polymer electrolyte containing mesoporous silica particles. *Journal of Power Sources* **245**, 656 (2014).

141. Jie Gao, Michael A. Lowe, Yasuyuki Kiya, Hector D. Abruna, Effects of Liquid Electrolytes on the Charge-Discharge Performance of Rechargeable Lithium/Sulphur Batteries: Electrochemical and in-Situ X-ray Absorption Spectroscopic Studies. *Journal of Physical Chemistry C* **115**, 25132 (2011).

142. Sen Xin, Lin Gu, Na-Hong Zhao, Ya-Xia Yin, Long-Jie Zhou, Yu-Guo Guo, Li-Jun Wan, Smaller Sulphur Molecules Promise Better Lithium-Sulphur Batteries. *Journal of the American Chemical Society* **134**, 18510 (2012).

143. B. Zhang, X. Qin, G. R. Li, X. P. Gao, Enhancement of long stability of sulphur cathode by encapsulating sulphur into micropores of carbon spheres. *Energy & Environmental Science* **3**, 1531 (2010).

144. Junghoon Kim, Dong-Ju Lee, Hun-Gi Jung, Yang-Kook Sun, Jusef Hassoun, Bruno Scrosati, An Advanced Lithium-Sulphur Battery. *Advanced Functional Materials* **23**, 1076 (2013).

145. Y. L. Liang, Z. L. Tao, J. Chen, Organic Electrode Materials for Rechargeable Lithium Batteries. *Advanced Energy Materials* **2**, 742 (2012).

146. Bernhard Haeupler, Andreas Wild, Ulrich S. Schubert, Carbonyls: Powerful Organic Materials for Secondary Batteries. *Advanced Energy Materials* **5**, 1402034 (2015).

147. Jaephil Cho, Liming Dai, Dirk Guldi, The Chemistry of Energy Conversion and Storage. *Chemistry-an Asian Journal* **11**, 119 (2016).

148. Xuan-Wen Gao, Yuan-Fu Deng, David Wexler, Guo-Hua Chen, Shu-Lei Chou, Hua-Kun Liu, Zhi-Cong Shi, Jia-Zhao Wang, Improving the electrochemical performance of the LiNi0.5Mn1.5O4 spinel by polypyrrole coating as a cathode material for the lithium-ion battery. *Journal of Materials Chemistry A* **3**, 404 (2015).

149. Zhi-Jia Zhang, Shu-Lei Chou, Qin-Fen Gu, Hua-Kun Liu, Hui-Jun Li, Kiyoshi Ozawa, Jia-Zhao Wang, Enhancing the High Rate Capability and Cycling Stability of LiMn2O4 by Coating of Solid-State Electrolyte LiNbO3. *ACS Applied Materials & Interfaces* **6**, 22155 (2014).

150. Liang Zhao, Junmei Zhao, Yong-Sheng Hu, Hong Li, Zhibin Zhou, Michel Armand, Liquan Chen, Disodium Terephthalate (Na2C8H4O4) as High Performance Anode Material for Low-Cost Room-Temperature Sodium-Ion Battery. *Advanced Energy Materials* **2**, 962 (2012).

151. Zhiping Song, Yumin Qian, Tao Zhang, Minoru Otani, Haoshen Zhou, Poly(benzoquinonyl sulphide) as a High-Energy Organic Cathode for Rechargeable Li and Na Batteries. *Advanced Science* **2**, 1500124 (2015).

152. Kai Zhang, Chunyang Guo, Qing Zhao, Zhiqiang Niu, Jun Chen, High-Performance Organic Lithium Batteries with an Ether-Based Electrolyte and 9,10-Anthraquinone (AQ)/CMK-3 Cathode. *Advanced Science* **2**, 1500018 (2015).

153. Shiwen Wang, Lijiang Wang, Kai Zhang, Zhiqiang Zhu, Zhanliang Tao, Jun Chen, Organic Li4C8H2O6 Nanosheets for Lithium-Ion Batteries. *Nano Letters* **13**, 4404 (2013).

154. Zhiping Song, Haoshen Zhou, Towards sustainable and versatile energy storage devices: an overview of organic electrode materials. *Energy & Environmental Science* **6**, 2280 (2013).

155. Meixiang Lv, Fen Zhang, Yiwen Wu, Mujuan Chen, Chunfeng Yao, Junmin Nan, Dong Shu, Ronghua Zeng, Heping Zeng, Shu-Lei Chou, Heteroaromatic organic compound with conjugated multi-carbonyl as cathode material for rechargeable lithium batteries. *Scientific Reports* **6**, 23515 (2016).

156. Haegyeom Kim, Ji Eon Kwon, Byungju Lee, Jihyun Hong, Minah Lee, Soo Young Park, Kisuk Kang, High Energy Organic Cathode for Sodium Rechargeable Batteries. *Chemistry of Materials* **27**, 7258 (2015).

157. Daniel Schmidt, Bernhard Haeupler, Christian Stolze, Martin D. Hager, Ulrich S. Schubert, Poly N-(10-oxo-2-vinylanthracen-9(10H)-ylidene)cyanamide as a Novel Cathode Material for Li-Organic Batteries. *Journal of Polymer Science Part a-Polymer Chemistry* **53**, 2517 (2015).

158. Martin E. Speer, Martin Kolek, Jean Jacques Jassoy, Jennifer Heine, Martin Winter, Peter M. Bieker, Birgit Esser, Thianthrene-functionalized polynorbornenes as high-voltage materials for organic cathode-based dual-ion batteries. *Chemical Communications* **51**, 15261 (2015).

159. Zhaohui Wang, Chao Xu, Petter Tammela, Peng Zhang, Kristina Edstrom, Torbjorn Gustafsson, Maria Stromme, Leif Nyholm, Conducting Polymer Paper-Based Cathodes for High-Areal-Capacity Lithium-Organic Batteries. *Energy Technology* **3**, 563 (2015).

160. Yi Fei Shen, Ding Ding Yuan, Xin Ping Ai, Han Xi Yang, Min Zhou, High Capacity and Cycling Stability of Poly(diaminoanthraquinone) as an Organic

Cathode for Rechargeable Lithium Batteries. *Journal of Polymer Science Part B-Polymer Physics* **53**, 235 (2015).

161. Zhiping Song, Yumin Qian, Minoru Otani, Haoshen Zhou, Stable Li-Organic Batteries with Nafion-Based Sandwich-Type Separators. *Advanced Energy Materials* **6**, 1501780 (2016).

162. B. Hille, *Ion channels of exitable membrane*. (Sinauer Sunderland, 2001).

163. X. Hou, W. Guo, L. Jiang, Biomimetic smart nanopores and nanochannels. *Chemical Society Reviews* **40**, 2385 (2011).

164. Hariharan Jayaram, Alessio Accardi, Fang Wu, Carole Williams, Christopher Miller, Ion permeation through a Cl^--selective channel designed from a CLC Cl^-/H^+ exchanger. *Proceedings of the National Academy of Sciences* **105**, 11194 (2008).

165. M. Nishizawa, V. P. Menon, C. R. Martin, Metal nanotubule membranes with electrochemically switchable ion-transport selectivity. *Science* **268**, 700 (1995).

166. H. Daiguji, Ion transport in nanofluidic channels. *Chemical Society Reviews* **39,** 901 (2010).

167. Y. H. Zhou, W. Guo, J. S. Cheng, Y. Liu, J. H. Li, L. Jiang, High-Temperature Gating of Solid-State Nanopores with Thermo-Responsive Macromolecular Nanoactuators in Ionic Liquids. *Advanced Materials* **24**, 962 (2012).

168. Jun Gao, Wei Guo, Dan Feng, Huanting Wang, Dongyuan Zhao, Lei Jiang, High-Performance Ionic Diode Membrane for Salinity Gradient Power Generation. *Journal of the American Chemical Society* **136**, 12265 (2014).

169. Wei Guo, Liuxuan Cao, Junchao Xia, Fu-Qiang Nie, Wen Ma, Jianming Xue, Yanlin Song, Daoben Zhu, Yugang Wang, Lei Jiang, Energy Harvesting with Single-Ion-Selective Nanopores: A Concentration-Gradient-Driven Nanofluidic Power Source. *Advanced Functional Materials* **20**, 1339 (2010).

170. L. Wang, Y. G. Wang, Y. Y. Xia, A high performance lithium-ion sulphur battery based on a Li2S cathode using a dual-phase electrolyte. *Energy & Environmental Science* **8**, 1551 (2015).

171. Weiyang Li, Qianfan Zhang, Guangyuan Zheng, Zhi Wei Seh, Hongbin Yao, Yi Cui, Understanding the Role of Different Conductive Polymers in Improving the Nanostructured Sulphur Cathode Performance. *Nano Letters* **13**, 5534 (2013).

172. Zhan Lin, Zengcai Liu, Nancy J. Dudney, Chengdu Liang, Lithium Superionic Sulphide Cathode for All-Solid Lithium–Sulphur Batteries. *ACS Nano* **7**, 2829 (2013).

173. Xia Li, Andrew Lushington, Qian Sun, Wei Xiao, Jian Liu, Biqiong Wang, Yifan Ye, Kaiqi Nie, Yongfeng Hu, Qunfeng Xiao, Ruying Li, Jinghua Guo, Tsun-Kong Sham, Xueliang Sun, Safe and Durable High-Temperature Lithium–Sulphur Batteries via Molecular Layer Deposited Coating. *Nano Letters* **16**, 3545 (2016).

174. K. Zhang, Q. Zhao, Z. L. Tao, J. Chen, Composite of sulphur impregnated in porous hollow carbon spheres as the cathode of Li-S batteries with high performance. *Nano Research* **6**, 38 (2013).

175. J. Wang, S. Y. Chew, Z. W. Zhao, S. Ashraf, D. Wexler, J. Chen, S. H. Ng, S. L. Chou, H. K. Liu, Sulphur-mesoporous carbon composites in conjunction with a

novel ionic liquid electrolyte for lithium rechargeable batteries. *Carbon* **46**, 229 (2008).

176. J. Lu, Q. Peng, W. Y. Wang, C. Y. Nan, L. H. Li, Y. D. Li, Nanoscale Coating of LiMO2 (M = Ni, Co, Mn) Nanobelts with Li+-Conductive Li2TiO3: Toward Better Rate Capabilities for Li-Ion Batteries. *Journal of the American Chemical Society* **135**, 1649 (2013).

177. Y. V. Mikhaylik, J. R. Akridge, Polysulphide shuttle study in the Li/S battery system. *Journal of the Electrochemical Society* **151**, A1969 (2004).

178. Byoungwoo Kang, Gerbrand Ceder, Battery materials for ultrafast charging and discharging. *Nature* **458**, 190 (2009).

179. S. Xin, L. Gu, N. H. Zhao, Y. X. Yin, L. J. Zhou, Y. G. Guo, L. J. Wan, Smaller Sulphur Molecules Promise Better Lithium-Sulphur Batteries. *Journal of the American Chemical Society* **134**, 18510 (2012).

180. C. F. Zhang, H. B. Wu, C. Z. Yuan, Z. P. Guo, X. W. Lou, Confining Sulphur in Double-Shelled Hollow Carbon Spheres for Lithium-Sulphur Batteries. *Angewandte Chemie-International Edition* **51**, 9592 (2012).

181. N. Jayaprakash, J. Shen, Surya S. Moganty, A. Corona, Lynden A. Archer, Porous Hollow Carbon@Sulphur Composites for High-Power Lithium-Sulphur Batteries. *Angewandte Chemie-International Edition* **50**, 5904 (2011).

182. Jiangxuan Song, Mikhail L. Gordin, Terrence Xu, Shuru Chen, Zhaoxin Yu, Hiesang Sohn, Jun Lu, Yang Ren, Yuhua Duan, Donghai Wang, Strong Lithium Polysulphide Chemisorption on Electroactive Sites of Nitrogen-Doped Carbon Composites For High-Performance Lithium-Sulphur Battery Cathodes. *Angewandte Chemie-International Edition* **54**, 4325 (2015).

183. Lifen Xiao, Yuliang Cao, Jie Xiao, Birgit Schwenzer, Mark H. Engelhard, Laxmikant V. Saraf, Zimin Nie, Gregory J. Exarhos, Jun Liu, A Soft Approach to Encapsulate Sulphur: Polyaniline Nanotubes for Lithium-Sulphur Batteries with Long Cycle Life. *Advanced Materials* **24**, 1176 (2012).

184. Jiulin Wang, Fengjiao Lin, Hao Jia, Jun Yang, Charles W. Monroe, Yanna NuLi, Towards a Safe Lithium-Sulphur Battery with a Flame-Inhibiting Electrolyte and a Sulphur-Based Composite Cathode. *Angewandte Chemie-International Edition* **53**, 10099 (2014).

185. Shuangqiang Chen, Xiaodan Huang, Hao Liu, Bing Sun, Waikong Yeoh, Kefei Li, Jinqiang Zhang, Guoxiu Wang, 3D Hyperbranched Hollow Carbon Nanorod Architectures for High-Performance Lithium-Sulphur Batteries. *Advanced Energy Materials* **4**, 1301761 (2014).

186. P. X. Xing, G. P. Robertson, M. D. Guiver, S. D. Mikhailenko, K. P. Wang, S. Kaliaguine, Synthesis and characterization of sulphonated poly(ether ether ketone) for proton exchange membranes. *Journal of Membrane Science* **229**, 95 (2004).

187. Klaus Schmidt-Rohr, Qiang Chen, Parallel cylindrical water nanochannels in Nafion fuel-cell membranes. *Nature Materials* **7**, 75 (2007).

188. B. Chu, B. S. Hsiao, Small-angle X-ray scattering of polymers. *Chemical Reviews* **101**, 1727 (2001).

189. N. Asano, M. Aoki, S. Suzuki, K. Miyatake, H. Uchida, M. Watanabe, Aliphatic/aromatic polyimide lonomers as a proton conductive membrane for fuel cell applications. *Journal of the American Chemical Society* **128**, 1762 (2006).

190. E. F. Pettersen, T. D. Goddard, C. C. Huang, G. S. Couch, D. M. Greenblatt, E. C. Meng, T. E. Ferrin, UCSF chimera - A visualization system for exploratory research and analysis. *Journal of Computational Chemistry* **25**, 1605 (2004).

191. D. N. Mastronarde, Automated electron microscope tomography using robust prediction of specimen movements. *Journal of Structural Biology* **152**, 36 (2005).

192. Feng Song, Ping Chen, Dapeng Sun, Mingzhu Wang, Liping Dong, Dan Liang, Rui-Ming Xu, Ping Zhu, Guohong Li, Cryo-EM Study of the Chromatin Fiber Reveals a Double Helix Twisted by Tetranucleosomal Units. *Science* **344**, 376 (2014).

193. PierreGilles De Gennes, *Scaling concepts in polymer physics*. Cornell university press, 1979.

194. P. G. Degennes, REPTATION OF A POLYMER CHAIN IN PRESENCE OF FIXED OBSTACLES. *Journal of Chemical Physics* **55**, 572 (1971).

195. Y. F. Chen, Z. H. Ni, G. M. Wang, D. Y. Xu, D. Y. Li, Electroosmotic flow in nanotubes with high surface charge densities. *Nano Letters* **8**, 42 (2008).

196. Nicolas Di Fiori, Allison Squires, Daniel Bar, Tal Gilboa, Theodore D. Moustakas, Amit Meller, Optoelectronic control of surface charge and translocation dynamics in solid-state nanopores. *Nature Nanotechnology* **8**, 946 (2013).

197. Michael J. O'Connell, Peter Boul, Lars M. Ericson, Chad Huffman, Yuhuang Wang, Erik Haroz, Cynthia Kuper, Jim Tour, Kevin D. Ausman, Richard E. Smalley, Reversible water-solubilization of single-walled carbon nanotubes by polymer wrapping. *Chemical Physics Letters* **342**, 265 (2001).

198. G. Y. Zheng, Q. F. Zhang, J. J. Cha, Y. Yang, W. Y. Li, Z. W. Seh, Y. Cui, Amphiphilic Surface Modification of Hollow Carbon Nanofibers for Improved Cycle Life of Lithium Sulphur Batteries. *Nano Letters* **13**, 1265 (2013).

199. P. G. Bruce, S. A. Freunberger, L. J. Hardwick, J. M. Tarascon, LigO 2 and LigS batteries with high energy storage. *Nature Materials* **11**, 19 (2012).

200. Brian L. Ellis, Kyu Tae Lee, Linda F. Nazar, Positive Electrode Materials for Li-Ion and Li-Batteries†. *Chemistry of Materials* **22**, 691 (2010).

201. Yuan Yang, Guangyuan Zheng, Yi Cui, Nanostructured sulphur cathodes. *Chemical Society Reviews* **42**, 3018 (2013).

202. D. Aurbach, E. Pollak, R. Elazari, G. Salitra, C. S. Kelley, J. Affinito, On the Surface Chemical Aspects of Very High Energy Density, Rechargeable Li-Sulphur Batteries. *Journal of the Electrochemical Society* **156**, A694 (2009).

203. Guangmin Zhou, Da-Wei Wang, Feng Li, Peng-Xiang Hou, Lichang Yin, Chang Liu, Gao Qing Lu, Ian R. Gentle, Hui-Ming Cheng, A flexible nanostructured sulphur-carbon nanotube cathode with high rate performance for Li-S batteries. *Energy & Environmental Science* **5**, 8901 (2012).

204. S. E. Cheon, K. S. Ko, J. H. Cho, S. W. Kim, E. Y. Chin, H. T. Kim, Rechargeable lithium sulphur battery - II. Rate capability and cycle characteristics. *Journal of the Electrochemical Society* **150**, A800 (2003).

205. M. Vijayakumar, Niranjan Govind, Eric Walter, Sarah D. Burton, Anil Shukla, Arun Devaraj, Jie Xiao, Jun Liu, Chongmin Wang, Ayman Karim, S. Thevuthasan, Molecular structure and stability of dissolved lithium polysulphide species. *Physical Chemistry Chemical Physics* **16**, 10923 (2014).

206. Jie Xiao, Jian Zhi Hu, Honghao Chen, M. Vijayakumar, Jianming Zheng, Huilin Pan, Eric D. Walter, Mary Hu, Xuchu Deng, Ju Feng, Bor Yann Liaw, Meng Gu, Zhiqun Daniel Deng, Dongping Lu, Suochang Xu, Chongmin Wang, Jun Liu, Following the Transient Reactions in Lithium-Sulphur Batteries Using an In Situ Nuclear Magnetic Resonance Technique. *Nano Letters* **15**, 3309 (2015).

207. Guo-Chun Li, Guo-Ran Li, Shi-Hai Ye, Xue-Ping Gao, A Polyaniline-Coated Sulphur/Carbon Composite with an Enhanced High-Rate Capability as a Cathode Material for Lithium/Sulphur Batteries. *Advanced Energy Materials* **2**, 1238 (2012).

208. Hailiang Wang, Yuan Yang, Yongye Liang, Joshua Tucker Robinson, Yanguang Li, Ariel Jackson, Yi Cui, Hongjie Dai, Graphene-Wrapped Sulphur Particles as a Rechargeable Lithium-Sulphur Battery Cathode Material with High Capacity and Cycling Stability. *Nano Letters* **11**, 2644 (2011).

209. Mohammad Rejaul Kaiser, Jiazhao Wang, Xin Liang, Hua-Kun Liu, Shi-Xue Dou, A systematic approach to high and stable discharge capacity for scaling up the lithium-sulphur battery. *Journal of Power Sources* **279**, 231 (2015).

210. Laura J. Cote, Franklin Kim, Jia Xing Huang, Langmuir-Blodgett Assembly of Graphite Oxide Single Layers. *J Am Chem Soc* **131**, 1043 (2009).

211. M. R. Cuervo, E. Asedegbega-Nieto, E. Diaz, S. Ordonez, A. Vega, A. B. Dongil, I. Rodriguez-Ramos, Modification of the adsorption properties of high surface area graphites by oxygen functional groups. *Carbon* **46**, 2096 (2008).

212. M. Phaner-Goutorbe, A. Sartre, L. Porte, SOFT OXIDATION OF GRAPHITE STUDIED BY XPS AND STM. *Microscopy Microanalysis Microstructures* **5**, 283 (1994).

213. J. L. Hueso, J. P. Espinos, A. Caballero, J. Cotrino, A. R. Gonzalez-Elipe, XPS investigation of the reaction of carbon with NO, O-2, N-2 and H2O plasmas. *Carbon* **45**, 89 (2007).

214. X. F. Wang, Z. X. Wang, L. Q. Chen, Reduced graphene oxide film as a shuttle-inhibiting interlayer in a lithium-sulphur battery. *Journal of Power Sources* **242**, 65 (2013).

215. E. Sosa, R. Cabrera-Sierra, M. T. Oropeza, F. Hernandez, N. Casillas, R. Tremont, C. Cabrera, I. Gonzalez, Chemical characterization of corrosion films electrochemically grown on carbon steel in alkaline sour environment. *Journal of the Electrochemical Society* **150**, B530 (2003).

216. Yuede Pan, Shu-Lei Chou, Hua-Kun Liu, Shi-Xue Dou, Improved cycling stability of lithium-sulphur batteries by enhancing the retention of active material with a sandwiched hydrothermally treated graphite film. *Rsc Advances* **6**, 34131 (2016).

217. Huilin Pan, Xiaoliang Wei, Wesley A. Henderson, Yuyan Shao, Junzheng Chen, Priyanka Bhattacharya, Jie Xiao, Jun Liu, On the Way Toward Understanding Solution Chemistry of Lithium Polysulphides for High Energy Li-S Redox Flow Batteries. *Advanced Energy Materials* **5**, 1500113 (2015).

218. Zhiping Song, Hui Zhan, Yunhong Zhou, Anthraquinone based polymer as high performance cathode material for rechargeable lithium batteries. *Chemical Communications*, **4**, 448 (2009).

219. Toshiki Nokami, Takahiro Matsuo, Yuu Inatomi, Nobuhiko Hojo, Takafumi Tsukagoshi, Hiroshi Yoshizawa, Akihiro Shimizu, Hiroki Kuramoto, Kazutomo Komae, Hiroaki Tsuyama, Jun-ichi Yoshida, Polymer-Bound

Pyrene-4,5,9,10-tetraone for Fast-Charge and -Discharge Lithium-Ion Batteries with High Capacity. *Journal of the American Chemical Society* **134**, 19694 (2012).

220. Z. Q. Zhu, M. L. Hong, D. S. Guo, J. F. Shi, Z. L. Tao, J. Chen, All-Solid-State Lithium Organic Battery with Composite Polymer Electrolyte and Pillar 5 quinone Cathode. *Journal of the American Chemical Society* **136**, 16461 (2014).

221. Yuki Hanyu, Yoshiyuki Ganbe, Itaru Honma, Application of quinonic cathode compounds for quasi-solid lithium batteries. *Journal of Power Sources* **221**, 186 (2013).

222. P. Arora, Z. M. Zhang, Battery separators. *Chemical Reviews* **104**, 4419 (2004).

223. Mingjie Liu, Lei Jiang, Dialectics of nature in materials science: binary cooperative complementary materials. *Science China Materials* **59**, 239 (2016).

224. Ji-Ae Choi, Sa Heum Kim, Dong-Won Kim, Enhancement of thermal stability and cycling performance in lithium-ion cells through the use of ceramic-coated separators. *Journal of Power Sources* **195**, 6192 (2010).

225. Myung-Hyun Ryou, Dong Jin Lee, Je-Nam Lee, Yong Min Lee, Jung-Ki Park, Jang Wook Choi, Excellent Cycle Life of Lithium-Metal Anodes in Lithium-Ion Batteries with Mussel-Inspired Polydopamine-Coated Separators. *Advanced Energy Materials* **2**, 645 (2012).

226. Jiadeng Zhu, Meltem Yanilmaz, Kun Fu, Chen Chen, Yao Lu, Yeqian Ge, David Kim, Xiangwu Zhang, Understanding glass fiber membrane used as a novel separator for lithium-sulphur batteries. *Journal of Membrane Science* **504**, 89 (2016).

227. H. Y. Liang, X. P. Qiu, S. C. Zhang, W. T. Zhu, L. Q. Chen, Study of lithiated Nafion ionomer for lithium batteries. *Journal of Applied Electrochemistry* **34**, 1211 (2004).

228. Hongbin Yao, Kai Yan, Weiyang Li, Guangyuan Zheng, Desheng Kong, Zhi Wei Seh, Vijay Kris Narasimhan, Zheng Liang, Yi Cui, Improved lithium-sulphur batteries with a conductive coating on the separator to prevent the accumulation of inactive S-related species at the cathode-separator interface. *Energy & Environmental Science* **7**, 3381 (2014).

229. Dan Li, Marc B. Muller, Scott Gilje, Richard B. Kaner, Gordon G. Wallace, Processable aqueous dispersions of graphene nanosheets. *Nature Nanotechnology* **3**, 101 (2008).

230. Xiaoyan Han, Caixian Chang, Liangjie Yuan, Taolei Sun, Jutang Sun, Aromatic carbonyl derivative polymers as high-performance Li-ion storage materials. *Advanced Materials* **19**, 1616 (2007).

231. Andrew J. Wain, Gregory G. Wildgoose, Charles G. R. Heald, Li Jiang, Timothy G. J. Jones, Richard G. Compton, Electrochemical ESR and Voltammetric Studies of Lithium Ion Pairing with Electrogenerated 9,10-Anthraquinone Radical Anions Either Free in Acetonitrile Solution or Covalently Bound to Multiwalled Carbon Nanotubes. *The Journal of Physical Chemistry B* **109**, 3971 (2005).

232. H. Daiguji, Ion transport in nanofluidic channels. *Chemical Society Reviews* **39**, 901 (2010).

233. W. Guo, C. Cheng, Y. Z. Wu, Y. A. Jiang, J. Gao, D. Li, L. Jiang, Bio-Inspired Two-Dimensional Nanofluidic Generators Based on a Layered Graphene Hydrogel Membrane. *Advanced Materials* **25**, 6064 (2013).

APPENDIX A: LIST OF PUBLICATIONS

1*. **Y. D. Pan**, S. L. Chou, H. K. Liu, S. X. Dou, Improved cycling stability of lithium-sulphur batteries by enhancing the retention of active material with a sandwiched hydrothermally treated graphite film. *RSC Adv.* **6**, 34131 (2016). (IF: 3.3)

2*. **Y. D. Pan**, Y. Zhou, Q. Zhao, S. L. Chou, F. Cheng, J. Chen, H. K. Liu, L. Jiang, and S. X. Dou, Introducing Ion-Transport-Regulating Nanochannels to Lithium-Sulfur Batteries. (*Nano Energy*, DOI: 10.1016/j.nanoen.2017.01.025) (IF: 11.6)

3*. **Y. D. Pan**, J. Hao, X. Zhu, Y. Zhou, Y. Dou, S. L. Chou, H. K. Liu, S. X. Dou, L. Jiang, An ion selective separator for lithium-organic batteries. (In preparation)

4*. **Y. D. Pan**, S. L. Chou, H. K. Liu, S. X. Dou, Functional membrane separators for next-generation high-energy rechargeable batteries. (submitted to *Natl. Sci. Rev.*, Under Review) (IF: 8.0)

5*. S. L. Chou, **Y. D. Pan**, J. Z. Wang, H. K. Liu, S. X. Dou, Small things make a big difference: binder effects on the performance of Li and Na batteries. *Phys. Chem. Chem. Phys.* **16**, 20347 (2014). (IF: 4.5)

6. Y. H. Dou, J. T. Xu, B. Y. Ruan, Q. N. Liu, **Y. D. Pan**, Z. Q. Sun, S. X. Dou, Atomic Layer-by-Layer Co3O4/Graphene Composite for High Performance Lithium-Ion Batteries. Adv. Energy Mater. **6**, 1501835, (2016). (IF: 15.2)

7. **Y. D. Pan**, S. L. Chou, H. K. Liu, S. X. Dou, etc., A novel polymer with sulphonate functional groups as binder for Li-S batteries. (In preparation)

8. **Y. D. Pan**, S. L. Chou, H. K. Liu, S. X. Dou, etc., A novel electrolyte with dual solvents for high-performance Li-S batteries (In preparation)

All the listed works listed are carried out during my PhD study.

The works marked with asterisks are exclusively included in this thesis.